TWO SPATIALLY AND TEMPORALLY DISTINCT SOURCES OF CALCIUM CONTRIBUTE TO VESICLE RELEASE AT THE ZEBRAFISH NEUROMUSCULAR JUNCTION

By

Jeffrey M. Hubbard

A DISSERTATION

Presented to the Neuroscience Graduate Program

and the Oregon Health and Science University

School of Medicine

in partial fulfillment of the requirements for the degree of

Doctor of Philosophy

November 2012

School of Medicine
Oregon Health & Science University

CERTIFICATE OF APPROVAL

This is to certify that the Ph.D. dissertation of
JEFFREY HUBBARD
has been approved on November 30, 2012

Advisor, Paul Brehm, PhD

Member and Chair, Laurence Trussell, PhD

Member, Tianyi Mao, PhD

Member, Henrique vonGersdorff, PhD

Member, David Naranjo, PhD

Dedicated to my parents, Francine and Bill

and in memory of grandad, C.K. Hubbard, M.D.

To my children, Emma and Alexander, remember, daddy loves you.

TABLE OF CONTENTS

LIST OF FIGURES

ACKNOWLEDGMENTS

It has been a long journey to arrive at this point in my life and career, during which time many individuals have supported me. For their help, love, and mentorship I will always be grateful. Thank you.

First, I would like to express my tremendous gratitude to my advisor, Dr. Paul Brehm. PB welcomed me into his lab in July of 2007 and his support never wavered despite the fact that my project changed numerous times in an attempt to "find something interesting." His guidance taught me to focus on relevant biological questions, rather than techniques, and the importance of a healthy dose of skepticism of published literature. I have never before encountered someone with such a zeal for, and dedication to science. Finally, his level of integrity is something I will always strive to emulate.

This thesis would not have been possible were it not for a great deal of patience and help from Dr. Hua Wen. I have immensely enjoyed our collaboration, and I truly appreciate her willingness to work closely with me in our efforts to investigate underlying mechanisms of synaptic transmission. To current and former members of the Brehm lab with whom I've had the pleasure of working alongside, thank you for helping make the lab a dynamic and enjoyable experience on a daily basis. In particular, my thanks to Dr. Michael Linhoff. Our frequent discussions of the latest data have been extremely valuable. I am also grateful to Dr. Gail Mandel and members of her lab for their encouragement and support. In addition, I wish to thank Dr. David Naranjo for joining my thesis committee while visiting the Brehm lab on sabbatical. His interest in my project provided valuable insight.

To my family, Mom, Gary, Dad, Jeanne and my brother Mike, thank you for your love and reassurance, especially when it was not at all certain that I would survive this process and achieve my ultimate goal. I don't think I have the words to adequately express my profound appreciation for the many years of support you have provided in so many ways.

To my wife, Charlotte, thank you. I will be forever grateful for your willingness to cross the globe and join me on this adventure of life. You have made countless sacrifices for which I am thankful. To my children, Emma and Alexander, you are my inspiration and I anxiously await the end of 2012, when we will be reunited.

"Ja! Kalzium, das ist alles!"
-Otto Loewi, 1959

PB: "Hagi, how far does calcium diffuse?"
Hagiwara: "Well…calcium doesn't diffuse."
-date unknown

ABSTRACT

The neuromuscular junction is a classic model synapse that has proved to be a rich source of scientific discovery for many decades. Accessibility made this synapse a favorite for researchers in the early days of electrophysiology. Zebrafish neuromuscular junction retains this key feature, but is also an optimal system for modern day molecular biology, genetics, and optical techniques. Moreover, the possibility to patch clamp motor neurons and simultaneously record from voltage clamped target muscle cells makes this a truly unique preparation. In this dissertation I will describe our efforts to examine two modes of vesicle release whose existence has been recognized since those early days of physiology on frog neuromuscular synapses. With paired recordings the distinction between synchronous and asynchronous release becomes clear. However, particularly with asynchronous transmission, the cause is decidedly less clear. At the zebrafish neuromuscular junction we have managed to isolate asynchronous release pharmacologically which has greatly facilitated its study. In the process, optical measurements of calcium dynamics throughout the motor neuron has uncovered a mechanism which explains key hallmarks of asynchronous release. Namely, why this mode of release is delayed, persistent and sensitive to the slow calcium chelator, EGTA.

Chapter 1: Introduction - Calcium and Synaptic Transmission

The central role of calcium channels in synaptic transmission is well established (Katz and Miledi, 1967; Zucker and Regehr, 2002). Neurotransmitter release through the fusion of vesicles to the plasma membrane involves many proteins that function to target, prepare, and trigger their release at specialized regions known as active zones in the presynaptic terminals of neurons. Many of these processes can be regulated in some way by Ca^{2+}, but the triggering molecules responsible for initiating exocytosis play a particularly critical role as Ca^{2+} sensors (James et al., 2009; Jockusch et al., 2007; Neher and Zucker, 1993; Sudhof, 2004). These proteins sense the acute rise in Ca^{2+} which occurs when an action potential (AP) invades a presynaptic bouton and causes the opening of voltage-gated Ca^{2+} channels (VGCCs). Recent research has been heavily focused on these molecules, many of which are part of the synaptotagmin family, because they are ideally poised to affect the timing and the Ca^{2+} sensitivity of release (Sudhof, 2004; Wadel et al., 2007). While these triggering molecules clearly impact when vesicles will undergo exocytosis, much of my work to be presented here focuses on the initial influx of Ca^{2+} through VGCCs, and how the spatial and temporal aspects of this Ca^{2+} entry may ultimately shape transmitter release.

Synaptic vesicle release in neurons can occur in any one of three "modes" which basically differ in their timing respective to an AP. Synchronous release is defined as fusion that is tightly coupled in time to the arrival of an AP, and multiple vesicles typically fuse simultaneously to an array of active release zones to produce a large evoked response in the postsynaptic cell. Asynchronous release is often defined as the exocytosis of a vesicle which is not phase locked with the AP and can also occur in the absence of APs following a period of

tetanic stimulation. It is generally accepted that elevated residual Ca^{2+} in the terminal, that is Ca^{2+} remaining from prior stimuli, plays a role in asynchronous release (Zucker and Regehr, 2002). Finally, spontaneous release is the ongoing fusion of individual vesicles irrespective of APs and whose Ca^{2+} dependence is debated. These fusion events underlie the miniature end plate potentials that Paul Fatt and Bernard Katz observed and reported on in 1952 during their recordings from the frog neuromuscular junction (NMJ) which first described the quantal nature of neurotransmitter release (Fatt and Katz, 1952). By measuring the current that individual exocytotic events produce in a postsynaptic cell when the neurotransmitter contents of a vesicle are released into the synaptic cleft and bind to their receptors we can infer the number of vesicles released during larger, multiquantal, events that are typically observed during synchronous and asynchronous release.

Synchronous Release

When an AP propagates from its initiation site, the axon initial segment (AIS), down the length of an axon and into presynaptic boutons, the brief membrane depolarization that occurs causes the opening of voltage dependent channels. Channels specifically permeable to Ca^{2+} allow divalent ions to rush from the extracellular space into the neuron largely during the repolarization phase of the AP. As the membrane potential recedes from its peak and moves further from the reversal potential of Ca^{2+} the driving force increases and Ca^{2+} floods in through the mouth of the channel (Borst and Sakmann, 1996; Chad and Eckert, 1984; Pumplin et al., 1981). Synchronous vesicle fusion occurs within this narrow window of time, coincident with the AP. During low frequency stimulation (<1Hz) most neurons release transmitter in a synchronous fashion. Several factors are thought to influence the synchronicity. First, the low affinity Ca^{2+} binding protein, synaptotagmin 1 (and at some synapses, synaptotagmin 2),

appears to be a critical mediator of synchronous release (Fernandez-Chacon et al., 2001; Geppert et al., 1994; Sudhof, 2004; Tang et al., 2006; Walter et al., 2011). Synaptotagmins (Syt) consist of a large family of proteins with a single transmembrane domain. Some isoforms contain two Ca^{2+} binding sites, C2A and C2B, which may be in part responsible for the steep Ca^{2+} dependence of exocytosis (Dodge and Rahamimoff, 1967; Pang et al., 2011; Sudhof, 2004). These proteins tend to reside on vesicles (except see Sugita et al., 2001) and interact with vital pieces of the fusion machinery, the SNARE (Soluble NSF Attachment protein REceptor) proteins, as well as with the lipid bilayer itself (Bai et al., 2004; Fernandez et al., 2001; Radhakrishnan et al., 2009; Schiavo et al., 1997). Upon Ca^{2+} influx and binding, synaptotagmins are thought to trigger the fusion of vesicle membrane to the plasma membrane and thus the release of transmitter through the fusion pore (Weber et al., 1998). The influx of Ca^{2+} is brief and restricted to a small area during an AP, which consequently limits the number of vesicles that actually detect enough Ca^{2+} to trigger a fusion event (Borst and Sakmann, 1996; Neher and Sakaba, 2008). Phasic synchronous release is thought to involve the vesicles which are tightly coupled to VGCCs, within the so-called nano or microdomain, where fast Ca^{2+} buffering restricts the diffusion of Ca^{2+} during low frequency firing. Because of its low affinity for Ca^{2+} and fast on-rate, Syt1 is ideally suited to sense the transient Ca^{2+} rise which occurs in the microdomain to trigger fast phasic transmission.

Proximity of synaptic vesicles to Ca^{2+} channels at release sites influences their ability to release in a synchronous manner (Wadel et al., 2007). This represents an important geometric consideration because terminals can be packed with 100's to 1000's of synaptic vesicles. Clearly a vesicle must come into close proximity with the plasma membrane in order to eventually fuse in a Ca^{2+}dependent manner, however there are additional steps in the vesicle cycle that are necessary to prepare the vesicle for eventual fusion. Processes such as docking and priming are

thought to involve interactions from multiple accessory proteins and importantly these reactions must take a certain amount of time to occur (Sudhof, 2004). Even if these processes occur very quickly it seems unlikely that a vesicle which must transit to the membrane and undergo a series of biochemical reactions could release without delay in response to the arrival of the AP. Therefore it is generally thought that vesicles releasing in a synchronous manner are part an immediately releasable pool, which consists of spatially privileged synaptic vesicles near Ca^{2+} channels. Whereas, the rest of the readily releasable pool (RRP) of vesicles are more distributed throughout the synapse (Richards et al., 2003; Rizzoli and Betz, 2004, 2005).

Asynchronous Release

Asynchronous release occurs after the end of an AP in a delayed manner (normally >1-2 msec after the AP), and often arises during trains of high frequency stimuli. This type of exocytosis can even continue long after a train of APs has halted and is sometimes seen as a jitter in the firing of a postsynaptic cell (Atluri and Regehr, 1998; Goda and Stevens, 1994; Manseau et al., 2010). While there is general consensus regarding the mechanisms underlying synchronous release, the cause of asynchronous release has remained mysterious and more controversial. Most of the focus has revolved around two possibilities. During repetitive stimulation the Ca^{2+} influx through channels at the nerve terminal can eventually overwhelm the fast endogenous Ca^{2+} buffers present. As this occurs the domain of elevated Ca^{2+} concentration expands and ever more distant vesicles are recruited to approach and fuse at the release sites. This slow expansion is thought to cause the delay in fusion with respect to the AP (Neher and Sakaba, 2008). When introduced into a neuron, the exogenous buffers such as the slow Ca^{2+} chelator EGTA, or the fast chelator BAPTA can reduce or altogether eliminate asynchronous release. This is taken as evidence that residual Ca^{2+} accumulating from sustained firing mediates

the slow asynchronous phase (Zucker and Regehr, 2002). Although there is good evidence that the microdomain can collapse as Ca^{2+} builds up, there must be other mechanisms in play since instantaneously raising intracellular Ca^{2+} with flash photolysis also reveals fast and slow phases of release.

A number of studies on vesicle exo and endocytosis have suggested that within a given synaptic terminal the vesicles themselves parse out into groups which have different biochemical characteristics. There is much debate as to whether these groupings are truly physical (vesicles possessing distinct molecular components) or merely operational (observed kinetic differences which are based on the state of the vesicle). Vesicles undergo a series of reactions and interactions with numerous proteins as they fuse and recycle so they surely exist in different states of preparedness as they proceed to ultimately release neurotransmitter into the cleft (Sudhof, 2004). Some groups favor the idea that vesicles maintain molecular signatures assigning them to defined groups that specifically undergo synchronous, asynchronous, or spontaneous release (Groffen et al., 2010; Pang et al., 2011; Raingo et al., 2012; Ramirez et al., 2012; Yao et al., 2011). The properties of their biochemical makeup would therefore determine the vesicular release kinetics rather than strictly their proximity to the Ca^{2+} source. Synaptotagmin-7 (Syt7), VAMP4 and Doc2b have now been implicated as Ca^{2+} sensors in asynchronous release but it is unclear if both synchronous and asynchronous sensors can be found on the same vesicle population (Raingo et al., 2012; Wen et al., 2010; Yao et al., 2011). In the case of Syt7, results from the zebrafish NMJ argue that both modes share a common pool of vesicles since eliminating either sensor individually only changes the mode of release and not the total number of vesicles that fuse during the stimuli (Otsu et al., 2004; Sun et al., 2007; Wen et al., 2010). Ideally an asynchronous sensor should have a slower on-rate than for Ca^{2+} than the synchronous sensor, in order to respond to global Ca^{2+} changes in the terminal which are much

lower than the concentrations present directly adjacent to an open Ca^{2+} channel. In addition, a slow Ca^{2+} binding rate could desynchronize vesicle fusion. Both Syt7 and Doc2b share these features, and importantly altering their expression selectively alters asynchronous release (Sugita et al., 2001; Wen et al., 2010; Yao et al., 2011).

Spontaneous Release

The third mode of release, spontaneous release, occurs in the absence of an AP. Early work on synaptic transmission at the frog NMJ concluded that these spontaneous events were caused by the random and intermittent fusion of individual vesicles. They were detected in the muscle as small depolarizations of consistent amplitude, called miniature end plate potentials (mEPPS). As the first ultrastructural images of synapses became available so did the realization that the small clear vesicles seen in the EM photos were in fact the carriers of acetylcholine responsible for the mEPPS (Fatt and Katz, 1952; Robertson, 1956). These studies established two important tenets of synaptic physiology, the quantal hypothesis and the vesicle hypothesis. Evoked release can then be explained as the fusion of multiple quanta. Over 60 years has passed since these early experiments and yet the purpose of spontaneous release is still unclear. There is speculation that it could be an important factor in maintaining synaptic connections. Moreover there is currently some debate as to whether or not spontaneous release and evoked release originate from the same pool of vesicles(Andreae et al., 2012; Fredj and Burrone, 2009; Groemer and Klingauf, 2007; Hua et al., 2010; Otsu et al., 2004; Sara et al., 2005; Wilhelm et al., 2010). In any case, given that much of our understanding of evoked release is based on the quantal hypothesis and hence the amplitude and kinetics of minis we can only hope that if vesicles in pools differ by what is present on their surface that they do not also differ by what they contain (or at least how much of it)! One aspect of spontaneous release which has

remained remarkably consistent across many experiments in numerous preparations is that when presumed Ca^{2+} sensors for fast phasic and slow tonic release are eliminated, rates of spontaneous release increase (Kochubey and Schneggenburger, 2011; Liu et al., 2009; Sun et al., 2007; Xu et al., 2009). My work concerns evoked transmitter release, both synchronous and asynchronous, and not spontaneous release, therefore I will limit future discussion to these two modes of exocytosis.

Ca^{2+} Channels

It is impossible to overstate the importance of Ca^{2+} in cellular function. Amongst its wide variety of roles, Ca^{2+} mediates muscle contraction, hormone secretion, synaptic transmission, gene transcription and generally serves as a cell's most versatile second messenger. One reason for this is that cells, and particularly neurons, have an exquisite capability to quickly introduce Ca^{2+} with a high degree of spatial fidelity. This is due to the extent to which free Ca^{2+} is buffered by a myriad of Ca^{2+} binding proteins in the cytoplasm when it enters the cell or is released from intracellular organelles through Ca^{2+} permeable channels. Neurons expend a good deal of energy creating the extreme Ca^{2+} gradient that exists between the extracellular space and the cytoplasm. The plasma membrane Ca^{2+} ATPase (PMCA) and sarcoplasmic/endoplasmic reticulum Ca^{2+} ATPase (SERCA) pump Ca^{2+} ions out of the cell and into intracellular stores respectively by harnessing the energy from ATP hydrolysis. Similarly, the Na^{+}/Ca^{2+} exchanger uses the power of the sodium gradient (generated by the Na^{+}/K^{+} pump) to transport Ca^{2+} out of the cell. The result of these efforts is a massive Ca^{2+} gradient of approximately 10,000 fold with cytoplasmic Ca^{2+} levels in the 100nM range while Ca^{2+} concentrations of ~2mM exist outside of the cell. Consequently, drastic changes in cytosolic Ca^{2+} concentration can occur, even during brief openings of Ca^{2+} channels. Voltage-gated Ca^{2+}

channels (VGCCs), found on the plasma membrane, respond to membrane potential depolarization by opening a Ca^{2+} selective pore allowing rapid influx of Ca^{2+} into the cell. Other Ca^{2+} channels such as ryanodine receptors and IP_3 receptors cause the efflux of Ca^{2+} from intracellular stores in response to either Ca^{2+} itself or the second messenger IP_3. In fact, many ligand and voltage gated channels as well as some transporters are permeable to Ca^{2+} with variable selectivity. For the purpose of this thesis work, I will be focusing on VGCCs and to a lesser extent the channels involved in release of intracellular Ca^{2+}.

VGCCs are large transmembrane proteins formed by multiple subunits. The α_1 subunit consists of four repeating domains (I-IV) which each contain six transmembrane segments (S1-S6) and a pore-forming reentrant loop (Catterall, 2000). Accessory subunits (α_2-δ, β, and γ) can alter various aspects of channel function, however it is the α_1 subunit that primarily differentiates the known Ca^{2+} channel subtypes. The sequences of α_1 can differ substantially and differences in voltage dependence, activation, inactivation, deactivation, pharmacology and subcellular localization exist. The VGCCs separate generally into two groups, high-voltage activated (HVA) and low-voltage activated (LVA) Ca^{2+} channels. HVA channels open at relatively depolarized potentials (-40mV) and these include L-type channels (CaV1.1, CaV1.2, CaV1.3, and CaV1.4), P/Q-type, N-type, and R-type channels (CaV2.1, CaV2.2, and CaV2.3 respectively). T-type Ca^{2+} channels are LVA, activating at more hyperpolarized potentials (-60mV). Three T-type isoforms have been identified (CaV3.1, CaV3.2, and CaV3.3). A number of Ca^{2+} channel mutations have been identified that are causal to serious human diseases (Lorenzon and Beam, 2008).

In the context of the vertebrate NMJ, P/Q-type, N-type, and to a lesser extent R-type have been implicated in mediating synaptic transmission (Urbano et al., 2002). In general

mammalian principally uses P/Q while lower vertebrates are thought to employ N-type channels. These distinctions have been made primarily on the pharmacological specificity of several Ca^{2+} channel toxins, however some results from our work at the zebrafish NMJ may call into question the validity of the presumed toxin specificity which will be discussed in chapter 4. A small contribution from L-type channels has been suggested, again based on pharmacology, at frog NMJ (Li et al., 2001). T-type channels have not been observed at presynaptic terminals of motor neurons, perhaps because their kinetics would not be well suited for fast synaptic transmission. Because of their particular importance in neuromuscular transmission, the emphasis here is on P/Q and N-type channels and how their activity is thought to produce synchronous vs. asynchronous release.

P/Q-type, N-type, and R-type Channels

Most synaptic transmission is mediated by a group of three Ca^{2+} channel subtypes; P/Q, N, and R-type. P/Q and N-type channels have been extensively studied and nature has evolved highly specific toxins (agatoxins from the funnel web spider, *Agelenopsis aperta* and the conotoxins, from cone snails *Conus* sp.) to target these important VGCCs. Less is known about R-type channels but they are effectively inhibited by a toxin derived from tarantula venom (*Hysterocrates gigas*, SNX-482). P/Q and N-type channels contain specific sequences assuring their central role in fast synaptic transmission. One intracellular domain, called the synprint site (for synaptic protein interaction), interacts specifically with critical plasma membrane SNARE proteins syntaxin-1A and SNAP-25 (Brunger, 2005; Catterall, 2010; Catterall and Few, 2008; Evans and Zamponi, 2006; Han et al., 2011). These proteins are contributors to the core SNARE complex and responsible for vesicle docking at the active zone in preparation for Ca^{2+} dependent fusion. In addition the C2B domain of synaptotagmin-1 can also interact with the

synprint site in a Ca^{2+} dependent manner, where high Ca^{2+} concentrations favor synaptotagmin binding over syntaxin binding (Sheng et al., 1996; Sheng et al., 1997).

P/Q and N-type channels are regulated in an activity dependent manner through a number of pathways. Modulation can occur by phosphorylation, phospholipid interactions, G proteins, Ca^{2+} dependent inactivation, both voltage dependent inactivation and voltage dependent facilitation and finally through Ca^{2+} dependent regulation by Ca^{2+} sensor proteins which can either facilitate or inactivate these channels. Some forms of short-term plasticity are likely caused by these types of modulation of P/Q-type and N-type channels (Catterall and Few, 2008; Leal et al., 2012). The literature on Ca^{2+} channel regulation is abundant and it is unclear whether or not channel modulation can alter the release mode between synchronous and asynchronous release.

A single gene (CaV2.1) encodes both the P- and Q-type channels, which are produced by alternative splicing. First described in Purkinje cells, P-type channels are resistant to ω-conotoxin and the L-type inhibitor, dihydropyridine (Llinas et al., 1989). However, the P/Q-type current is sensitive to agatoxin, which does not affect N-type channels (Mintz et al., 1992a; Mintz et al., 1992b). P/Q-type channels exist throughout the central and peripheral nervous system and while often found at presynaptic terminals, they are not limited to that subcellular localization. At the mammalian neuromuscular junction, numerous studies have shown the presence of P/Q channels which, based on blockade of transmission by agatoxin, appears to be responsible for the majority of Ca^{2+} influx during stimulation (Bowersox et al., 1995; Protti and Uchitel, 1993; Uchitel et al., 1992). Specific antibody labeling of P/Q channels at presynaptic terminals of rat spinal motor neurons has been reported (Westenbroek et al., 1998). N-type channels were also observed at some terminals innervating skeletal muscle, however in much

lower abundance (Westenbroek et al., 1998). When neuromuscular transmission was tested in a P/Q-type Ca^{2+} channel knockout mouse, compensation was observed due to Ca^{2+} current mediated by both R-type and N-type channels (Westenbroek et al., 1998). Despite the compensation by the other two members of the CaV2 family, the gene deletion was not without consequence, as quantal content was smaller than that for WT mice. In addition, paired-pulse facilitation was abolished and post-synaptic receptor clusters were smaller (Urbano et al., 2003). Mutations in mammalian P/Q-type VGCCs have also been shown to give rise to severe ataxias (Lorenzon and Beam, 2008).

In 1985, Nowycky, Fox, and Tsien published their discovery of a third type of Ca^{2+} channel. At this time HVA and LVA channels were known to exist (Hagiwara et al., 1975) and their currents could be isolated by their voltage dependence of activation (L-type = HVA, T-type = LVA) and sensitivity to dihydropyridines (L-type). The N-type channel had activation kinetics similar to L-type channels but inactivated more quickly like T-type (Fox et al., 1987a, b; Nowycky et al., 1985). Isolation of ω-conotoxin GVIA, a peptide neurotoxin from the venom of *Conus geographus*, was an important step for Ca^{2+} channel classification and it has become the "gold standard" for pharmacological identification of N-type currents due to its apparent specificity (Hille, 2001; Olivera et al., 1984).

At the frog NMJ, ω-conotoxin GVIA sensitive Ca^{2+} current is primarily responsible for acetylcholine (ACh) release (Katz et al., 1995; Kerr and Yoshikami, 1984; Koyano et al., 1987; Sano et al., 1987; Yazejian et al., 1997). Given the discrimination of agatoxin and ω-conotoxin GVIA for P/Q and N-type channels respectively in the mammalian CNS, it has been widely assumed that this specificity holds true in the lower vertebrates. Fluorescently tagged ω-conotoxin GVIA shows strong labeling at presynaptic terminals of the frog NMJ (Cohen et al.,

1991; Robitaille et al., 1990) as does indirect immunostaining of channels using fluorescent antibodies raised against ω-conotoxin GVIA (Torri Tarelli et al., 1991). Pre and postsynaptic voltage clamp was used in an embryonic *Xenopus* nerve-muscle coculture to directly assess the ionic contribution of different VGCC isoforms when pharmacological blockers were applied. This study found that while ω-conotoxin GVIA could effectively abolish >90% of the Ca^{2+} current, some of the total conductance was also sensitive to DHP blockade. Both nitrendipine and nimodipine reduced Ca^{2+} currents by as much as 30%. Around 17% of the postsynaptic current could be inhibited with application of nitrendipine alone (Sand et al., 2001; Thaler et al., 2001). These results suggest that ω-conotoxin GVIA may not be as specific to N-type channels as previously believed. Furthermore, we hope that our identification of a zebrafish Ca^{2+} channel mutant will shed more light on non-N-type inhibition by ω-conotoxin GVIA.

In relation to synchronous release, the roles of P/Q and N-type channels at presynaptic terminals of the NMJ seems clear. Their association with exocytosis machinery, active zone proteins and synaptic vesicles ideally suits them for fast synchronous release. In general it has been assumed that these same channels must also provide the Ca^{2+} source for asynchronous release as well. Through the repetitive openings of these Ca^{2+} entry points it is thought that nearby Ca^{2+} buffers saturate and give way to an expanding cloud of Ca^{2+} capable of initiating asynchronous vesicle fusion (Neher and Sakaba, 2008). A recent report from the Catterall lab has added a twist to this theory by finding a persistent Ca^{2+} current which outlasts the stimulus by hundreds of milliseconds. The current is mediated by a CaV2 channel and could potentially account for asynchronous release providing another possible mechanism for this phenomenon. Their work shows that when these channels are activated repetitively by multiple depolarizing voltage steps they are able to remain open even after the membrane is repolarized. This persistent Ca^{2+} conduction (termed I_{async}) requires a rise in internal Ca^{2+} as it is blocked by 10

mM EGTA and can last hundreds of msec following repolarization (Few et al., 2012). While the authors do not provide a direct link from this asynchronous current to asynchronous transmitter release, they note that the time-courses of onset and duration following a train of stimuli are similar for each in cultured hippocampal neurons.

L-type Channels

The skeletal muscle L-type Ca^{2+} channel was the first voltage gated Ca^{2+} channel to be cloned and expressed (Tanabe et al., 1987). T-tubules of myocytes are a rich source of CaV1.1 protein which proved pivotal in its isolation. It was already known at this time that multiple Ca^{2+} channels can and must exist in certain preparations such as starfish egg and canine atrial cardiac cells based on voltage dependence of activation, inactivation kinetics and dihydropyridine (DHP) sensitivity (Bean, 1985). The other three subtypes (CaV1.2, CaV1.3, and CaV1.4) were soon cloned by sequence homology (Lipscombe et al., 2004). Like the CaV2 channels, CaV1 Ca^{2+} channels are principally activated at depolarized potentials, although some recent studies have questioned this belief, particularly for the neuronal CaV1.3 subtype (Helton et al., 2005; Xu and Lipscombe, 2001). However, these channels differ from P/Q, N, and R-type channels in that they are slowly inactivating (Lipscombe et al., 2004). L-type channels are found on the soma of mouse motor neurons (Carlin et al., 2000; Jiang et al., 1999; Westenbroek et al., 1998) and *Xenopus* motor neurons (Li et al., 2001). They have also been implicated in coupling Ca^{2+} influx with gene expression through the activation of CREB (Dolmetsch et al., 2001).

T-type Channels

With their unusual voltage dependence, T-type channels are distinctly different from their high voltage activated cousins. These Ca^{2+} channels begin opening around -60mV and inactivate quickly (Cain and Snutch, 2010; Evans and Zamponi, 2006; Hille, 2001; Perez-Reyes,

2003). Despite the small transient conductance observed in single channel recordings (Fox et al., 1987a, b), T-type channels can play important roles in neuronal excitability. Recent studies have found that T-type channels can affect the action potential waveform, shape AP bursting patterns, and even influence the position of Na^+ channel clusters along the axon initial segment (Bender and Trussell, 2009; Bender et al., 2012; Grubb and Burrone, 2010). Although their involvement in transmitter release at neuromuscular synapses has not been shown, some T-type contribution has been observed in the soma of *Xenopus* motor neurons (Li et al., 2001).

Store Release Channels

Intracellular organelles such as the endoplasmic reticulum (ER) and mitochondria are capable of storing large quantities of Ca^{2+}. It is estimated that micromolar to millimolar concentrations of Ca^{2+} may exist within the lumen of these organelles at any given time (Berridge et al., 2000). With the ability to act as a Ca^{2+} sink, these stores can limit the duration of elevated cytoplasmic Ca^{2+} following entry through VGCCs. Conversely they can act as a source of Ca^{2+} when triggered by either Ca^{2+} itself through Ca^{2+} induced Ca^{2+} release (CICR) or the second messenger IP_3. Ryanodine receptors (RyR) and IP_3 receptors are Ca^{2+} release channels which line the surface of the ER and respond to Ca^{2+} and IP_3 respectively by opening and releasing additional Ca^{2+} into the cytoplasm causing large global Ca^{2+} changes. These two channels share similar structural features, both are formed as tetramers of identical subunits (Capes et al., 2011; Taylor and Prole, 2012). Three RyR genes have been identified encoding RyR1, RyR2 and RyR3. Low Ca^{2+} concentrations can increase RyR activity while high concentrations inhibit RyR opening. IP_3 is generated by phospholipase C (PLC) when the lipid phosphotidylinositol 4,5-bisphosphate is hydrolyzed. This activity can be induced by G protein and tyrosine kinase linked receptors. IP_3 receptors on the ER bind IP_3 causing the receptor to

open and release Ca^{2+}, much like RyR activation. Three genes have been identified which encode IP_3 receptors and cells often express multiple isoforms. Many of the same principles of regulation appear to apply to both RyRs and IP_3 receptors, such as the biphasic effect of Ca^{2+}.

There has been significant recent interest in the potential involvement of internal Ca^{2+} stores with vesicle release (Bardo et al., 2006; Berridge, 1998; Berridge et al., 2003; Berridge et al., 2000; Fitzjohn and Collingridge, 2002). Both mitochondria and ER membrane are thought to be present in most presynaptic boutons, but it is unclear of their proximity to release sites (Bouchard et al., 2003; Verstreken et al., 2005). Kuba's group has focused on RyR mediated Ca^{2+} release and how it relates to transmission during tetanic stimulation at the frog NMJ (Kubota et al., 2005; Soga-Sakakibara et al., 2010). Their work has linked Ca^{2+} efflux from RyRs, and in particular RyR3, to asynchronous release (Narita et al., 2000; Narita et al., 1998). In the CNS, a number of studies lend support to a role for presynaptic intracellular store Ca^{2+} release in synaptic transmission, including increased mEPSC frequencies and postsynaptic firing (Sharma and Vijayaraghavan, 2003), underlying large mIPSCs in Purkinje cells (Llano et al., 2000), changes in short-term plasticity (Emptage et al., 2001), enhanced evoked release (Galante and Marty, 2003), induction of LTD at CA3-CA3 synapses (Unni et al., 2004), and mobilization of endogenous cannabinoids (Isokawa and Alger, 2006). I will note that disagreement exists about the role of presynaptic intracellular stores in short-term plasticity (Carter et al., 2002).

In the work presented here I hope to convince readers that with the zebrafish NMJ we have available to us an ideal preparation to address questions about synchronous and asynchronous release with paired recordings, live imaging, transgenics, mutants, and pharmacology. Using these tools we identify a previously undescribed mechanism by which

delayed asynchronous vesicle release may manifest during periods of intense stimulation and attempt to localize and alter key mediators of this process.

Results presented here show that synchronous transmitter release at the zebrafish NMJ is dependent on Ca^{2+} influx through a ω-conotoxin GVIA sensitive P/Q-type Ca^{2+} channel. Application of ω-conotoxin GVIA in conjunction with prolonged high frequency stimulation of the primary motor neuron will evoke delayed asynchronous release, while the synchronous component is completely absent. Using the toxin to isolate asynchronous release, the properties of this mode of transmission were studied. The onset of asynchronous release can be further delayed by increasing the concentration of EGTA within the patch pipette. In addition, the delay itself results from the slow propagation of a calcium wave, whose arrival at synaptic terminals is coincident with the onset of the delayed asynchronous release. The identity of the initiating factor and mechanism underlying the propagating calcium wave are presently unknown. However, the demonstration of a calcium wave as causal to delayed release represents an altogether new mechanism by which asynchronous release may manifest

Chapter 2: Materials and Methods

Zebrafish Preparation

Day 3-5 (72-120 hpf) zebrafish (*Danio rerio*) embryos were used. A detailed description of the preparation, including videos, is published in the Journal of Visualized Experiments (Wen and Brehm, 2010). First the fish is decapitated and pinned through the notochord to the bottom of a Sylgard coated recording chamber using electrolytically sharpened tungsten. The chamber is filled with bath recording solution (BRS). Using a small hook, a flap of skin is pulled up next to the rostral pin. With fine forceps the skin is then removed by grabbing hold of the flap and gently pulling toward the tail, taking care to avoid tearing muscle cells in the process. Once the muscle is exposed the solution is exchanged for BRS containing 10% formamide (2 M). After a period of no more than 2 minutes the formamide solution is replaced by normal BRS. Dorsal muscle is then removed using a suction pipette (~15 um tip diameter, TW150F-4, World Precision Instruments, Sarasota, FL) fashioned with a horizontal pipette puller (P-97 Flaming/Brown Micropipette Puller, Sutter Instruments, Novato, CA). At this point the dura is exposed and prepared for patch clamp experiments on the underlying neurons in the spinal cord. The ventral muscle remains intact and suitable for imaging. Additional suction of superficial slow muscle on the ventral side is necessary in the case of paired motor neuron and fast skeletal muscle recordings.

Solutions

Bath Recording Solution (BRS)

134 mM NaCl, 2.9 mM KCl, 2.1 mM $CaCl_2$, 1.2 mM MgCl, 10 mM glucose, 10 mM HEPES, pH to 7.4 with NaOH, ~290 mOsm. All chemicals were from Sigma-Aldrich (St. Louis, MO) except glucose from BDH Chemicals (supplied by VWR, Brisbane, CA). In some experiments low Ca^{2+} solutions (100, 200, and 500 uM $CaCl_2$) were used. Some synaptopHluorin experiments include 50 mM NH_4Cl (Sigma-Aldrich, St. Louis, MO).

Spinal Neuron Internal Solution (SN)

115 mM K-gluconate, 15 mM KCl, 2 mM MgCl, 4 mM Mg-ATP, 10 mM HEPES, pH to 7.2 with KOH, ~290 mOsm. 500 μM or 5 mM EGTA was used. All chemicals were from Sigma-Aldrich (St. Louis, MO). For Ca^{2+} imaging the following indicators were used: 100 μM Fluo-4, 100 μM Fluo-5F, 100 μM Fluo-4FF, 100 μM Oregon Green BAPTA-1 Dextran conjugate (Invitrogen-Molecular Probes, Eugene, OR). Most experiments also included the morphological marker Alexafluor-647 hydrazide (40 μM, Invitrogen-Molecular Probes, Eugene, OR).

Pharmacology

The following drugs were used in experiments: ω-conotoxin GVIA (Alamone Labs, Jerusalem, Israel), TTX (Alamone Labs, Jerusalem, Israel), Ni^{2+} (Sigma-Aldrich, St. Louis, MO), Cd^{2+} (Sigma-Aldrich, St. Louis, MO), Mibefradil (Sigma-Aldrich, St. Louis, MO), Nimodipine (Sigma-Aldrich, St. Louis, MO), Ryanodine (Sigma-Aldrich, St. Louis, MO), Ruthenium Red (Sigma-Aldrich, St. Louis, MO), SNX-482 (Tocris, Bristol, UK), Nifedipine (Tocris, Bristol, UK), Isradipine (Tocris, Bristol, UK), Amlodipine (Tocris, Bristol, UK), Verapamil (Tocris, Bristol, UK), SN-6 (Tocris, Bristol, UK), CPA

(Tocris, Bristol, UK), 2-APB (Tocris, Bristol, UK), Xestospongin-C (Tocris, Bristol, UK), TTA-P2 (Merck, Whitehouse Station, NJ).

Staining

Alpha-Bungarotoxin-555 (Invitrogen, Carlsbad, CA) conjugate was diluted into BRS (1:2000). Skinned zebrafish were incubated with the α-Btx for 15 minutes and subsequently washed with BRS. Fast muscle staining was achieved with phalloidin-555 (Invitrogen, Carlsbad, CA) and for slow muscle staining, a slow myosin specific antibody was used (f59-647, Developmental Studies Hybridoma Bank, University of Iowa).

Mutants and Transgenic Fish

SynaptopHluorin fish were generated by Hua Wen. The original description of synaptopHluorin can be found here (Miesenbock et al., 1998). *Tb204a* and *relaxed* mutants were acquired from the original Tubingen screen (Granato et al., 1996). *Gemini* mutants were kindly donated by the Nicolson lab (Vollum Institute, OHSU, Portland, OR). *Island beat* mutants were kindly donated by the Rottbauer lab (University of Ulm, Ulm, Germany). SynaptopHluorin/*tb204a* and synaptopHluorin/relaxed fish were generated and screened in the Brehm lab.

Physiology

CaP Motor Neuron

Whole cell patch clamp recordings of the CaP primary motor neuron were performed using a Heka EPC 10/2 amplifier (Heka Elektronik, Lambrecht/Pfalz, Germany) as described (Wen and Brehm, 2005, 2010). Briefly, patch pipettes were fashioned with a long narrow shank and small

tip (~1 μm, 12-18 MΩ resistance). Spinal neuron internal solution was used and normally included the Alexafluor-647 hydrazide dye (40 μM) for morphological reconstruction as well as a Ca^{2+} indicator (normally 100 μM). The spinal dura was penetrated under positive pressure and the identified CaP motor neuron was approached. Once the gigaohm seal was achieved, slight negative pressure was sufficient to attain whole cell configuration. Input resistance was generally 180-220 MΩ. In current clamp mode, 2 msec 50 pA current injection steps were applied until an AP was evoked (typically 400-450 pA). Various AP trains were evoked using the appropriate level current injection.

Fast Skeletal Muscle

Whole cell voltage clamp recordings of the fast skeletal muscle were performed using a Heka EPC 10/2 amplifier (Heka Elektronik, Lambrecht/Pfalz, Germany) as described (Wen and Brehm, 2005, 2010). Patch pipettes were fashioned (~3 μm tip, 3-5 MΩ resistance). Spinal neuron internal solution was used and sometimes included the Alexafluor-555 hydrazide dye (40 μM) for morphological reconstruction. For paired recordings, the CaP motor neuron was patched first followed by the innervated fast skeletal muscle. In voltage clamp mode the muscle cell was held at -90 mV to measure end plate currents.

Imaging

Images were acquired with a Stanford Photonics 620 Turbo ICCD camera (Stanford Photonics, Palo Alto, CA) typically with 33msec exposure (30 fps) on a Zeiss Axioskop FS2 Plus with a Zeiss Plan-Apochromat 40x/1.0 W objective (Zeiss, 421462-9900) or Achroplan 63x/0.95 W (Zeiss, 440067-9901). Focal changes in the z-direction were made by a Mipos 100SG piezo device

attached to the objective and controlled by a NV40/1 controller (Piezosystem Jena, Jena, Germany). Resolution with the 40x objective is 286 nm/pixel, resolution with the 63x objective is 185 nm/pixel. Yokogawa CSU-10 spinning disc (Yokogawa Electric Corporation, Tokyo, Japan) was used for confocal imaging with a dichroic beamsplitter (Di01-T404/488/568/647-13x15x0.5, Semrock, Rochester, NY). Excitation at 488nm was produced by a DLS200 argon laser (Dynamic Laser, Salt Lake City, UT), 561nm by a Sapphire 561-50 CW CDRH solid state laser (Coherent, Santa Clara, CA) and 640nm by a Chromalase II diode laser (CLAS2639-040C, Blue Sky Research, Milpitas, CA). Excitation wavelength was controlled by a NEOS AOTF through a Gooch and Housego RF driver (Melbourne, FL) and custom DAC controller (Solamere Technology Group, Salt Lake City, UT). Beams were launched into a single mode fiber optic attached to the spinning disc. Emission filters were arranged in an ASI-1000 filter wheel (ASI Imaging, Eugene, OR). For Ca^{2+} and synaptopHluorin imaging an HQ 535/60 (EM) filter was used, for α-bungarotoxin staining an HQ/605/55 (EM) filter was used, and for morphology an ET 700/75 (EM) filter was used (Chroma Technology Corporation, Bellows Falls, VT). Piper Control 2.5.04 was used for image acquisition (Stanford Photonics, Palo Alto, CA) as was μManager for some synaptopHluorin imaging (NIH, Bethesda, MD). Images were analyzed with ImageJ (NIH, Bethesda, MD). Additional analysis was performed with Microsoft Excel (Microsoft, Redmond, WA) and Igor Pro 6.12 (Wavemetrics, Lake Oswego, OR).

Ca^{2+} Measurements

After whole cell configuration was attained, Ca^{2+} indicator and Alexafluor-647 dye was allowed to dialyze throughout the CaP motor neuron for 10 minutes. Focus was adjusted to image 10-20 synaptic boutons in the field based on the Alexa fill. For lower magnification experiments, effort was made to find an image plane that included preferably the soma, AIS, part of the axon prior

to branching, and synaptic boutons, including branch points. Ca^{2+} signals from boutons were measured with circular ROIs (15 pixel diameter) and were background subtracted with measurements of local background for the duration of the movie. The indicator was excited using the argon laser (488 nm). Typically images were acquired with 33 msec exposures. Slight movement during imaging could normally be compensated for by either registering the stack using the ImageJ plugin, StackReg, or another plugin, Time Series Analyzer 2.0, which automatically makes small X/Y adjustments to the ROI in order to track the center of light within the region. ROI movement was < 3 pixels typically. Image analysis was performed with ImageJ (NIH, Bethesda, Maryland).

SynaptopHluorin Measurements

SynaptopHluorin imaging was performed much in the same way as Ca^{2+} imaging, except that often stacks (typically 10 individual 1 μm steps) were acquired. The stacks were maximally projected offline and subsequently analyzed in a similar manner as the Ca^{2+} measurements. SynaptopHluorin experiments typically included the Alexafluor-647 dye but no Ca^{2+} indicator. SynaptopHluorin fluorescence was excited with the 488 nm argon laser.

Morphological Reconstruction

Neuronal morphology reconstruction was performed with Imaris FilamentTracer software (BitPlane, Zurich, Switzerland). Motor neurons were reconstructed using the images acquired during multiple z-steps through the 50-70 μm volume of the cell. An Alexafluor-647 morphological fill was used to develop this precise reconstruction in three dimensions (Figure 2.1). During Ca^{2+} imaging, acquisition was normally limited to a single z-section in order to

improve temporal resolution. The Ca^{2+} imaging ROIs were matched with the reconstruction of the neuron in order to localize the responses with respect to the overall morphology of the cell. This procedure allowed for accurate measurements to be made from the three dimensional model for individual regions of interest observed in the live imaging experiments. In Figure 2.2 the Alexafluor-647 fill is seen in panel A (same as in Figure 2.1). In addition to the filament reconstruction (Fig. 2.2B, same as Figure 2.1 transparent overlay). The colored filaments (Figure 2.2 C-T) demonstrate progressively more distant locations (from the soma) of ROIs found in the single z-section for the live Ca^{2+} imaging. This is the basis for the distance vs. delay plots to be presented.

Figure 2.1 – The Axon and Field of Synaptic Boutons of a CaP Motor Neuron Reconstructed in Imaris FilamentTracer

The CaP motor neuron is filled with Alexafluor-647 and a stack of images (at 63x) has been acquired and reconstructed offline using the Imaris software. The transparent overlay shows the neuronal tracing manually performed using the FilamentTracer plugin. Place a blank piece of white paper between the transparent overlay and Figure 2.1 to best visualize the reconstructed filament.

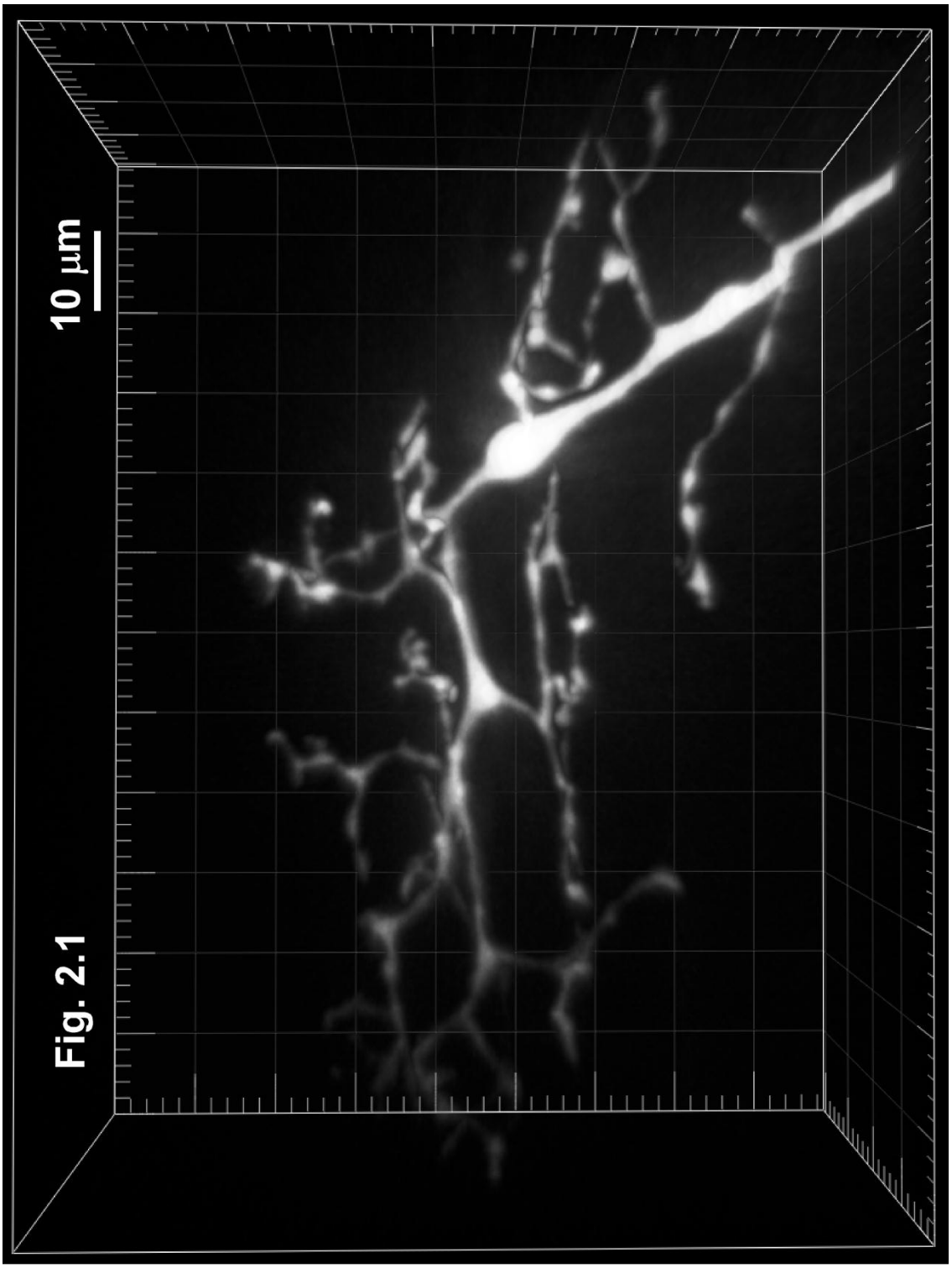

Fig. 2.1

Figure 2.2 – Distance Measurements Throughout the CaP Axon

(A) The same CaP motor neuron as in Fig. 2.1 filled with Alexafluor-647. (B) The traced neuron as seen in the transparent overlay from Fig. 2.1. (C-T) The colored filaments are used to measure distances that correspond to ROIs chosen from the single focal plane Ca^{2+} imaging.

Fig. 2.2

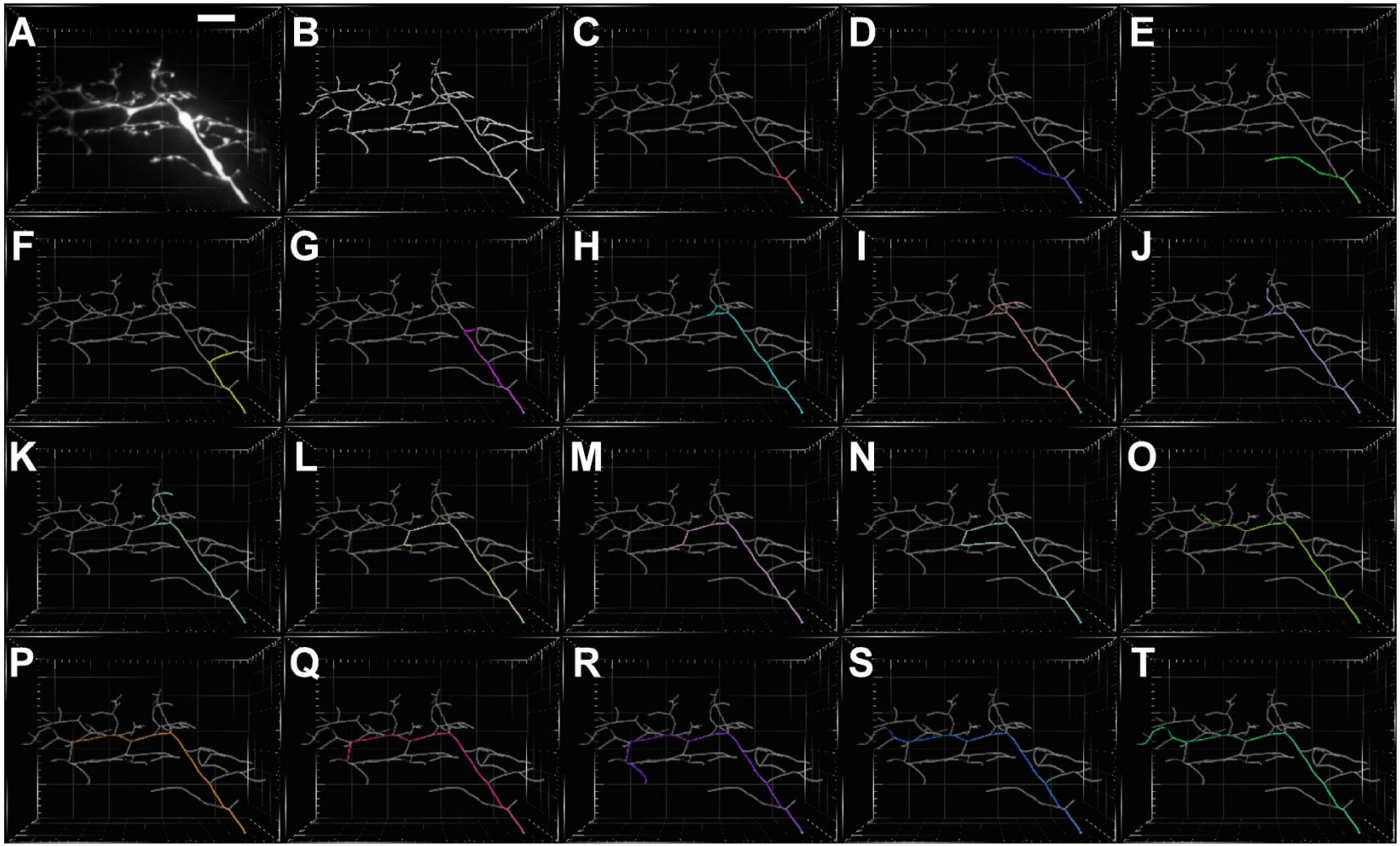

Chapter 3: Zebrafish Model System

Body Plan and Innervation

Zebrafish (*Danio rerio*) has gained traction as a useful model system for the study of synapse development and function in the last 20 years . Somatogenesis begins within the first 24 hours after fertilization, and myocytes in each individual segment (dorsal and ventral) receive innervation from one of three primary motor neurons (CaP-caudal primary motor neuron, MiP-medial primary motor neuron, and RoP-rostral primary motor neuron) emanating from the ventral root (CaP motor neuron, Fig. 3.1). Numerous secondary motor neurons are also present but their axonal branching and neuromuscular synapses are less extensive than that of the three primary motor neurons. This pattern is repeated for each segment down the trunk of the fish, and by day three of development functional neuromuscular synapses are present and complex survival behaviors are possible, such as the escape response.

At day 3-4 of development (72-96 hours post fertilization, hpf), 1-2 layers of superficial slow skeletal muscle are present beneath the skin (Fig. 3.2A and B) which are highly electrically coupled to one another via gap junctions (Luna and Brehm, 2006). Below the slow muscle fibers lie the layers of fast skeletal muscle (Fig. 3.2B and C) which have little gap junctional coupling (Luna and Brehm, 2006). Each wedge shaped segment, or chevron, of the trunk is separated by connective tissue at the myocommata. The three primary motor neurons in each segment innervate a non-overlapping field of muscle fibers in a characteristic fashion. Multiple fast skeletal muscle fibers are innervated by an individual primary motor neuron which forms *en passant* type synapses reminiscent of those found in the CNS, however on a larger scale. The CaP motor neuron, our primary cell of study, is situated medially in the spinal cord near the

myoseptum. Its axon projects caudally as it exits the ventral nerve root, bundled with the axons from the MiP and RoP motor neurons as well as axons of secondary motor neurons (Fig. 3.1). As the axon continues ventrally, it arches over the notochord across the midline. The axonal branching begins approximately 100-150 microns from the soma and tends to originate from deep layers of muscle projecting superficially. Along the primary branch of the axon we find that the diameter of the axon can widen substantially, but it is unclear what these enlargements represent. Myelination of motor neuron axons is thought to occur by 72 hpf for the primary axon branches and extend to the terminals by 96 hpf (Kucenas et al., 2008).

Axonal varicosities and branch points are almost invariably associated with juxtaposed ACh receptors (Fig. 3.3, 86% N = 65 from 9 fish, and 96% N = 24 from 9 fish respectively) as evidenced by fluorescent conjugated alpha-bungarotoxin (α-Btx) staining. This is a good indication that these structures are indeed synapses. Confocal imaging shows that the postsynaptic receptors form a cup like structure around the presynaptic boutons. Using structured illumination to gain better resolution we observe the pretzel-like structure (Mike Linhoff, personal communication) which has previously been described at the mammalian NMJ (Sanes and Lichtman, 2001). In contrast the axon initial segment never shows α-Btx staining (Fig. 3.3, 0%, N = 9 from 9 fish). The receptor juxtaposition with boutons, branch points and the AIS was visualized using the Imaris software. Receptor clusters were assessed by eye to determine if they were associated with these specific regions on the motor neuron. The regions analyzed correspond to ROIs that were chosen from Ca^{2+} imaging movies. The percentage of ROIs associated with receptor for each group (boutons, branch points and AIS) was then calculated. Prior to branching, large amorphous clusters of receptor can be seen near the axon. These clusters likely represent the early stage postsynaptic receptors located centrally on muscle fibers thought to help guide the growing axon as it travels ventrally (Beattie, 2000;

Hutson and Chien, 2002; Panzer et al., 2006). The myocommata also stain heavily with fluorescently tagged α-Btx, which appear to be innervated by both primary and secondary motor neurons.

Physiology

For studying synaptic physiology, zebrafish NMJ offers a number of unique opportunities. Accessibility to the spinal cord in early stage intact zebrafish is relatively easy and the primary motor neurons are readily identifiable and amenable to the patch clamp technique. Given the non-overlapping nature of primary motor neuron innervation, one knows that the CaP motor neuron will always be found to synapse onto approximately two-thirds of the ventral fast muscle (Fig. 3.1), which makes finding paired motor neuron and target fast skeletal muscle nearly certain. A key feature is that the myocytes are small and isopotential, lending themselves to voltage-clamp technique. Thus, the zebrafish preparation is the only vertebrate which allows one to perform paired patch clamp recordings of motor neuron and target muscle voltage clamp in an intact animal (Wen and Brehm, 2005).

Physiological characteristics of this synapse are ideally suited for the study of synchronous and asynchronous vesicle release for several reasons. First, unlike many CNS synapses, the release probability is very close to "1" (Wen et al., 2010). In addition, as a cholinergic synapse, the decay kinetics are fast, making quantal analysis easier and techniques such as deconvolution unnecessary (Neher and Sakaba, 2001, 2003; Wen and Brehm, 2005; Wen et al., 2010). Quantal size is approximately 0.5 nA and the quantal content is around 10 (Wen et al., 2010). This combination of high release probability, fast kinetics, large quantal size and small quantal content makes it possible to precisely parse release into vesicles that fuse synchronously (within the time window of the known synaptic delay and the rise and decay of

the synaptic current, 1.5 msec) and those that fuse asynchronously, occurring either before or after this narrow window of time. During low frequency stimulation (i.e. 0.2 or 1 Hz) all release is synchronous. However, during high frequency trains, several forms of synaptic plasticity manifest and asynchronous release can account for over 50% of the total as the balance shifts from an initially synchronous mode to a primarily asynchronous mode of transmission (Wen et al., 2010). APs can follow frequencies as high as 500 Hz and during 100 Hz stimulation EPC failures rarely occur until after at least 5 seconds (Hua Wen personal communication and see chapter 4). A 10 second train of such tetanic stimuli can effectively depress all EPCs in most experiments, presumably due to vesicle depletion (see chapter 4). Recovery time from this type of exhaustive stimulation is rather slow (approximately 10% after 40 seconds, Hua Wen personal communication).

The paired recording paradigm has become a major driver of research in the Brehm lab. In addition to providing an excellent means to examine forms of release and plasticity, the technique also allows for straight forward testing of potentially interesting mutants which have particular defects in neuromuscular transmission. Forward genetics in zebrafish is a powerful, unbiased approach for understanding both pre and postsynaptic protein function and the paired recordings have been instrumental for many of the studies on these novel mutants. In terms of the present work, findings based on the pharmacology of Ca^{2+} influx from paired recordings was the impetus to develop Ca^{2+} imaging of the NMJ in our lab.

Imaging

Given that development occurs externally and the embryos are transparent, zebrafish has become a popular system for imaging studies. Immunofluorescence staining of fixed tissue is commonplace and FM dyes have been used to observe vesicle dynamics at the NMJ (Li et al.,

2003). Recently, genetically encoded Ca^{2+} indicators, optogenetics, and live imaging in partially restrained animals have been employed to explore the intrinsic circuitry underlying various swimming behaviors (Ahrens et al., 2012; Muto et al., 2011; Ritter et al., 2001; Wyart et al., 2009). For the most part, these studies have relied on the bulk loading of fluorescent dyes (such as Ca^{2+} indicators, dyes for morphological analysis or FM dyes) or the expression of genetically encoded indicators which is not limited to an isolated cell or even a single cell type.

During my time in the Brehm lab I have utilized bulk loading of FM dyes and a transgenic line expressing a pH dependent version of GFP fused to the vesicular SNARE protein, VAMP, called synaptopHluorin to monitor exo and endocytosis optically. In the initial experiments with FM dyes, motor neurons were stimulated extracellularly and live imaging was performed with a spinning disc confocal microscope. However, in order to better correlate imaging data with the paired recordings we turned to patch clamp of the CaP motor neuron. Given that synaptopHluorin is capable of tracking both exo and endocytosis and no dye loading protocols are necessary, it became the system of choice for optical recordings of vesicle dynamics. Both techniques show similar kinetics for exocytosis during a 100 Hz 10 second stimulation protocol, and the fluorescence change observed for synaptopHluorin over that 10 second period mirrors the cumulative charge from paired recordings nicely.

Introducing a fluorescent dye, such as Alexa-647 hydrazide, via the patch the pipette into the CaP neuron allows for precise morphological reconstruction in three dimensions (Fig. 2.1). At day three, a CaP motor neuron is roughly 200-250 μm long, depending on which segment it is in. In the z-direction a typical CaP neuron travels within an approximately 50-60 μm volume. When laid out flat and pinned to the bottom of the chamber, the soma and axon initial segment lie in the same plane as parts of the main axon branch and the axonal arbor,

including many boutons in most cases. This fortuitous orientation allows for live imaging of several subcellular compartments simultaneously at high temporal resolution. In addition, with the proper magnification the entire length of the neuron can be captured within the imaging field (Fig. 3.1).

Recently, Ca^{2+} imaging has become a focus of our studies. Again, by dialyzing the CaP neuron with fluorescent Ca^{2+} indicators (Oregon Green BAPTA-1, Fluo-4, Fluo-5F, Fluo-4FF, and Oregon Green BAPTA-1 dextran have been used to date) through the patch electrode, signal is limited to the neuron of interest. Excellent signal to noise is achieved using this approach and generally Fluo-4 and Fluo-5F have been the indicators of choice due to their large dynamic range and low basal fluorescence. In general, these various imaging approaches have been a wonderful compliment to the power of the paired recordings where the quantification of vesicle release characteristics is unmatched. I will show in the following chapters that the ability to localize vesicle release, monitor the Ca^{2+} dynamics underlying transmission, and model the structure of the motor neuron through imaging have also provided valuable insights. By applying both techniques, either individually or more recently simultaneously, we find a novel mechanism by which asynchronous vesicle release can arise and a surprising result regarding a key mediator of synchronous release at the zebrafish NMJ.

Figure 3.1 – Entire CaP Motor Neuron Reconstructed in Imaris

Using the Alexafluor-647 dye fill, the motor neuron morphology is constructed from soma to most distal terminals. (A-E) Rotating view of the neuron demonstrates the path of the axon as it exits the spinal cord and arches over the notochord. A field of ventral fast skeletal muscle is in innervated by the arborized axon, en passant synapses, and synaptic terminals. R is rostral, C is caudal, V is ventral and D is dorsal. Scale bar is 20 μm.

Fig. 3.1

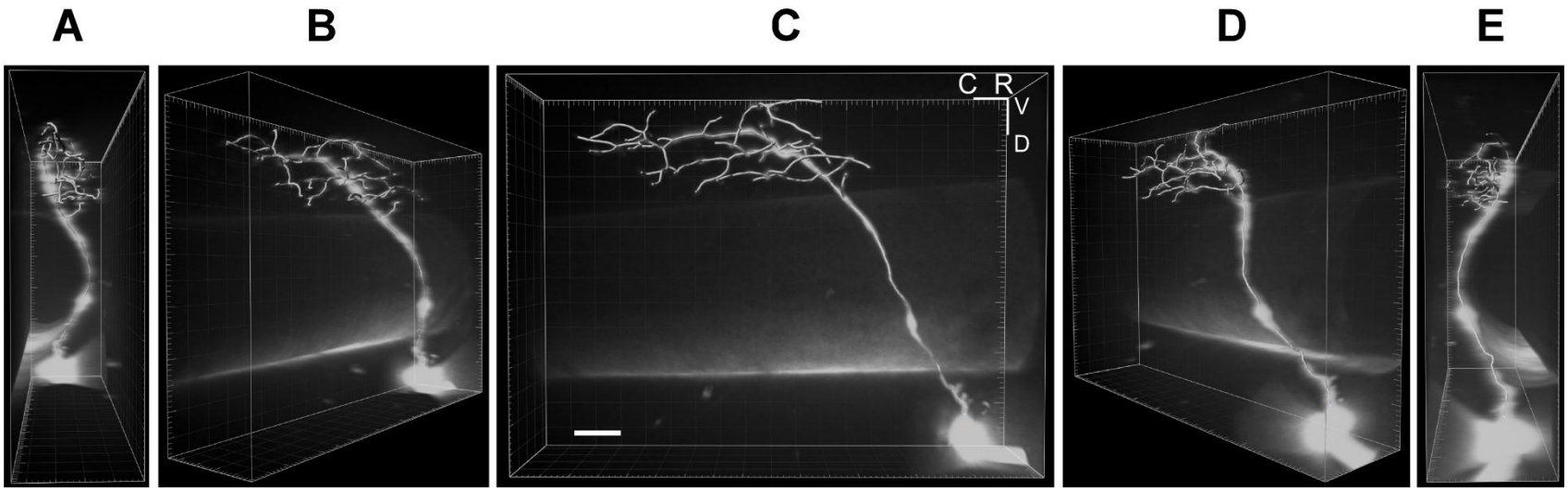

Figure 3.2 – Zebrafish Fast and Slow Muscle

Whole mount zebrafish stained with a slow myosin marker, F59-647 (green), labeling the slow skeletal muscle layer and phalloidin-555 to label fast skeletal muscle cells (courtesy of Michael Linhoff). (A) One to two superficial layers of slow muscle (green) run longitudinally between the myocommata of each segment. (B) Angled view to demonstrate the segregation of fast and slow muscle layers. (C) Fast skeletal muscle (red) is targeted by primary motor neurons. R is rostral, C is caudal, V is ventral and D is dorsal. Scale bar is 50 μm.

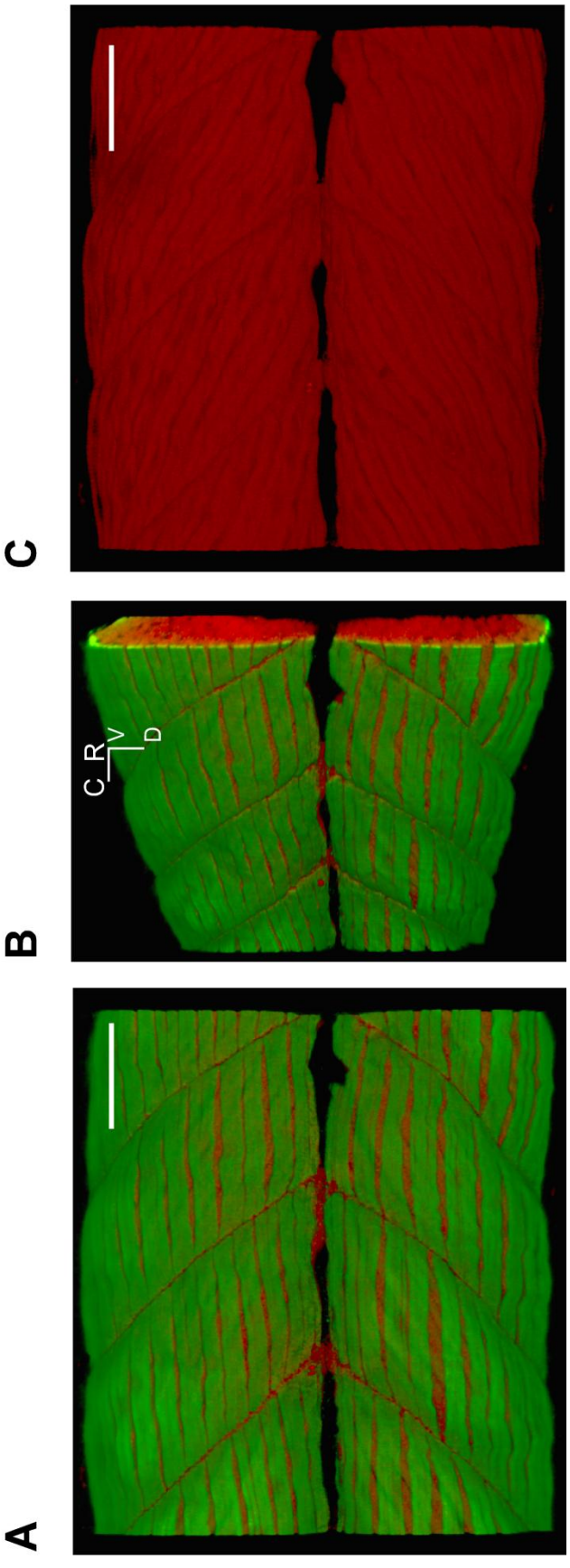

Fig. 3.2

Figure 3.3 – CaP Motor Neuron and the AChRs

(A) The CaP neuron is patched and filled with Alexafluor-647 (green). (B) AChRs are labeled with Alexafluor-555 conjugated α-Btx (red). (C) Overlay of panel A and B. Scale bar = 10 μm.

Fig. 3.3

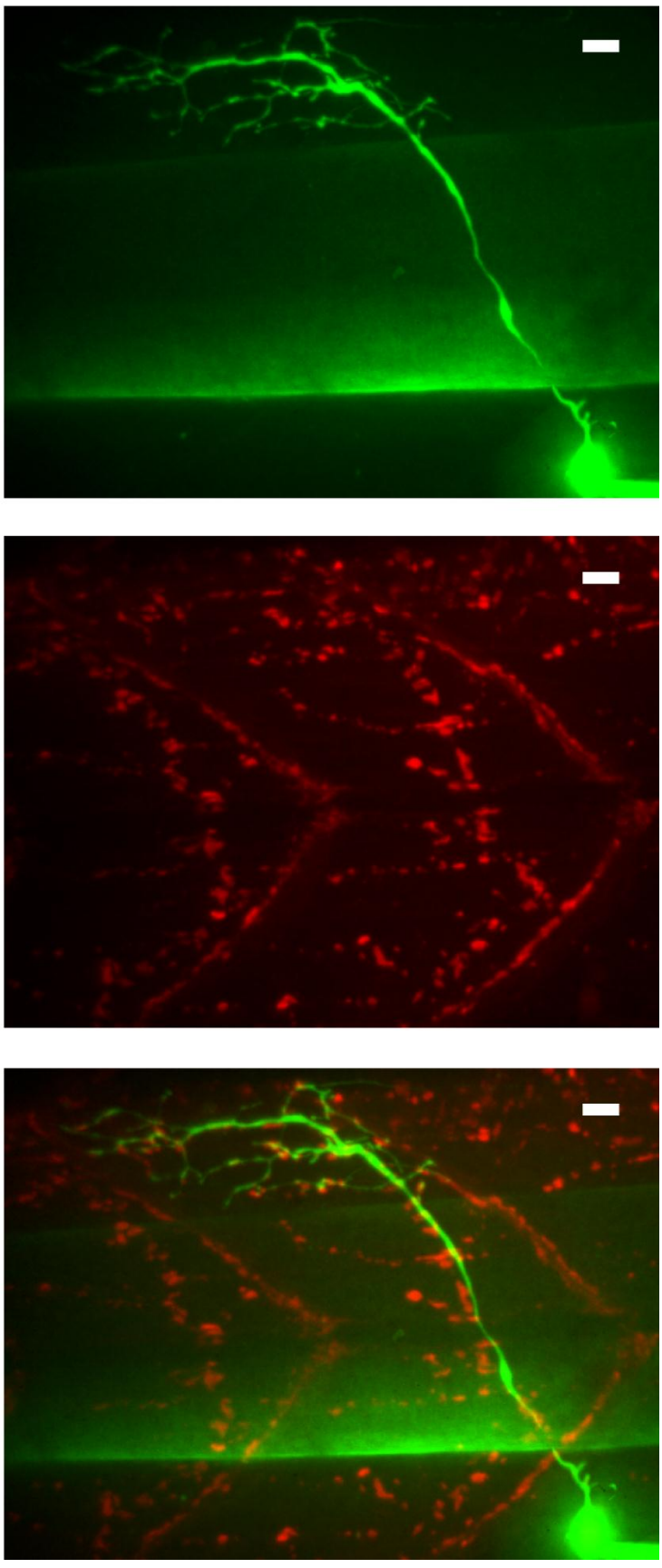

Chapter 4: Synchronous Release

Our method for investigating synchronous release at the NMJ relies fundamentally on two approaches, pharmacology and forward genetics. Paired recordings from the CaP motor neuron and the target fast skeletal muscle were made on 72-96 hpf zebrafish. In current clamp mode, the motor neuron was held at -80 mV and positive current (typically 400-450 pA) was injected for 2 msec to evoke an action potential. The innervated muscle cell was held at -50 mV in whole cell voltage clamp mode in order to inactivate sodium channels. During low frequency stimulation (0.2 Hz), EPCs are entirely synchronous with the motor neuron AP and this is also true during the first second of high frequency stimulation (Wen and Brehm, 2005; Wen et al., 2010). An example of 10 APs and associated EPCs from a 100Hz train in an untreated wild type fish is shown in Figure 4.1A. Given that the mean quantal size is approximately 500 pA (Wen and Brehm, 2005), then the quantal content for the first evoked response would correspond to roughly 12 vesicles (Fig. 4.1A). Quantal content is smaller for the subsequent stimuli but remains synchronized with the following 9 APs. In an effort to determine the identity of the Ca^{2+} channel responsible for synchronous vesicle release we first applied 1μM ω-conotoxin GVIA, a toxin that is generally considered to be highly specific for N-type VGCCs. Treatment with GVIA completely abolished synchronous transmitter release, arguing that an ω-conotoxin GVIA sensitive VGCC mediates the Ca^{2+} influx necessary for release tightly coupled to the invading AP (Fig. 4.2B).

The second approach used to assess synchronous release was a product of the fortuitous identification of a mutant zebrafish called *tb204a*. Originally identified in a large scale genetic screen, *tb204a* has a reduced locomotion phenotype in response to touch (Granato et

al., 1996). In paired patch clamp recordings, *tb204a* embryos lack almost all synchronous release (Fig. 4.1C, courtesy of Hua Wen). When compared to wild type fish, total release is dramatically decreased in *tb204a* mutants, as evidenced by the cumulative charge of EPCs during a 1 second 100 Hz stimulus train. Total release in wild type is 302 ± 140 pC (N = 15) whereas *tb204a* -/- homozygotes only achieve 33.2 ± 18 pC (N = 9, Fig. 4.2A, courtesy of Hua Wen). Some release is observed in *tb204a* as opposed to wild type fish treated with ω-conotoxin GVIA (wild type = 0 ± 0 pC, N = 3, Fig. 4.2B, courtesy of Hua Wen).

Calcium imaging of synaptic terminals in both wild type and *tb204a* fish points to significantly reduced Ca^{2+} influx in mutant boutons. CaP motor neurons were patched and dialyzed with Fluo-5F Ca^{2+} indicator and an Alexafluor-647 fill. Synaptic terminals were imaged as the neuron was stimulated at 100 Hz for 100 msec. Average fluorescence increase for wild type boutons was approximately 4% Δ G/R (Fig. 4.3A, black trace). All boutons responded with an increase in fluorescence during the 10 APs, however measurements of the peak responses from individual boutons were not homogeneous (Δ G/R = 4.4 ± 0.33 %, Fig. 4.3B, black circles). Ca^{2+} influx for *tb204a* boutons was severely attenuated, with an average increase of 1% Δ G/R (Fig. 4.3A, red trace). Peak responses for individual boutons were similarly decreased, and in many cases difficult to differentiate from the noise in the recording (Δ G/R = 1.5 ± 0.11 %, Fig. 4.3B, red squares). These results suggest that the *tb204a* mutation imparts a specific defect on Ca^{2+} influx rather than a fault in exocytosis machinery. Positional cloning of *tb204a* has confirmed a point mutation (Y1662N) near S6 of domain IV on the intracellular side of a P/Q-type Ca^{2+} channel (Wen et al., submitted).

Aside from paired recordings as an assay to quantify vesicle release, optical tools can also be useful in determining where exocytosis is occurring. In our hands, synaptopHluorin

imaging is not sufficiently sensitive to track individual fusion events, however short trains of high frequency stimulation can provide suitable signal to noise for analysis. An example of a synaptopHluorin experiment is shown in Fig. 4.4. Here the CaP motor neuron is patched and dialyzed with the Alexa fill and stimulated for 1 second at 100 Hz. Images are maximal intensity projections obtained from 10 individual 1μm z-sections. SynaptopHluorin fluorescence signal is seen on the plasma membrane prior to stimulation (Fig. 4.4A), and increases in a stimulus dependent manner (Fig. 4.4B). The increase in fluorescence is particularly evident at varicosities and branch points, which can be visualized by subtracting a pre-stimulus image from the post-stimulus image (Fig. 4.4C). This was done by averaging 10 consecutive images prior to the stimulus and 10 consecutive images after the stimulation and subsequently subtracting the pre-stimulus image from the post-stimulus image using ImageJ. To demonstrate these synaptopHluorin hot spots, the subtracted image from Fig. 4.4C is false colored green in Fig. 4.4D, the morphological fill is false colored red in Fig. 4.4E and the overlay is seen in Fig. 4.4F. Three sample regions of interest were chosen for this cell (Fig. 4.5A, red, green and blue circles) and the corresponding fluorescence responses are shown in Fig. 4.5B (red, green and blue traces). Because multiple z-sections were acquired during the experiment the overall temporal resolution is poor (1.3 sec/frame, 1 frame=10 1μm z-sections). Despite this limitation, when multiple regions from multiple cells are analyzed, the 1 second 100 Hz stimulation generates an average fluorescence increase of 19.3 ± 3.7 % (N = 53 boutons from 5 cells, Fig. 4.5C). Fitting the synaptopHluorin relaxation back to baseline with a single exponential approximates the rate of endocytosis (τ=37 seconds, Fig. 4.5C red trace). Paired recordings show that 300-400 vesicles are released onto a single fiber during this stimulus regimen (Hua Wen, personal communication).

During longer bouts of high frequency stimulation there is a shift from solely synchronous release to asynchronous release (Fig. 4.6A). These transitions are shown in detail by the 100 msec snippets labeled "1" (synchronous, Fig. 4.6B) and "2" (asynchronous, Fig. 4.6C). The CaP motor neuron is able to faithfully fire APs at 100 Hz for extended periods of time, but a 20 second train will cause eventual EPC failures (Fig. 4.6C). SynaptopHluorin measurements of boutons in response to a 10 second 100 Hz stimulus show a robust fluorescence increase (ΔF = 124.3 ± 13.1 %, N = 89 boutons from 5 cells) which slowly relaxes to baseline (τ = 242 seconds, Fig. 4.7A). However, even with extended stimulation, a significant fraction of vesicles do not undergo release in some boutons. When 50 mM NH_4Cl is applied to the neuron, the entire synaptopHluorin pool is revealed due to the alkylinization of previously acidified vesicles causing the unquenching of the fluorophore, GFP. This procedure was done following the 10 second 100 Hz protocol to see the fraction of the total pool that is released by the AP train. Overall, boutons on average released approximately 50% of the total pool (Fig. 4.7B, N = 56 boutons from 4 cells). When the fractional release from individual boutons is parsed out and binned, we find that there exists a broad range of release profiles, meaning that some terminals release only 20% of the total synaptopHluorin pool while others will release their full complement of vesicles (Fig. 4.7C).

Calcium imaging was performed for the 10 second 100 Hz protocol as well. A wild type CaP motor neuron was patched and Fluo-5F Ca^{2+} indicator as well as the Alexa-647 fill were allowed to diffuse throughout the cell for 10 minutes. Figure 4.8A presents the morphology of the entire neuron and the Imaris FilamentTracer reconstruction. In addition, four ROIs are marked, a blue region at the AIS, and three regions on the axonal arbor at progressively more distal synaptic boutons (red, green and orange, Fig. 4.8A). A series of timepoints (pre-stimulus, 1, 2, 3, and 4 seconds) from the Ca^{2+} imaging are shown in Fig. 4.8B. These images are taken in a

single focal plane at video rate (30 fps) and the increased Ca^{2+} fluorescence is apparent rapidly throughout the motor neuron (Fig. 4.8B). Traces of the fluorescence change induced by the AP train are shown in Fig. 4.8C for each colored ROI. Responses from individual boutons and the AIS were background subtracted and normalized to their peak fluorescence to facilitate the direct comparison of the timing of Ca^{2+} rise. The time to reach 20% of the maximal fluorescence was fast regardless of the location of the ROI in relation to the motor neuron soma (Fig. 4.8D, colored circles correspond to ROIs of the respective color). This would be expected, particularly for responses in the terminals given that the VGCC opening is dependent on the arrival of the AP which travels significantly faster than our acquisition rate. Cumulative data is plotted and individual ROIs from all cells were binned by their distance from the soma (25 μm bins, Fig. 4.9). All regions reached the 20% level on average within 500 msec.

Figure 4.1 – Synchronous Release is Mediated by a ω-conotoxin GVIA Sensitive Channel

Paired motor neuron and target fast skeletal muscle recordings. Top, black traces, are APs from CaP motor neurons in current clamp mode stimulated by 2 msec current injections at 100 Hz for 100 msec. Bottom, red traces, are whole cell patch clamp recordings of EPCs from muscle fibers innervated by the CaP neuron in voltage clamp mode (-50 mV holding potential). (A) Paired recording from a wild type motor neuron and muscle cell. Evoked EPCs respond to CaP APs without fail and variable amplitude. (B) Paired recording from a wild type motor neuron and muscle cell treated with 1 μM ω-conotoxin GVIA. Synchronous EPCs are never observed in this condition. (C) Paired recording from a *tb204a* motor neuron and muscle cell. Some small synchronous EPCs are evoked by the CaP APs in addition to many failures (panel C courtesy of Hua Wen).

Fig. 4.1

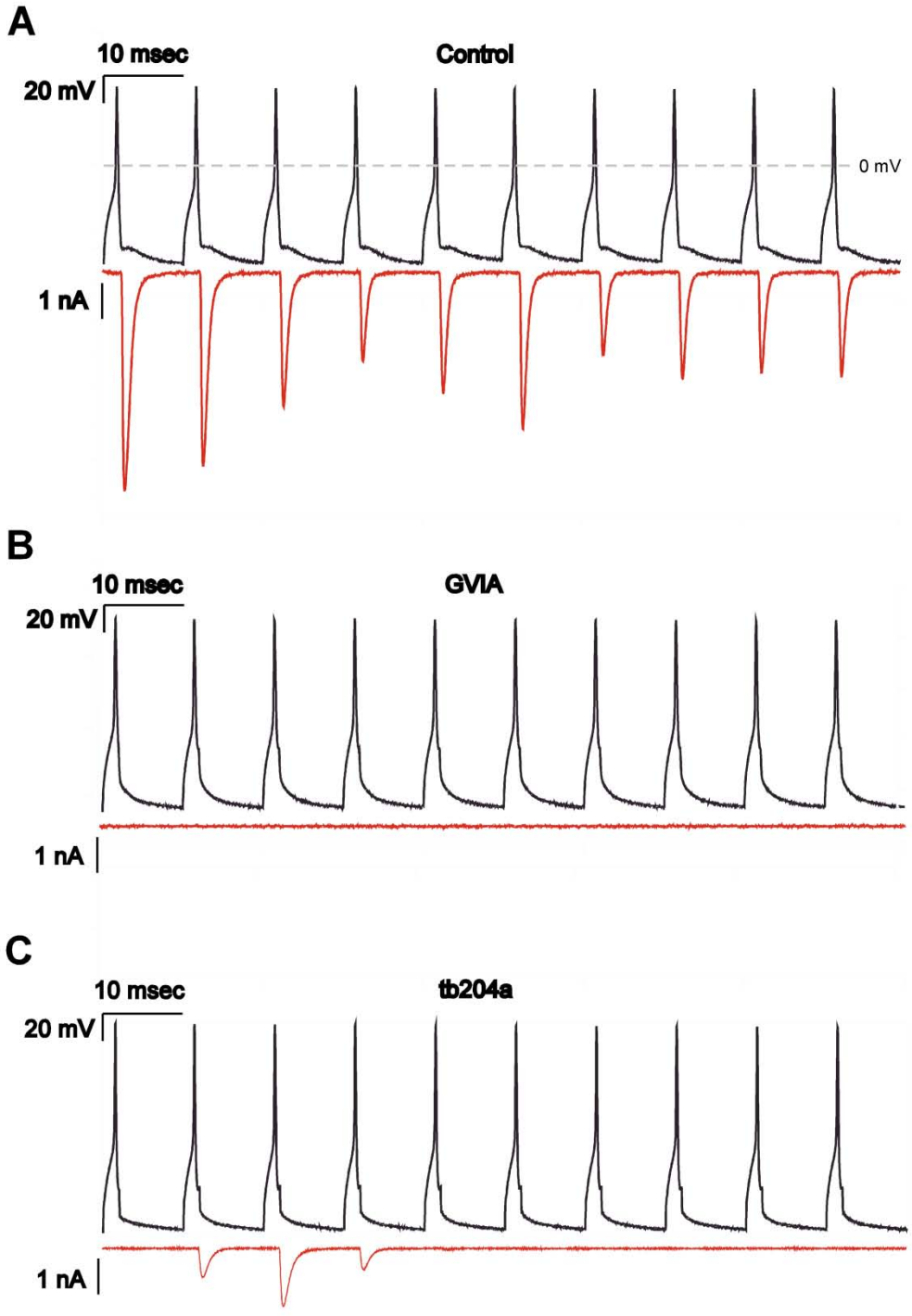
A
10 msec
Control
20 mV
0 mV
1 nA
B
10 msec
GVIA
20 mV
1 nA
C
10 msec
tb204a
20 mV
1 nA

Figure 4.2 – Total Release in Both ω-conotoxin GVIA Treated Wild Type and *tb204a* CaP Motor Neurons is Severely Attenuated

Paired recordings of motor neuron and muscle cells during 1 second 100 Hz stimulation. Scatterplots of individual experiments comparing wild type and *tb204a* release measured as cumulative charge. (A) Wild type cumulative charge (302 ± 140 pC, N = 15) compared to *tb204a* (33.2 ± 18 pC, N = 9, courtesy of Hua Wen). (B) Comparison of total charge from *tb204a* (same as in A) and wild type treated with 1 μM ω-conotoxin GVIA (0 ± 0 pC, N = 3, courtesy of Hua Wen). Data are shown as mean ± S.D. and *** indicates $P < 0.001$.

Fig. 4.2

A

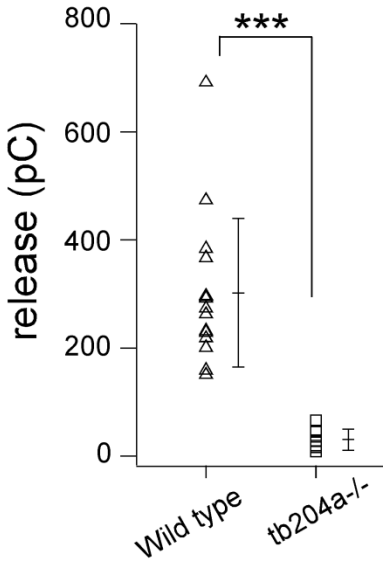
800
600
400
200
0
release (pC)
***
Wild type
tb204a-/-

B

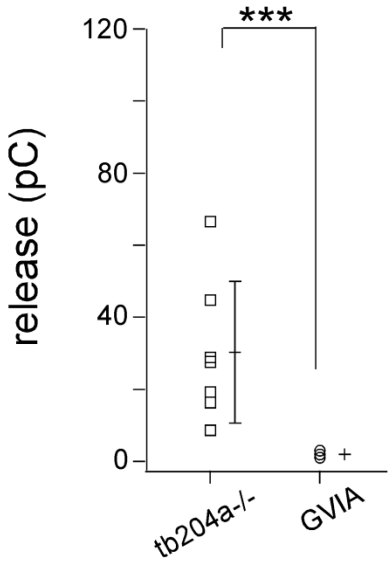
120
80
40
0
release (pC)
***
tb204a-/-
GVIA

Figure 4.3 – Synaptic Boutons From *tb204a* Mutants Show Reduced Calcium Influx as Compared to Wild Type

Calcium imaging of Fluo-5F (100 μM) fluorescence responses in during a 100 msec 100 Hz stimulus train. CaP motor neurons were co-labeled with Alexafluor-647 (40 μM) for visualization and normalization. (A) Average responses from wild type (black trace) and *tb204a* (red trace) synaptic boutons. (B) Scatterplots of the peak Ca^{2+} response from synaptic boutons of wild type (Δ G/R = 4.4 ± 0.33 %, black circles, N = 52 boutons from 4 cells) and *tb204a* (Δ G/R = 1.5 ± 0.11 %, red squares, N = 59 boutons from 4 cells) motor neurons. Data are presented as the ratio of G/R and are shown as mean ± S.E.M. and *** indicates $P < 0.001$.

Fig. 4.3

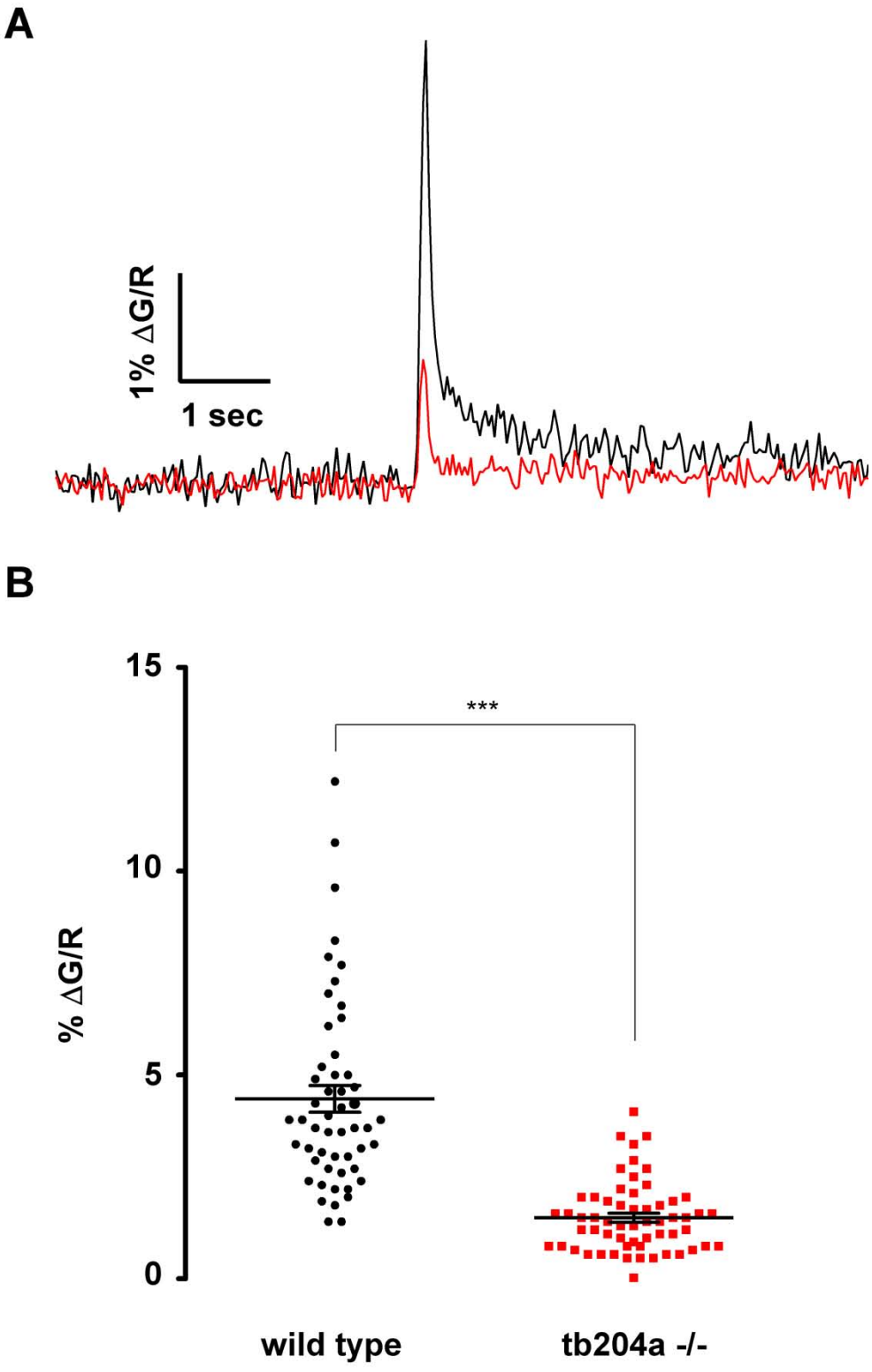

Figure 4.4 – SynaptopHluorin Reveals Vesicle Release at Synaptic Terminals of the CaP Motor Neuron

The example CaP motor neuron was stimulated for 1 second at 100 Hz. (A) SynaptopHluorin fluorescence (average of 10 images taken at 33 msec exposure) prior to the beginning of the stimulus train. (B) SynaptopHluorin fluorescence (average of 10 images taken at 33 msec exposure) following the 1 second train of APs. (C) A difference image of the average post-stimulation fluorescence (panel B) subtracted by the average pre-stimulus fluorescence (panel A), showing the boutons in which release occurred. (D) A green false colored image of C. (E) The Alexafluor-647 fill of the CaP motor neuron false colored in red. (F) Overlay of D and E showing where release occurs in relation to the axonal morphology. Varicosities throughout the image appear to be "hot spots" for vesicle release. Images are all maximal intensity projections of 10 z-sections taken in 1 μm steps. Calibration bar is 10 μm.

Fig. 4.4

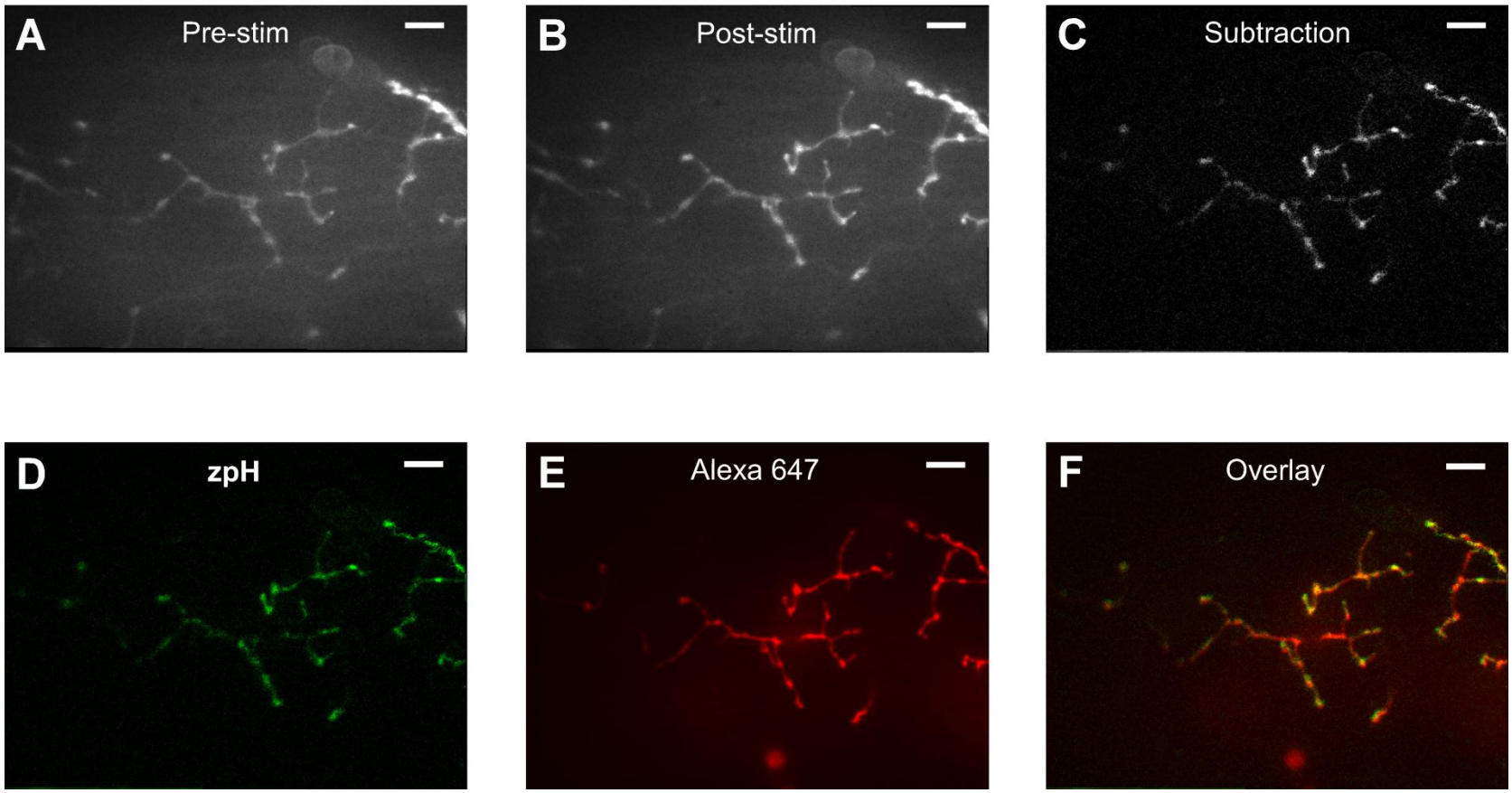
A
Pre-stim
B
Post-stim
C
Subtraction
D
zpH
E
Alexa 647
F
Overlay

Figure 4.5 – SynaptopHluorin Imaging Tracks Exo and Endocytosis at CaP Motor Neuron Synaptic Terminals

Imaging analysis of the motor neuron presented in Figure 4.4 and cumulative data from similar experiments using the 1 second 100 Hz stimulus protocol after a 30 second baseline. (A) The synaptopHluorin difference image from Figure 4.4C with three colored sample ROIs placed on synaptic boutons. (B) Change in synaptopHluorin fluorescence for the sample ROIs, with the colored circles in A corresponding to the colored traces in B. Responses were background subtracted and divided by the average pre-stimulation fluorescence ($\Delta F/F_0$) . (C) Average synaptopHluorin response from individual experiments on 5 different cells (N = 51 boutons) ± S.E.M. Multiple z-sections were acquired therefore each time point reflects the time needed to move the objective with the piezo device and take an image (1.3 seconds for the 10μm stack). The endocytosis phase was fit with a single exponential with a τ=37 seconds. Responses in panel C were normalized to the first time point after background subtraction.

Fig. 4.5

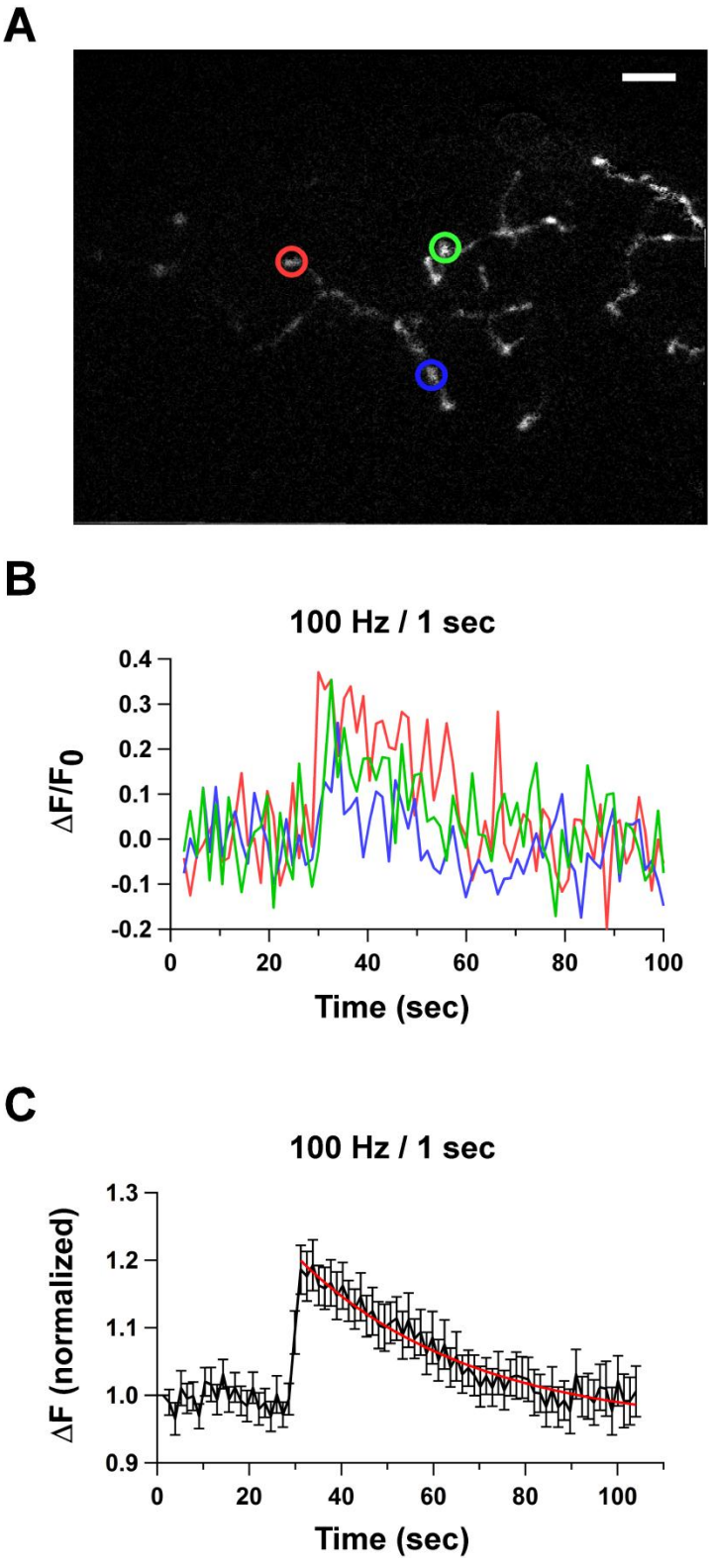
A
B
100 Hz / 1 sec
ΔF/F0
0.4
0.3
0.2
0.1
0.0
-0.1
-0.2
0
20
40
60
80
100
Time (sec)
C
100 Hz / 1 sec
ΔF (normalized)
1.3
1.2
1.1
1.0
0.9
0
20
40
60
80
100
Time (sec)

Figure 4.6 – High Frequency Stimulation for Long Durations Causes a Transition From Synchronous to Asynchronous Release

Paired motor neuron target muscle recording. (A) APs from a CaP motor neuron in current clamp mode (top, black trace) evoked by 2 msec current injections at 100 Hz for 20 seconds. Whole cell patch clamp recordings of EPCs from a muscle fiber innervated by the CaP neuron in voltage clamp mode (bottom, red trace, -50 mV holding potential). Exploded 100 msec snippets are shown labeled as 1-3. (B) #1 corresponds to the 1st 100 msec of stimulation. The expanded view shows the EPCs are entirely synchronized with the APs. (C) The 2nd set of traces (#2) is 100 msec of APs and EPCs occurring 3 seconds into the stimulation. At this point there is a mixture of synchronous and asynchronous release. (C) The 3rd set of traces (#3) is 100 msec of APs and EPCs occurring 10 seconds into the stimulus train. At this stage of the stimulus many EPC failures occur.

Fig. 4.6

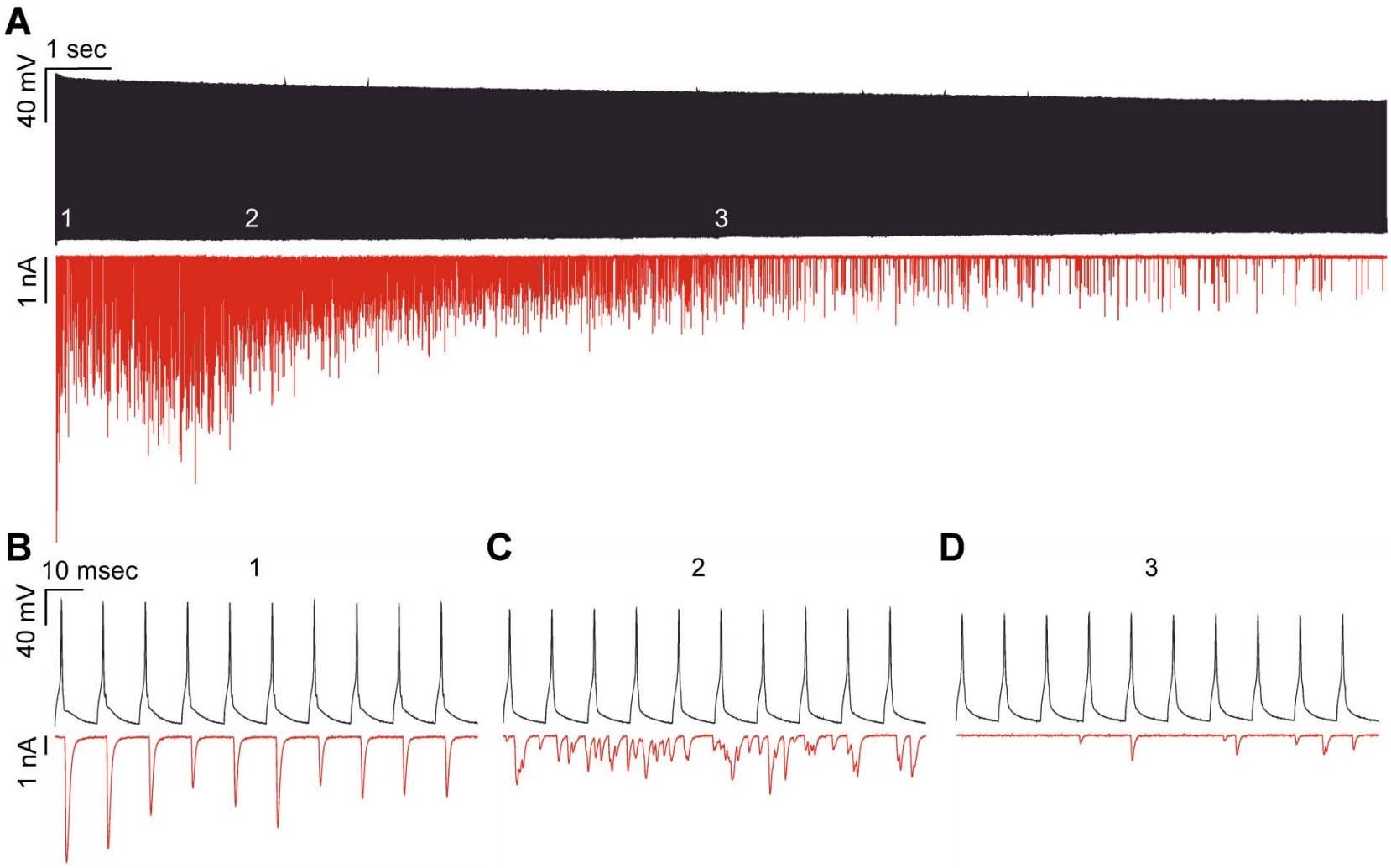

Figure 4.7 – SynaptopHluorin Responses During High Frequency Stimulation are Immediate But Not Homogeneous

CaP motor neurons from synaptopHluorin transgenic fish were patched clamped and APs were stimulated at 100 Hz for 10 seconds in current clamp mode. SynaptopHluorin fluorescence responses were measured for individual boutons and normalized to the first time point. (A) Average fluorescence change in response to the 10 second 100 Hz stimulation (black arrow, N = 89 boutons from 5 cells). (B) Average fluorescence change in response to the 10 second 100 Hz stimulation (black arrow), followed by application of 50 mM NH_4Cl to reveal the total synaptopHluorin pool (N = 56 boutons from 4 cells). ROIs in B were not background subtracted because of the temporary effect of the solution exchange on background fluorescence. (C) The fraction of the total pool of vesicles released by the stimulus train was determined for individual boutons. To determine the percentage of vesicles released, the peak of the stimulus evoked response was divided by the NH_4Cl elicited fluorescence. Bouton responses were binned according to the fraction of vesicles released (bin width = 10%) and plotted as a histogram (N = 56 boutons from 4 cells).

Fig. 4.7

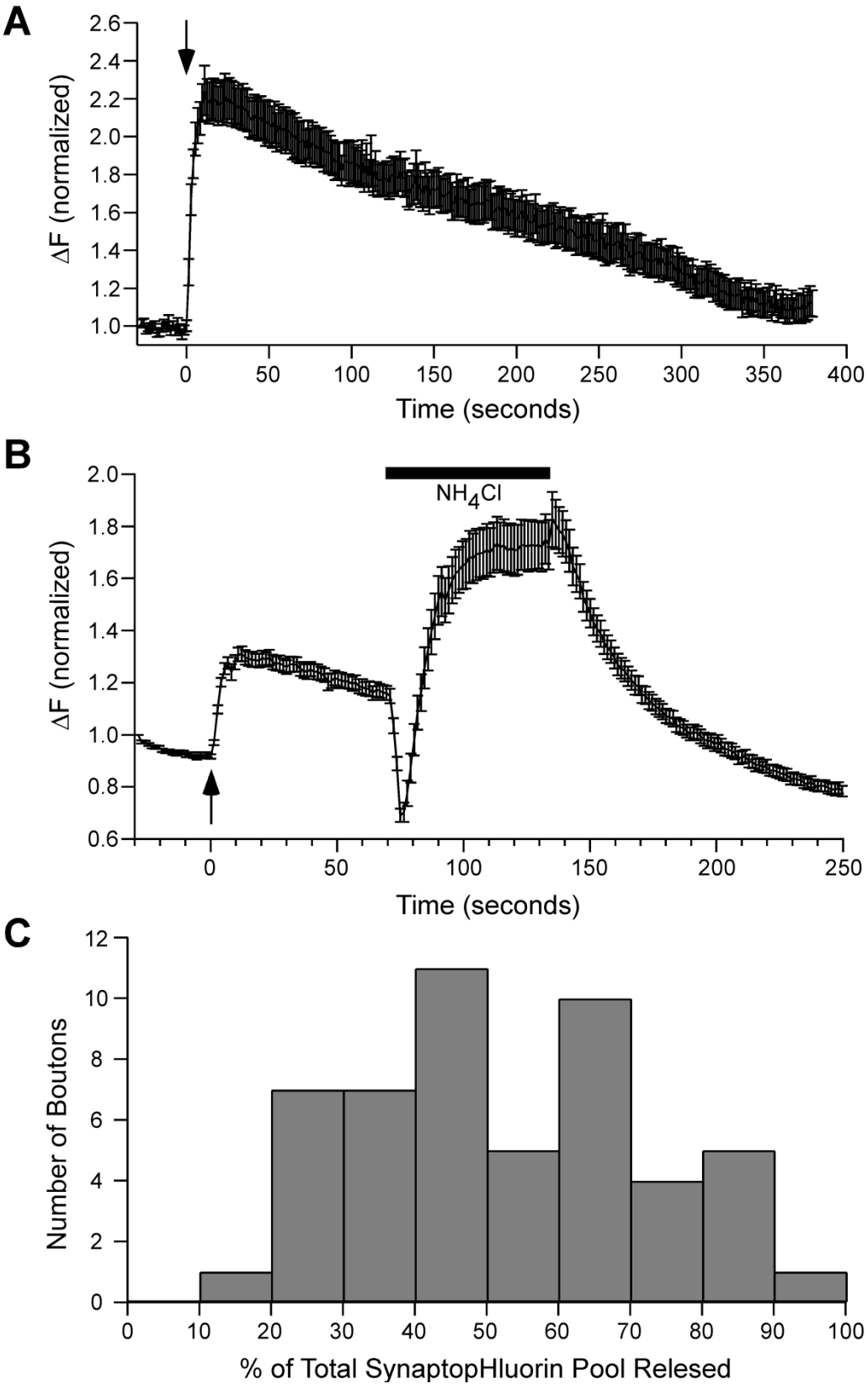
A
ΔF (normalized)
Time (seconds)
B
NH4Cl
ΔF (normalized)
Time (seconds)
C
Number of Boutons
% of Total SynaptopHluorin Pool Relesed

Figure 4.8 – Calcium Rises Nearly Simultaneously Throughout the Motor Neuron During High Frequency Stimulation

Calcium imaging of a patched CaP motor neuron filled with 100 μM Fluo-5F Ca^{2+} indicator and stimulated at 100 Hz for 10 seconds. In addition the cell was dialyzed with the morphological fill, Alexafluor-647 (40 μM). (A) Imaris FilamentTracer reconstruction of the motor neuron based on the morphology from the Alexafluor-647 fluorescent dye. Four colored sample ROIs are positioned on the reconstruction which correspond to the colored traces in C and colored markers in D. (B) Sequential images of the change in Ca^{2+} during the 100Hz stimulation, beginning with a pre-stimulus image and followed by images from 1, 2, 3, and 4 seconds into the train of APs. The ROIs in A are also in B, highlighting the AIS (blue circle) and three sample boutons (red, green and orange). (C) Fluorescence changes observed in the sample ROIs (trace colors match the corresponding colored ROIs) during the 100Hz stimulation. Local background fluorescence is subtracted and the responses are normalized to their peak fluorescence. The dashed line marks the 20% level of the maximal fluorescence. (D) The plot of the location of individual ROIs (presented as distance from soma in μm) versus the time it took to reach 20% of the maximal fluorescence signal for that particular ROI. The example ROIs from A, B, and C are represented in the same color in D. Calibration bar is 20μm for all images.

Fig. 4.8

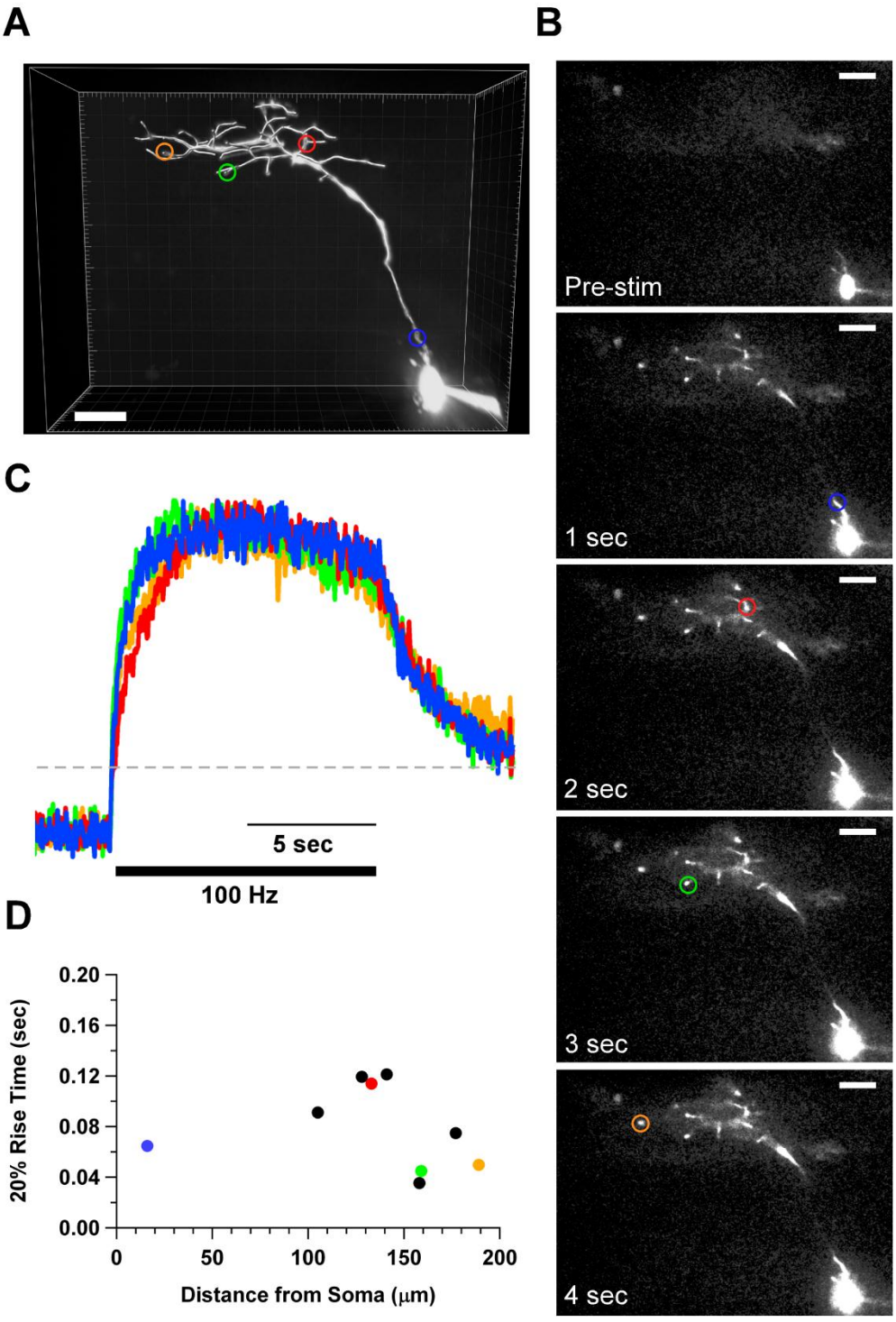
A
B
Pre-stim
1 sec
2 sec
3 sec
4 sec
C
5 sec
100 Hz
D
20% Rise Time (sec)
0.20
0.16
0.12
0.08
0.04
0.00
0
50
100
150
200
Distance from Soma (μm)

Figure 4.9 – Calcium Rises Quickly Regardless of Location in Wild Type Motor Neurons During High Frequency Stimulation

Cumulative distance vs. delay for wild type motor neurons stimulated at 100 Hz for 10 seconds. Fluo-5F Ca^{2+} indicator (100 μM) was used to measure the Ca^{2+} response to stimulation. ROIs from wild type motor neurons were sorted, depending on their distance from the soma (25 μm bins) as measured using Imaris FilamentTracer software and plotted as the mean ± S.E.M. for both distance and delay.

Fig. 4.9

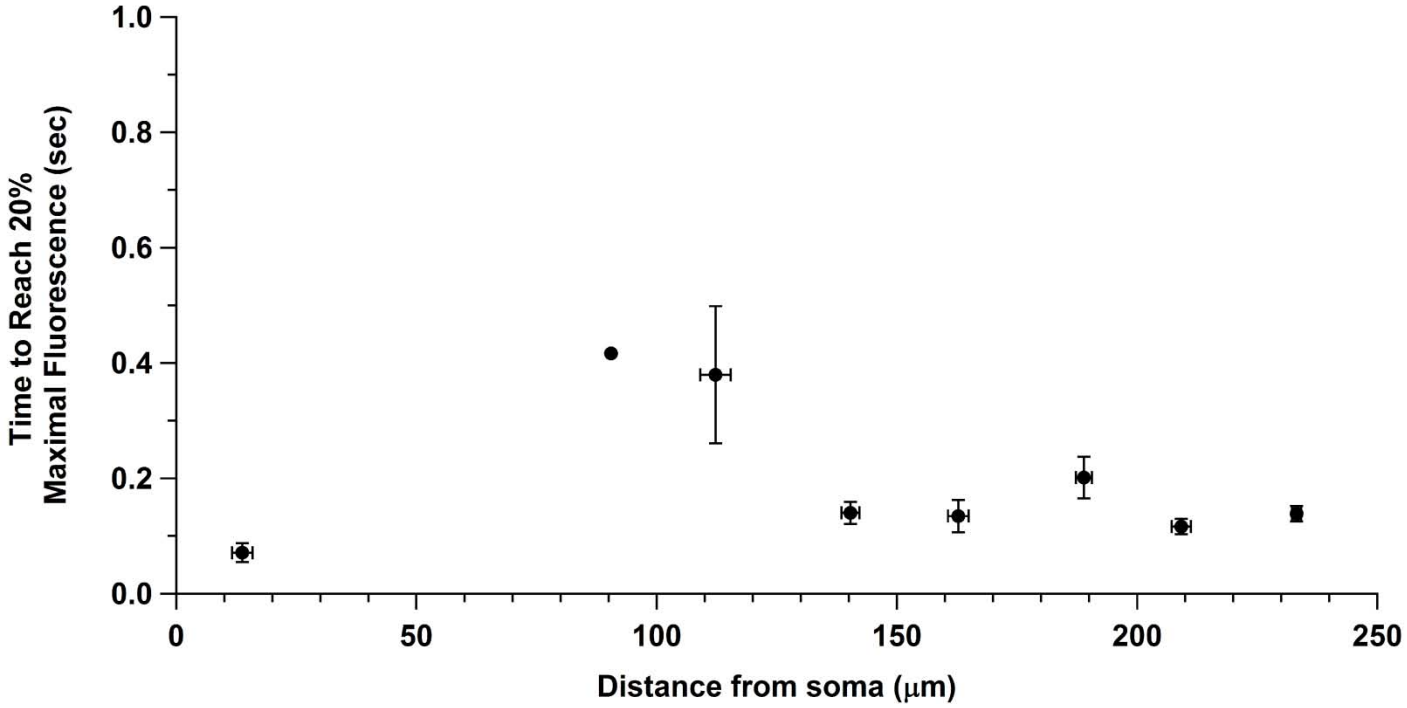
Time to Reach 20% Maximal Fluorescence (sec)
1.0
0.8
0.6
0.4
0.2
0.0
0
50
100
150
200
250
Distance from soma (μm)

Chapter 5: Asynchronous Release

At the zebrafish NMJ, asynchronous transmitter release can manifest during prolonged high frequency stimulation (Fig. 4.6), but it is always preceded by a period of exclusively synchronous release. Pharmacological block of Ca^{2+} influx with 1 μM ω-conotoxin GVIA was shown to completely eliminate synchronous release and the results from the *tb204a* mutant indicate that synchronous release is principally mediated by a P/Q-type Ca^{2+} channel (Fig. 4.1, 4.2). We found that both the pharmacological approach and P/Q channel mutant could also be used to effectively isolate asynchronous release when the CaP motor neuron was stimulated at high frequency for extended periods. Figure 5.1A and B show the EPCs produced by 100 Hz stimulation of the CaP motor neuron in both *tb204a* (Fig. 5.1A, 10 second stimulation, courtesy of Hua Wen) and wild type treated with 1 μM ω-conotoxin GVIA (Fig. 5.1B, 20 second stimulation). The *tb204a* mutation is not a functional null and consequently, some synchronous release remains (Fig. 4.1C). By contrast, application of ω-conotoxin GVIA to wild type motor neurons eliminates nearly all release during the first ten seconds of stimulation. However, in both ω-conotoxin GVIA treated and *tb204a* robust asynchronous release is observed after the first seconds of stimulation (Fig. 5.2A).

As an independent means of assessing the delayed release, I used synaptopHluorin transgenic lines. As presented in chapter 4, the synaptopHluorin fluorescence signal rises upon vesicle release, when the fluorophore becomes unquenched as it is exposed to the extracellular space during fusion to the plasma membrane. SynaptopHluorin measurements comparing optical recordings from boutons of tb204/synaptopHluorin (Fig. 5.1C, blue traces) and ω-conotoxin GVIA treated synaptopHluorin fish (Fig. 5.1C, red traces) confirm the delay observed

in the paired recordings in Fig. 5.1A and B. Figure 5.1C shows three examples, each of which compares synaptopHluorin fluorescence responses from a bouton in wild type (black trace), *tb204a* (blue trace), and ω-conotoxin GVIA treated wild type fish (red trace). In the wild type, bouton fluorescence increases immediately in response to the start of the 100 Hz 20 second stimulation (black traces), whereas the synaptopHluorin/*tb204a* mutant shows an intermediate delay (blue traces) and the ω-conotoxin GVIA treated synaptopHluorin fish has the longest delay (red traces).

Cumulative charge curves obtained by paired recordings and optical measurements of synaptopHluorin fluorescence changes are presented in Figure 5.2. Paired recordings were made in wild type (black traces, 8 pairs), *tb204a* (blue traces, 7 pairs), and ω-conotoxin GVIA treated wild type fish (red traces, 5 pairs). To quantitate release, we measured charge by integrating the synaptic current produced during each second of stimulation. The cumulative charge recorded in muscle during a 10-20 second 100 Hz stimulation of the CaP motor neuron is normalized and plotted versus time for each condition to compare the onset of release (Fig. 5.2A, courtesy of Hua Wen). Some variability is seen in both the *tb204a* and ω-conotoxin GVIA treated fish but the delay is clearly greatest with ω-conotoxin GVIA present, consistent with the examples shown in Fig. 5.1A and B and the imaging data in Fig. 5.1C. Figure 5.2B shows a histogram of ensemble data from synaptopHluorin imaging experiments. The 50% rise time of the synaptopHluorin response from individual synaptic terminals in control (black bars, 8 cells, 127 boutons), *tb204a* (blue bars, 2 cells, 5 boutons), and ω-conotoxin GVIA treated fish (red bars, 4 cells, 23 boutons) are presented in Figure 5.2B. *Tb204a*/synaptopHluorin data are limited as these transgenic fish were only recently generated. In addition, signal to noise for both the *tb204a*/synaptopHluorin fish and synaptopHluorin fish treated with ω-conotoxin GVIA is less than optimal, making responses from individual terminals difficult to obtain. Regardless

of these limitations, the optical method of tracking vesicle release appears to be in good agreement with the electrophysiological measurements as expected.

Numerous studies have shown that altering the strength of Ca^{2+} buffering within neurons can have dramatic effects on asynchronous release, where higher buffering leads to a decrease in asynchronous release (Atluri and Regehr, 1998; Hefft and Jonas, 2005; Lu and Trussell, 2000). We tested the sensitivity of asynchronous release to changes in buffer strength by altering the concentration of EGTA in the patch pipette internal solution. Asynchronous release was isolated through application of 1 μM ω-conotoxin GVIA and internal concentrations of 500 μM and 5 mM EGTA were tested during 20 second long 100 Hz stimulus trains. In the low calcium buffering condition of 500 μM EGTA, asynchronous release occurred after approximately two seconds of stimulation (Fig. 5.3A). The delay was increased to approximately ten seconds when the buffer strength was increased tenfold to 5 mM EGTA (Fig. 5.3B). Summary cumulative charge data (measured as in Fig. 5.2A) show that the increased delay with an increase in buffer strength is consistent and reproducible (Fig. 5.3C, black traces are control with no ω-conotoxin GVIA, green traces are 500 μM EGTA, and red traces are 5 mM EGTA, courtesy of Hua Wen). Increasing the internal EGTA concentration to 25 mM eliminates all stimulus evoked release (Hua Wen, personal communication).

Using Ca^{2+} imaging, the delay imparted by EGTA was examined for the *tb204a* mutant and wild type fish in the presence and absence of ω-conotoxin GVIA. In order to do this, a fluorescent Ca^{2+} indicator was introduced to the cell via the patch pipette and measurements of synaptic bouton fluorescence were made during 10-20 second long bouts of 100 Hz stimulation. The time from the onset of stimulation to reach 20% of peak fluorescence was compared for wild type (Fig. 5.4, white bars), ω-conotoxin GVIA treated wild type (red bars), and *tb204a*

synaptic boutons (blue bars). In wild type motor neurons (white bars) the 20% rise time was 0.18 ± 0.02 seconds with 500 μM EGTA (4 fish, 64 boutons) and 0.71 ± 0.08 seconds with 5 mM EGTA (3 fish, 38 boutons) present in the internal solution of the patch electrode. In wild type motor neurons treated with ω-conotoxin GVIA (red bars) the 20% rise time was 1.98 ± 0.10 seconds with 500 μM EGTA (6 fish, 69 boutons) and 5.42 ± 0.26 seconds with 5 mM EGTA (4 fish, 56 boutons) present in the internal solution of the patch electrode. Finally, for *tb204a* motor neurons (blue bars) the 20% rise time was 0.60 ± 0.04 seconds with 500 μM EGTA (4 fish, 57 boutons) and 4.26 ± 0.15 seconds with 5 mM EGTA (2 fish, 30 boutons) present in the internal solution of the patch electrode. These results were consistent with the paired recording data, indicating that the higher EGTA concentration increased the delay of Ca^{2+} rise just as the delay increased for release in paired recordings.

The delayed Ca^{2+} response in both the ω-conotoxin GVIA treated cells and *tb204a* mutants was expected given the delay observed in both paired recordings and synaptopHluorin measurements of vesicle release. However, to be certain the delayed Ca^{2+} response was causal to delayed asynchronous release I performed simultaneous paired motor neuron target muscle patch clamp recordings and Ca^{2+} imaging (Fig. 5.5). The CaP motor neuron was visualized with an Alexafluor-647 fluorescent dye and the innervated fast skeletal muscle was filled with an Alexafluor-555 fluorescent dye (Fig. 5.5A). As before, action potentials were elicited for 20 seconds at 100 Hz and the post-synaptic response in voltage-clamped muscle was recorded (Fig. 5.5B). In the example shown, delayed asynchronous release occurred after approximately 12 seconds of stimulation (Fig. 5.5B). Six boutons that appeared to contact the surface of the muscle fiber were identified by eye with the aid of Imaris software. Fluo-5F fluorescence was measured for each of these boutons and the responses were normalized to their maximal fluorescence and averaged. The data from these boutons is plotted on the same timescale as

the paired recording (Fig. 5.5C). During the initial 10 seconds of stimulation a small steady rise in Ca^{2+} was observed, until around 12 seconds into the AP train where an inflection point was reached and the Ca^{2+} response rapidly increased. This rapid increase correlated with the arrival of the delayed release as measured by the EPCs (Fig. 5.5B and C), providing good evidence that the delayed Ca^{2+} rise is causal to the delayed asynchronous release.

Two questions arose from the observations of delayed asynchronous release in ω-conotoxin GVIA treated neurons. First, what is the source of the Ca^{2+} responsible for this form of transmitter release? Second, what could account for the delay in the Ca^{2+} rise? Calcium imaging experiments were critical in addressing these questions. As shown, the delayed release seen in paired recordings was reflected in the delayed rise in Ca^{2+} at synaptic boutons. Moreover, the delayed Ca^{2+} response was longer for boutons that were further from the cell body. In fact, when the entire motor neuron was imaged there was an apparent Ca^{2+} wave which travels from the soma along the axon and out to distal boutons. This came as quite a surprise because to our knowledge propagating Ca^{2+} waves have never been reported in axons of motor neurons. An example of this dynamic Ca^{2+} response is shown in Figure 5.6. The neuron was filled with both the Alexafluor-647 morphological dye (Fig. 5.6A) and Fluo-5F Ca^{2+} indicator, introduced through the patch electrode. A single z-section of the motor neuron is shown, which included the soma, axon initial segment, sections of axon and boutons (Fig. 5.6A). A large section of axon distal to the initial segment is absent as this is the portion that arches over the notochord, out of the plane of focus. The subsequent panels are sequential time frames taken from the Ca^{2+} imaging movie prior to stimulation (Fig. 5.6B) and at 1, 2, 3, and 4 seconds into the stimulus train (Fig. 5.6C-F). Calcium levels are represented as a heat map where red indicates high levels of Ca^{2+} and dark blue areas indicate the lowest levels of Ca^{2+}. In the pre-stimulus image, the soma and patch pipette are seen in the lower right corner and the axonal arbor is not

visible (due to low basal fluorescence of Fluo-5F). Some autofluorescence can be seen in the upper half of the image and can be distinguished from the neuron itself when compared with the image of the neuronal fill (Fig. 5.6B and A). After 1 second of stimulation the signal in the axon initial segment is readily apparent and a slight increase can be seen in parts of the axon (Fig. 5.6C). At 2 seconds the primary branch of the axon continues to brighten, as do some axon branch points and secondary branches of the axon (Fig. 5.6D). By 3 seconds of 100 Hz stimulation most of the proximal axonal arbor Ca^{2+} signal has increased, particularly at swellings along the axon and at branch points. A rise in Ca^{2+} at some distal boutons (far from the soma) is now apparent as well (Fig. 5.6E). Finally, after 4 seconds of stimulation, the most distal boutons (furthest from the soma) within the focal plane report a rise in Ca^{2+} (Fig. 5.6F, upper left corner).

The distance dependence of the delayed Ca^{2+} rise was quantified by reconstructing a motor neuron offline and matching regions of interest from the Ca^{2+} imaging to locations on the morphological reconstruction (Fig. 5.7A). A 60 μm z-stack of the Alexafluor-647 fill was acquired (in 1 μm steps) and subsequently used to create a three dimensional image of the entire motor neuron. Using Imaris FilamentTracer software, the entire axon of the motor neuron was traced and precise distances between regions of interest along the axon (i.e. boutons, branch points, etc.) and the cell body were determined (Fig. 5.7A). Sample ROIs are shown on the reconstruction (blue-AIS, red-axon, green-axonal varicosity, orange-axonal varicosity, Fig 5.7A). The timepoints (pre-stimulus, 1, 2, 3, and 4 seconds) from the Ca^{2+} imaging are shown in Figure 5.7B along with the colored ROIs (same cell as Fig. 5.6). The fluorescence changes for each colored ROI (trace color corresponds to the ROI color) in response to the 10 second 100 Hz train are shown (Fig. 5.7C). It is clear that the Ca^{2+} rise is not simultaneous for individual regions as it was for the control experiment in the absence of ω-conotoxin GVIA (Fig. 4.8). When regions are plotted with respect to their distance from the soma we find that the time to reach 20% of the

maximal signal is longer for more distal boutons (Fig. 5.7D, individual ROIs are marked according to their corresponding colors in Fig. 5.7A-C). The cumulative data for ω-conotoxin GVIA treated cells is plotted (Fig. 5.8, open circles) alongside the control data from Figure 4.9 (Fig. 5.8, closed circles). Individual ROIs from each cell were binned (25 μm bins) according to their relative distance from the soma (Fig. 5.8). Under these conditions the distance vs. delay relationship is highly linear and the inverse of the slope gives an apparent velocity of approximately 60 μm/second. Another illustration of the Ca^{2+} wave in a ω-conotoxin GVIA treated neuron is shown using a higher magnification and NA objective (63x, 1.0 NA), but in this example only the axonal arbor is visible in the imaging field (Fig. 5.9A). The Imaris reconstruction was produced from the Alexafluor-647 morphological fill and regions of interest were chosen at proximal and distal locations (Fig. 5.9B). Calcium responses for a control cell (only the fluorescence traces are shown for this cell) and for the ω-conotoxin GVIA treated cell (from Fig. 5.9A and B) were normalized and plotted (Fig. 5.9C and D). With the distance data obtained from the morphology, the distance vs. delay graph was generated, once again demonstrating the distance dependence of the delayed rise of Ca^{2+} along the length of the motor neuron (Fig. 5.9E).

The existence of a ω-conotoxin-insensitive source of Ca^{2+}, located some distance from release sites, could explain the observed delay if this Ca^{2+} is indeed traveling along the axon and eventually arriving at active zones. However, we worried that the apparent propagating Ca^{2+} wave could be an artifact of the experimental design given that fluorescent Ca^{2+} indicators such as Fluo-4 are themselves Ca^{2+} buffers in addition to being reporters of changes in cytosolic Ca^{2+}. The indicators alter the buffering capacity of the cell therefore I wanted to test indicators with differing intrinsic Ca^{2+} affinities to determine if the delay occurred similarly. In addition, we wanted to test an indicator with low mobility in the cytosol to see if the wave persists with a highly immobile Ca^{2+} dye. To test these possibilities, first, Ca^{2+} indicators with different inherent

affinities for Ca^{2+} were tested in the presence and absence of ω-conotoxin GVIA. The delay in boutons was similar in control and ω-conotoxin GVIA treated fish for two different Ca^{2+} indicators tested (Fig. 5.10A, control white bars, ω-conotoxin GVIA red bars, Fluo-4, K_d = 345 nM, Fluo-5F, K_d = 2.3 μM). The second approach was to test a more immobile buffer to see if the propagating Ca^{2+} wave remained intact. For this purpose I used Oregon Green BAPTA-1 dextran conjugate which diffuses very slowly throughout the cell. Results from a ω-conotoxin GVIA treated neuron using OGB-1 dextran were similar to those of the mobile indicators (Fig. 5.10B, green circles). Given the fact that the paired recordings do not contain a fluorescent Ca^{2+} indicator and changing Ca^{2+} indicators had virtually no effect, I feel confident that our experimental conditions are not inducing the observed phenomena.

Another concern was whether or not ω-conotoxin GVIA block of the P/Q-type channels was complete at a concentration of 1 μM. I worried that despite the evidence for an apparent Ca^{2+} wave, perhaps there was instead a slow accumulation of Ca^{2+} through unblocked P/Q-type channels at release sites. If Ca^{2+} was slowly accumulating in this manner then we might also observe delayed Ca^{2+} signals in boutons with Ca^{2+} imaging and delayed release with paired recordings. However, this would not explain the apparent propagation through the bouton field. Nonetheless, to directly address this possibility, two types of experiments were performed. The first was to simply increase the ω-conotoxin GVIA concentration used in the bath solution to 10 μM and perform paired recordings. No changes were observed with a higher concentration of toxin, and the delayed asynchronous release proceeded as it had in 1 μM ω-conotoxin GVIA (data not shown). The second experiment, which we called the "killswitch," was to stimulate the motor neuron for a period of time while monitoring for the onset of EPCs, with a goal of abruptly stopping the stimulation prior to the actual onset of the post-synaptic currents. One successful experiment is shown in Figure 5.11A. In this cell the 100

Hz stimulation was stopped several seconds prior to the onset of the EPCs (Fig. 5.11A, courtesy of Hua Wen). The delayed asynchronous release occurred well after the end of the stimuli, indicating that the Ca^{2+} responsible for the EPCs is not likely accumulating through unblocked P/Q-type channels since those channels would no longer be activated by APs. A similar "killswitch" experiment was used to look at the Ca^{2+} signal itself. For reference, a wild type untreated neuron is given a 10 second 100 Hz stimulus train and the Ca^{2+} fluorescence was measured for a proximal (black trace) and distal (red trace) region of the axon (Fig. 5.11B). The Ca^{2+} signals for each region were nearly identical. Another motor neuron was treated with ω-conotoxin GVIA and a 4 second AP train was induced (Fig. 5.11C). In this case the proximal region (black trace) responded with a rise in Ca^{2+} which accelerated after three seconds of stimulation and peaked at the end of the AP train (Fig. 5.11C). In contrast, the distal region (red trace) Ca^{2+} rise occurred more slowly than the proximal region in response to the start of the stimulus. In fact, the rapid rise of Ca^{2+} did not occur until approximately one second after the stimulation stopped (Fig. 5.11C, red trace). These data argue against the possibility that the Ca^{2+} source for delayed release could be the P/Q-type channels. Instead, the "killswitch" experiments point to a process where a regenerative Ca^{2+} wave can be initiated and sustained even after the cell is no longer stimulated.

To further explore the mechanism underlying the delayed asynchronous release we wanted to test the possibility that the Ca^{2+} wave could be triggered in the absence of action potentials. By applying 1 μM TTX to the preparation action potentials were inhibited. In voltage clamp mode the motor neuron was depolarized from -80 mV to +50 mV. Surprisingly, under these conditions a propagating wave traveled from the soma to the most distal boutons of the neuron (Fig. 5.12). The duration of depolarization necessary to evoke this wave varied in cells tested as did the velocity of propagation. In one case the Ca^{2+} wave reached the end of the

neuron and actually reflected back, traveled the length of the axon, and reached the cell body. In the example shown a doublet of Ca^{2+} waves were seen (Fig. 5.12B). Clearly this scenario is not physiological (unless perhaps a zebrafish encounters a feisty puffer fish), but it does provide some evidence that a fundamental mechanism exists within CaP motor neurons to propagate a Ca^{2+} wave the entire length of the cell. A regenerative mechanism such as Ca^{2+} induced Ca^{2+} release (CICR) of internal stores may be responsible for this wave but at this time the experiments to test this idea have not been adequately explored.

Knowing that cadmium application could effectively block all release, we suspected that a secondary (non-ω-conotoxin GVIA sensitive) VGCC might trigger the propagating Ca^{2+} wave. This sparked a painstaking search for some pharmacological inhibitor of wave initiation. Paired recordings were made in the presence of 1 μM ω-conotoxin GVIA, 100 μM Ni^{2+} and 5 μM mibefradil and a 25 second 100 Hz train of action potentials was evoked in the CaP motor neuron. Overall release decreased and was further delayed (Fig. 5.13A, courtesy of Hua Wen). Calcium imaging was performed on the motor neuron before and after application of ω-conotoxin GVIA, 100 μM Ni^{2+} and 5 μM mibefradil in response to 2 second 100 Hz trains. In this condition, both the axon initial segment (Fig. 5.13B) and boutons (Fig. 5.13C, example from a single bouton) showed a reduced response in the presence of the drugs. An approximate 75% reduction in Ca^{2+} signal was seen at the initial segment and 90% reduction was observed in this example bouton.

These results led us to believe that a T-type Ca^{2+} current could perhaps trigger the Ca^{2+} wave in the presence of ω-conotoxin GVIA because the Ni^{2+} and mibefradil concentrations used for those experiments are supposedly specific for CaV 3.3 channels (Randall and Tsien 1997, Lee et al. 1999, McDonough and Bean, 1998). To test this possibility we applied a proprietary

compound developed by Merck (TTA-P2) that is also reported to be specific for T-type Ca^{2+} channels (Dreyfus et al. 2010, Choe et al. 2011). Once again, in the presence of 1 μM ω-conotoxin GVIA, 5 μM TTA-P2 was applied to the motor neuron, but this time the action potentials were stimulated at 100 Hz for 10 seconds to test for the presence of the calcium wave. Robust Ca^{2+} signals were recorded throughout the motor neuron and the previously described delay remained intact (Fig. 5.14). Here, the Ca^{2+} responses were not normalized to their respective maximal signals in order to provide an example of variation in amplitude normally observed at distinct regions of the motor neurons. The full neuronal reconstruction necessary to determine the distance vs. delay plot was not performed in this case, but the delay between the AIS (red trace) and the other regions is clear. The most distal boutons often show small amplitude responses (i.e. grey trace rising at ~3.5 seconds). In addition, paired recordings utilizing these same conditions failed to show a significant reduction in release following ω-conotoxin GVIA and TTA-P2 application (Hua Wen, personal communication).

Mibefradil can also inhibit Ca^{2+} current mediated by L-type Ca^{2+} channels, although typically at higher concentrations than 5 μM. Therefore, we continued our search for a pharmacological blocker of the Ca^{2+} wave seen in the presence of ω-conotoxin GVIA. Numerous Ca^{2+} channel blockers were tested and notably the L-type antagonists, 100-200 μM verapamil and 50 μM amlodipine looked rather promising. However, their action was likely due to inhibition of APs early in the stimulus trains (data not shown). The R-type toxin, 200 nM SNX-482, did not appear to affect the Ca^{2+} wave (data not shown). Nor did the Na^{+}/Ca^{2+} exchanger antagonist, 30 μM SN-6 (data not shown). Due to the robust nature of the Ca^{2+} wave, one approach that was adopted was to lower external Ca^{2+} to 100 μM, 200 μM, or in some experiments 500 μM. The 100 μM and 200 μM Ca^{2+} concentrations do not support release, however weak Ca^{2+} waves could be induced and observed with Ca^{2+} imaging when the motor

neuron was stimulated at 100 Hz for 20 seconds with either 100 μM or 200 μM Ca^{2+} in the bath solution. Using this approach, the L-type Ca^{2+} channel antagonist, 50 μM nimodipine, showed promising results (Fig. 5.15A and B). The weak Ca^{2+} wave (200 μM bath Ca^{2+}) seen in the presence of ω-conotoxin GVIA was blocked when 50 μM nimodipine was also present, although some Ca^{2+} current persisted in the AIS and axon. The AIS Ca^{2+} plateaued when both nimodipine and ω-conotoxin GVIA were in the bath, while cells tested with ω-conotoxin GVIA alone showed a steady rise (Fig. 5.15A). This indicates that even under 200 μM bath Ca^{2+} conditions with ω-conotoxin GVIA and 50 μM nimodipine present, a slight amount of residual Ca^{2+} influx persists. Further from the soma, the Ca^{2+} signal in the axon also reported a rise in Ca^{2+} but the inflection and acceleration of the Ca^{2+} response was never observed in the presence of both ω-conotoxin GVIA and nimodipine (Fig. 5.15B). Therefore, despite the persistence of some Ca^{2+} influx with 1 μM ω-conotoxin GVIA and 50 μM nimodipine present (in 200 μM bath Ca^{2+}), the addition of nimodipine abolishes the weak Ca^{2+} wave whereas ω-conotoxin GVIA alone does not. The integral of the Ca^{2+} responses from individual experiments (both AIS and axonal ROIs) were determined after 20 seconds of stimulation to quantify the effect of adding nimodipine (Fig. 5.15C). Average value for the AIS treated with ω-conotoxin GVIA was 32.29 ± 6.39. AIS treated with ω-conotoxin GVIA and nimodipine was 10.23 ± 3.26. Average value for the axon treated with ω-conotoxin GVIA was 66.29 ± 13.41. Axon treated with ω-conotoxin GVIA and nimodipine was 24.24 ± 4.25 (N = 5 for both conditions, all data are mean ± S.E.M). Because variability in the timing of wave onset was common in these experiments, I have plotted Ca^{2+} imaging traces from the individual experiments (Fig. 5.16A-D).

With some indication that an L-type channel could be involved as a triggering mechanism for the propagating Ca^{2+} wave, based on the nimodipine experiments, I acquired

embryos from two different mutant zebrafish lines. The first to be tested was *gemini*, a CaV 1.3 mutant (Sidi et al. 2004). Using the 200 μM Ca^{2+} paradigm, I found that the weak Ca^{2+} wave was not blocked (data not shown). Another mutant line, called *island beat*, was obtained from the Rottbauer lab in Germany, which encodes a dysfunctional CaV 1.2 channel (Rottbauer et al. 2001). In normal Ca^{2+}, with GIVA present, there was no inhibition of the Ca^{2+} wave when the CaP neuron was stimulated at 100 Hz for 10 seconds (data not shown). While the nimodipine result was encouraging we were disappointed by the lack of effect in the fish lines with mutations in L-type channels. However, nimodipine has also been reported to antagonize T-type Ca^{2+} channels as well (Randall and Tsien 1999). As we saw in chapter 4 with the surprising finding that ω-conotoxin GVIA blocks P/Q-type channels in zebrafish, it is clear that positive pharmacological identification of channels can be difficult and sometimes unpredictable.

A limited number of experiments designed to test the involvement of Ca^{2+} release from internal stores were performed. Because I suspected that CICR may be responsible for the propagating calcium wave, I tested several inhibitors of internal store Ca^{2+} release. Thapsigargin, 2-APB and CPA were bath applied and the motor neuron was stimulated at 100 Hz for 10 seconds in the presence of ω-conotoxin GVIA (data not shown). None of these inhibitors of CICR blocked the propagating Ca^{2+} wave. While these experiments suggest that CICR does not underlie the observed wave, these compounds were only tested a few times. A more thorough investigation of CICR involvement should be done to formally rule out the possibility that it underlies the Ca^{2+} wave.

Figure 5.1 – Genetic and Pharmacological Isolation of Asynchronous Release

Delayed asynchronous release was elicited through tetanic stimulation of either mutant (*tb204a*) or ω-conotoxin GVIA treated wild type CaP motor neurons. (A) A sample paired recording (motor neuron APs not shown) showing EPCs in target fast skeletal muscle voltage-clamped at -50 mV evoked by a 10 second 100 Hz stimulation of a *tb204a* CaP motor neuron (courtesy of Hua Wen). (B) A paired recording (motor neuron APs not shown) showing EPCs evoked by a 20 second 100 Hz stimulation of a CaP motor neuron from a WT fish treated with ω-conotoxin GVIA. (C) Examples of fluorescence changes recorded from synaptic boutons of synaptopHluorin (black traces), ω-conotoxin GVIA treated synaptopHluorin (red traces), and *tb204a*/synaptopHluorin (blue traces) transgenic fish in response to 10 second 100 Hz stimulus trains applied to CaP motor neurons.

Fig. 5.1

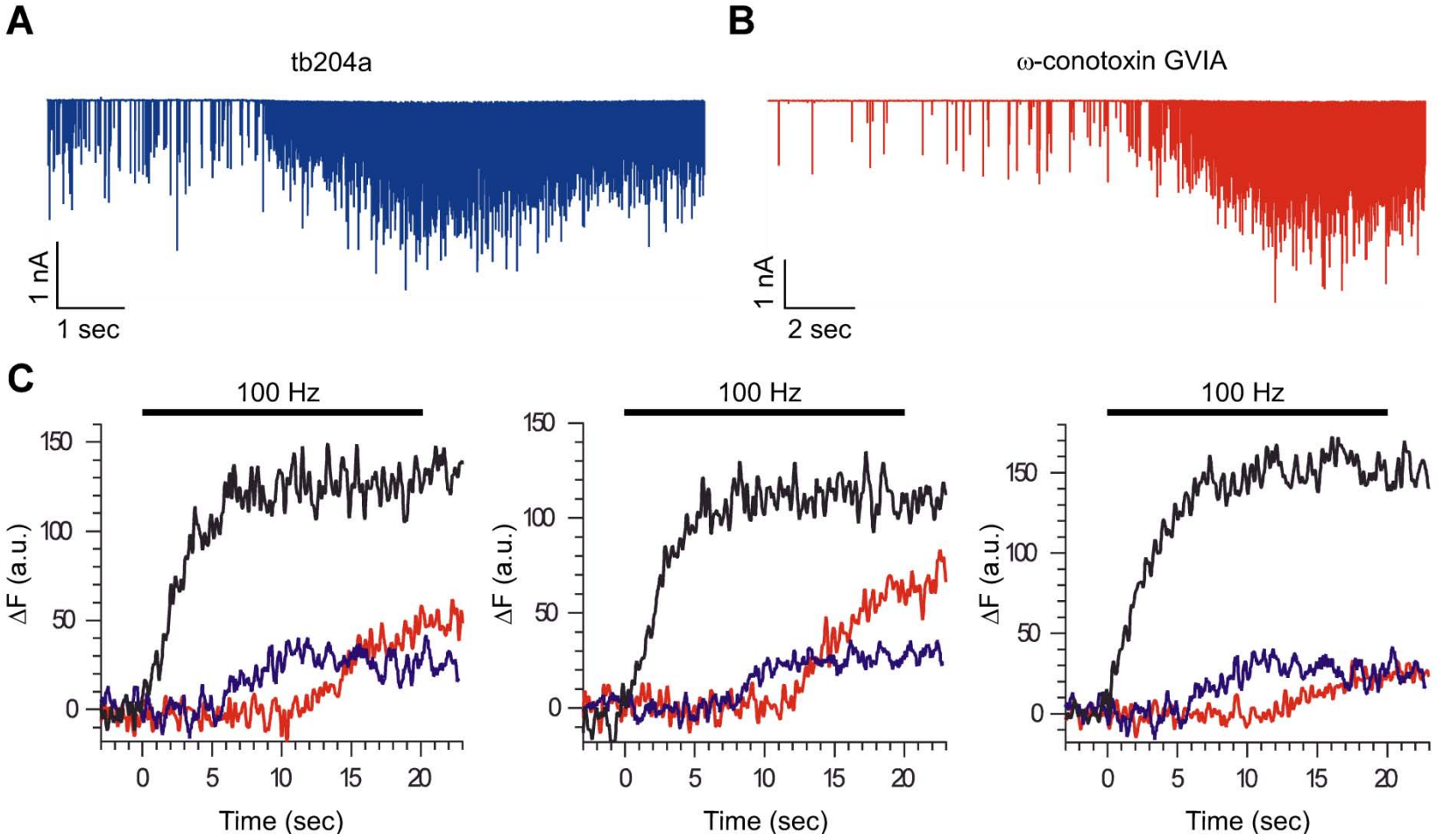
A
tb204a
1 nA
1 sec
B
ω-conotoxin GVIA
1 nA
2 sec
C
100 Hz
ΔF (a.u.)
Time (sec)
100 Hz
ΔF (a.u.)
Time (sec)
100 Hz
ΔF (a.u.)
Time (sec)

Figure 5.2 – Paired Recordings and Imaging Confirm Delayed Asynchronous Release in *tb204a* Fish and ω-conotoxin GVIA Treated Wild Type Fish

(A) Cumulative postsynaptic charge associated with 100 Hz stimulation of WT (black traces), *tb204a* (blue traces), and ω-conotoxin GVIA treated WT (red traces) motor neurons (as in Fig. 5.1A and B, courtesy of Hua Wen). Cumulative postsynaptic charge was binned at 1 second intervals and normalized to the to the maximal response. (B) Ensemble data from synaptopHluorin imaging of WT (black bars), tb204 (blue bars), and ω-conotoxin GVIA treated WT (red bars) synaptic boutons during 100 Hz stimulation of the motor neuron. SynaptopHluorin fluorescence responses from individual boutons were determined as the time required to reach 50% of their peak fluorescence.

Fig. 5.2

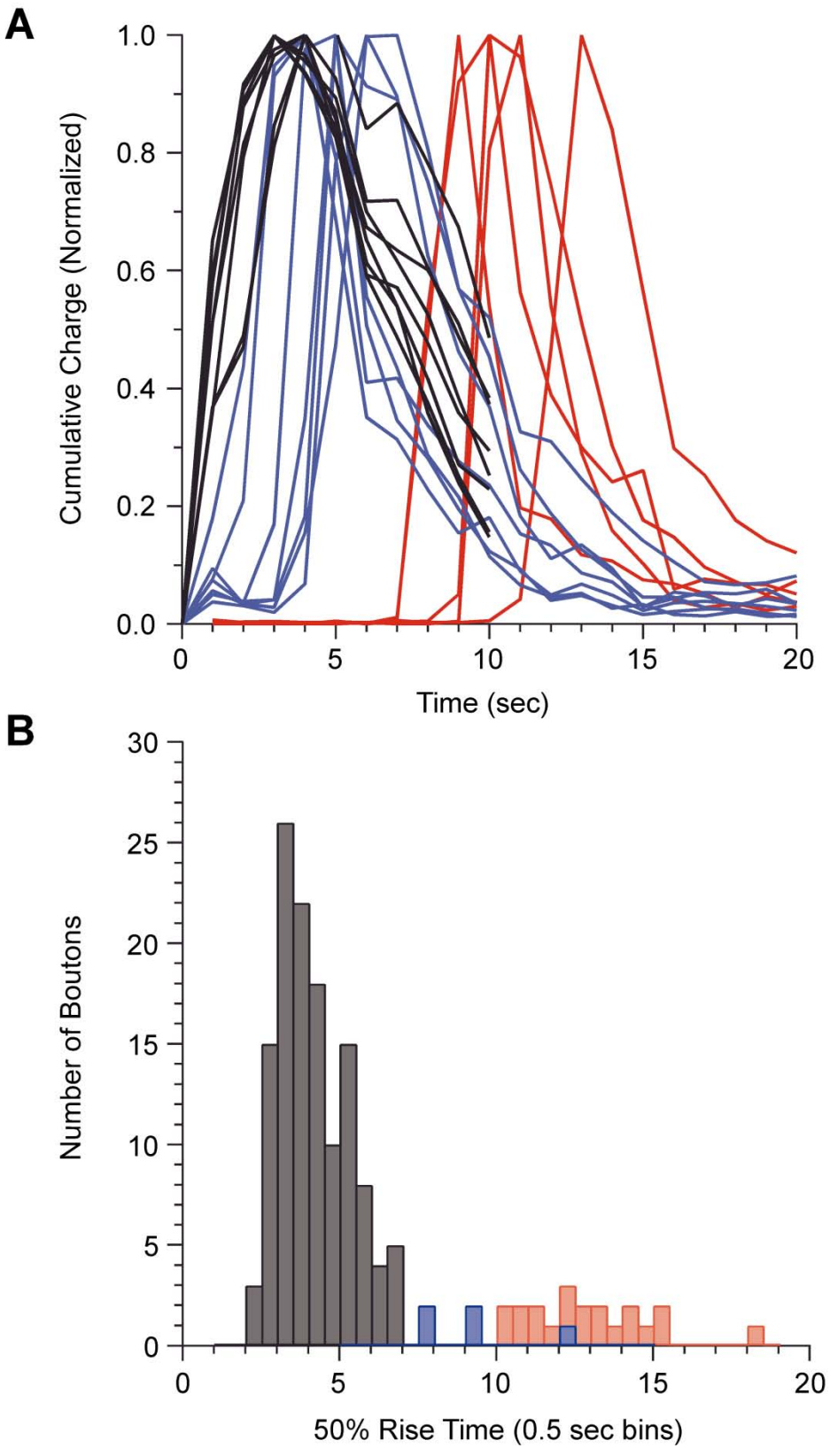
A
1.0
0.8
0.6
0.4
0.2
0.0
Cumulative Charge (Normalized)
0
5
10
15
20
Time (sec)
B
30
25
20
15
10
5
0
Number of Boutons
0
5
10
15
20
50% Rise Time (0.5 sec bins)

Figure 5.3 – Calcium Buffering Affects the Delay of Asynchronous Release

Sample EPCs from paired recordings of WT CaP motor neurons and target fast muscle cells in the presence of ω-conotoxin GVIA with 500 μM EGTA (A) or 5 mM EGTA (B) in the patch pipette internal solution. EPCs were evoked by a 20 second 100 Hz stimulus train. (C) Cumulative postsynaptic charge from 100 Hz stimulation of WT control (black traces) or ω-conotoxin GVIA treated WT CaP neurons dialyzed with 500 μM EGTA (green traces) or 5 mM EGTA (red traces, courtesy of Hua Wen).

Fig. 5.3

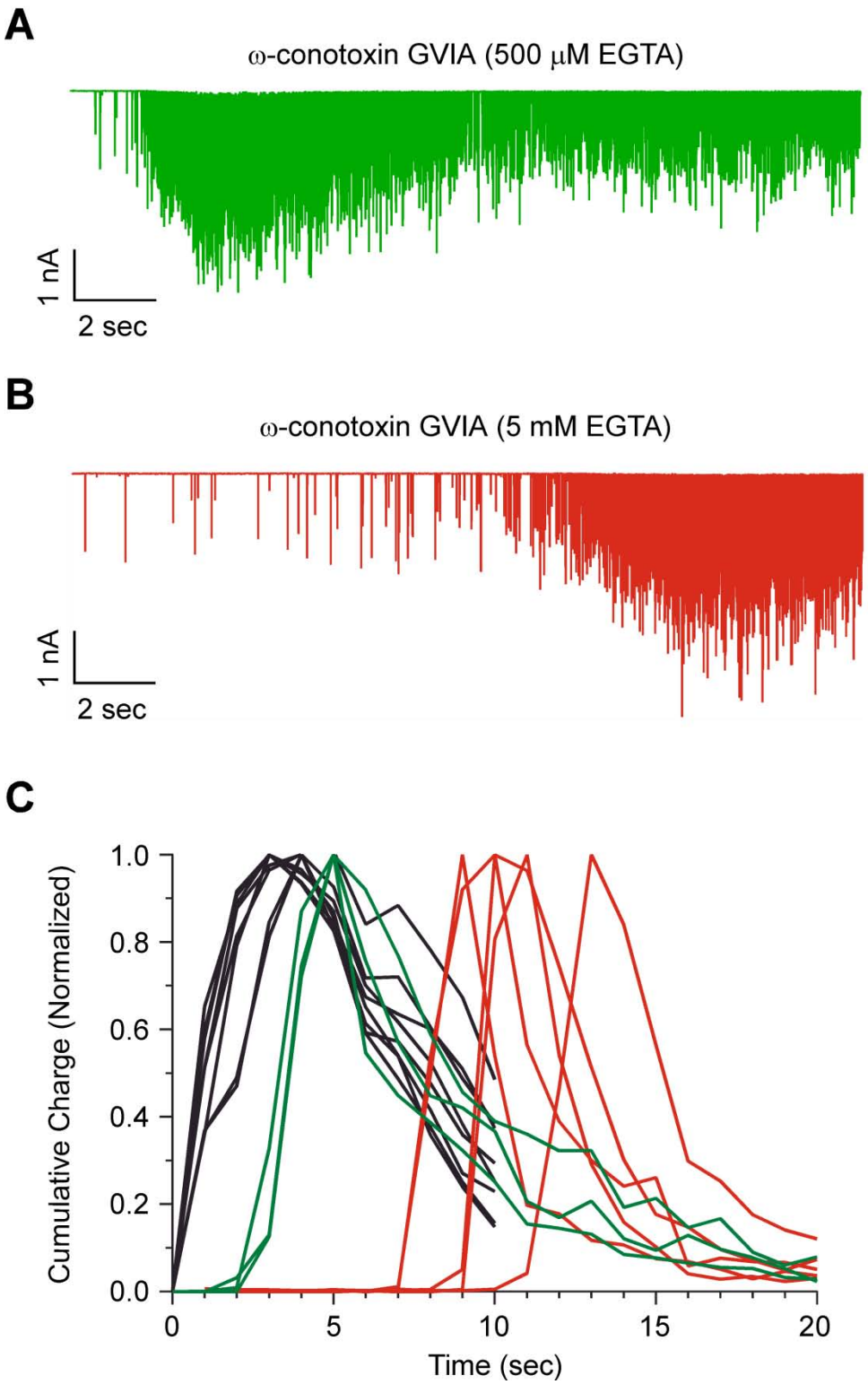
A
ω-conotoxin GVIA (500 μM EGTA)
1 nA
2 sec
B
ω-conotoxin GVIA (5 mM EGTA)
1 nA
2 sec
C
Cumulative Charge (Normalized)
1.0
0.8
0.6
0.4
0.2
0.0
0
5
10
15
20
Time (sec)

Figure 5.4 – Dependence of Delayed Calcium Rise in Synaptic Boutons on Intracellular Calcium Buffering

Fluo-4 calcium signals from synaptic boutons of CaP motor neurons in WT (white bars), ω-conotoxin GVIA treated WT (red bars), and *tb204a* fish (blue bars) were measured with 500 μM EGTA or 5 mM EGTA present in the patch pipette internal solution and the time to reach 20% of the maximal fluorescence was determined. For ** $P < 0.05$, and for *** $P < 0.001$.

Fig. 5.4

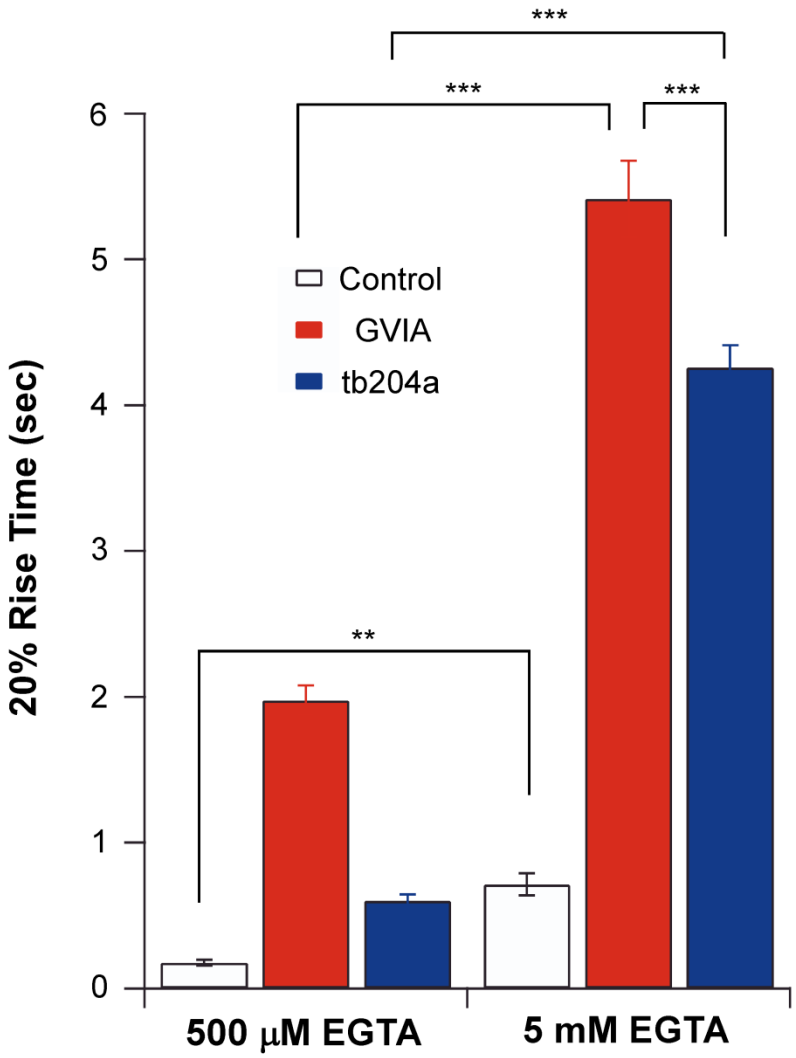
***
***
***
**
Control
GVIA
tb204a
20% Rise Time (sec)
0
1
2
3
4
5
6
500 μM EGTA
5 mM EGTA

Figure 5.5 – Simultaneous Paired Recording and Calcium Imaging

(A) A CaP motor neuron is dye filled with Alexafluor-647 (green) and target muscle cell is dye filled with Alexafluor-555 (red). Multiple synaptic boutons contacting the patched muscle cell are visible near the main axonal branch, appearing as yellow varicosities (scale bar = 10 μm). (B) Paired recording of the motor neuron and target muscle shown in A, where the neuron is stimulated for 20 seconds at 100 Hz (APs are the upper black traces) and the corresponding EPCs in the muscle cell are recorded (lower red traces). (C) Fluo-5F Ca^{2+} signals (normalized to peak fluorescence) from 6 synaptic boutons appearing to contact the patched muscle cell. The timescales in B and C are matched to one another, therefore the Ca^{2+} response in C corresponds to the stimulus seen in B.

Fig. 5.5

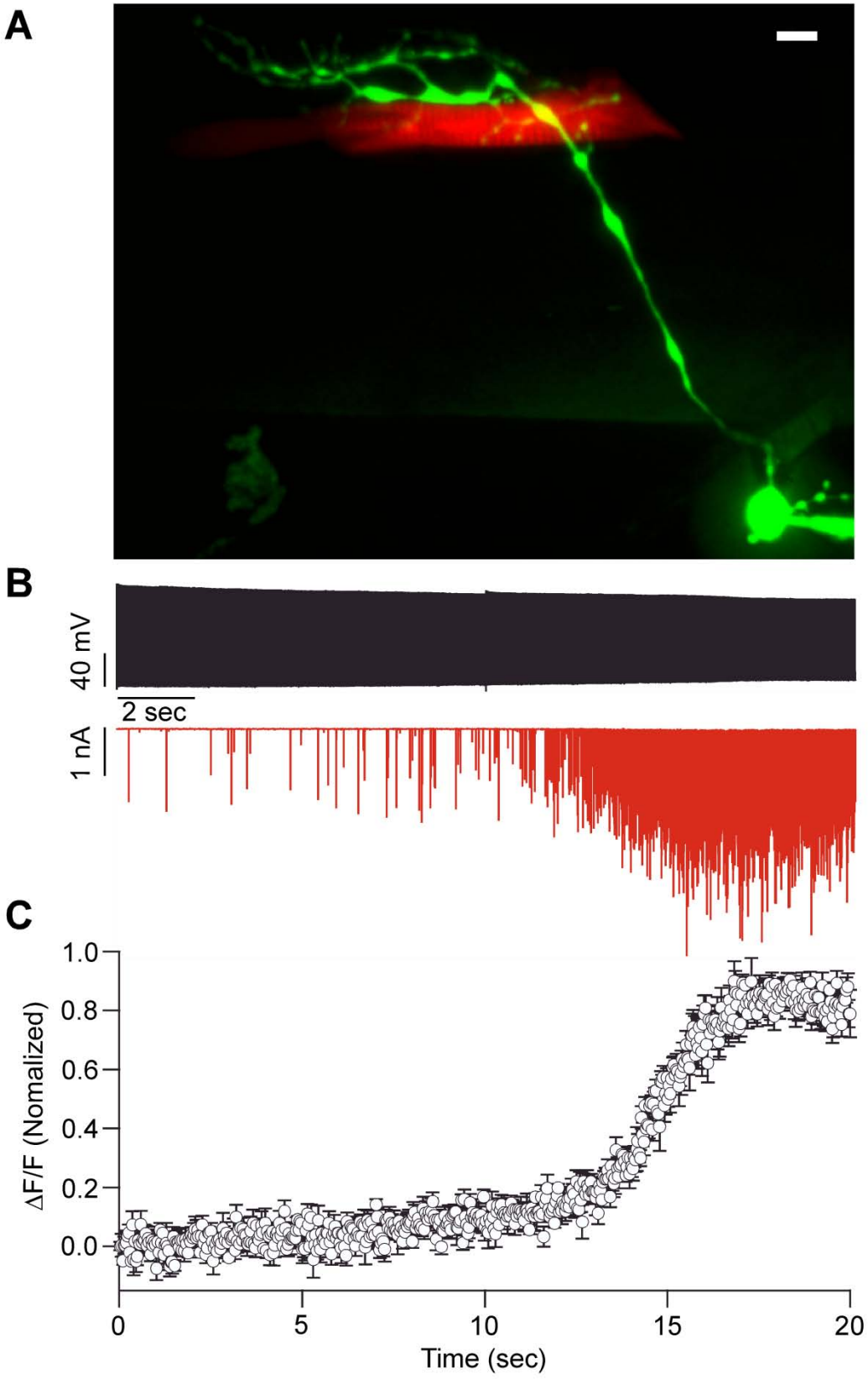
A
B
40 mV
2 sec
1 nA
C
ΔF/F (Nomalized)
1.0
0.8
0.6
0.4
0.2
0.0
0
5
10
15
20
Time (sec)

Figure 5.6 – A Delayed Calcium Wave is Generated During Prolonged High Frequency Stimulation in the Presence of ω-conotoxin GVIA

(A) A CaP motor neuron dye filled with Alexafluor-647. Image is taken from a single focal plane, corresponding to the focal plane used for the Ca^{2+} imaging in panels B-F (scale bar = 10 μm and applies to all panels). (B) Fluo-5F Ca^{2+} imaging of the motor neuron in A prior to 100 Hz stimulation with the soma apparent in the lower right corner. Intensity of the Ca^{2+} signal is represented by a heat map (shown in panel F) where red indicates high levels of Ca^{2+} and dark blue represents low Ca^{2+}. (C) An image taken after 100 APs shows a large increase in the Ca^{2+} signal in the axon initial segment while the axonal arbor remains virtually unchanged, with the exception of weak signals in several areas of the principal branch of the axon. (D) After 2 seconds of stimulation more distal sections of the primary axon branch have elevated Ca^{2+} levels. (E) 3 seconds into the stimulus all but the most distal synaptic boutons have experienced a rise in Ca^{2+}. (F) By 4 seconds the most distal boutons (upper left corner) have higher Ca^{2+} levels.

Fig. 5.6

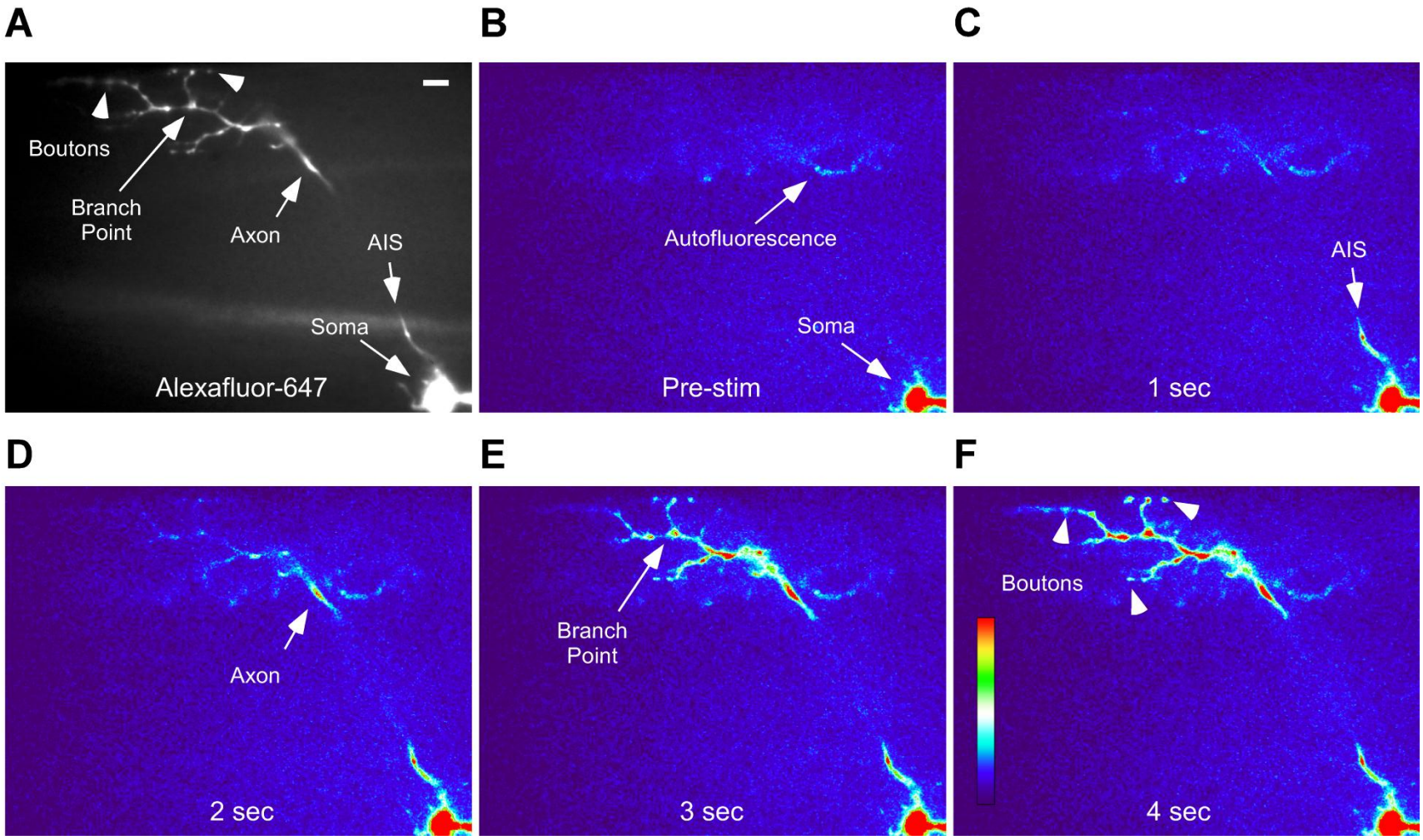
A
B
C
Boutons
Branch Point
Axon
AIS
Soma
Alexafluor-647
Autofluorescence
Soma
Pre-stim
AIS
1 sec
D
E
F
Axon
2 sec
Branch Point
3 sec
Boutons
4 sec

Figure 5.7 – Distance Dependence of Calcium Rise is Determined by Morphological Analysis

Imaris FilamentTracer software was used to create accurate morphological reconstructions of the 3D structure of CaP motor neurons and regions of interest from Ca^{2+} imaging were then mapped to this structure to determine the distance dependence of the timecourse of Ca^{2+} rise. (A) An Imaris reconstruction superimposed on a 60 μm stack of 60 Alexafluor-647 1 μm images of a CaP motor neuron. Four colored ROIs are represented on the reconstruction which correspond to regions where Ca^{2+} were measured in B and C (scale bar = 20 μm for A and B). (B) Fluo-4 Ca^{2+} imaging of the CaP motor neuron during a 10 second 100 Hz stimulus train in the presence of ω-conotoxin GVIA. The series of Ca^{2+} images are the same as those in Fig. 5.6 and show the four sample ROIs measured. (C) Traces of the Ca^{2+} responses from the ROIs in B, with the most proximal region in blue, and progressively more distal regions in red, green and orange, respectively. For each region (and others not represented here) the time to reach 20% of the maximal fluorescence was determined (dashed line). (D) Plot of time to reach 20% of the maximal fluorescence and the corresponding distance from the soma for each region shown in A-C (colored circles) as well as other regions measured from the same experiment (black circles).

Fig. 5.7

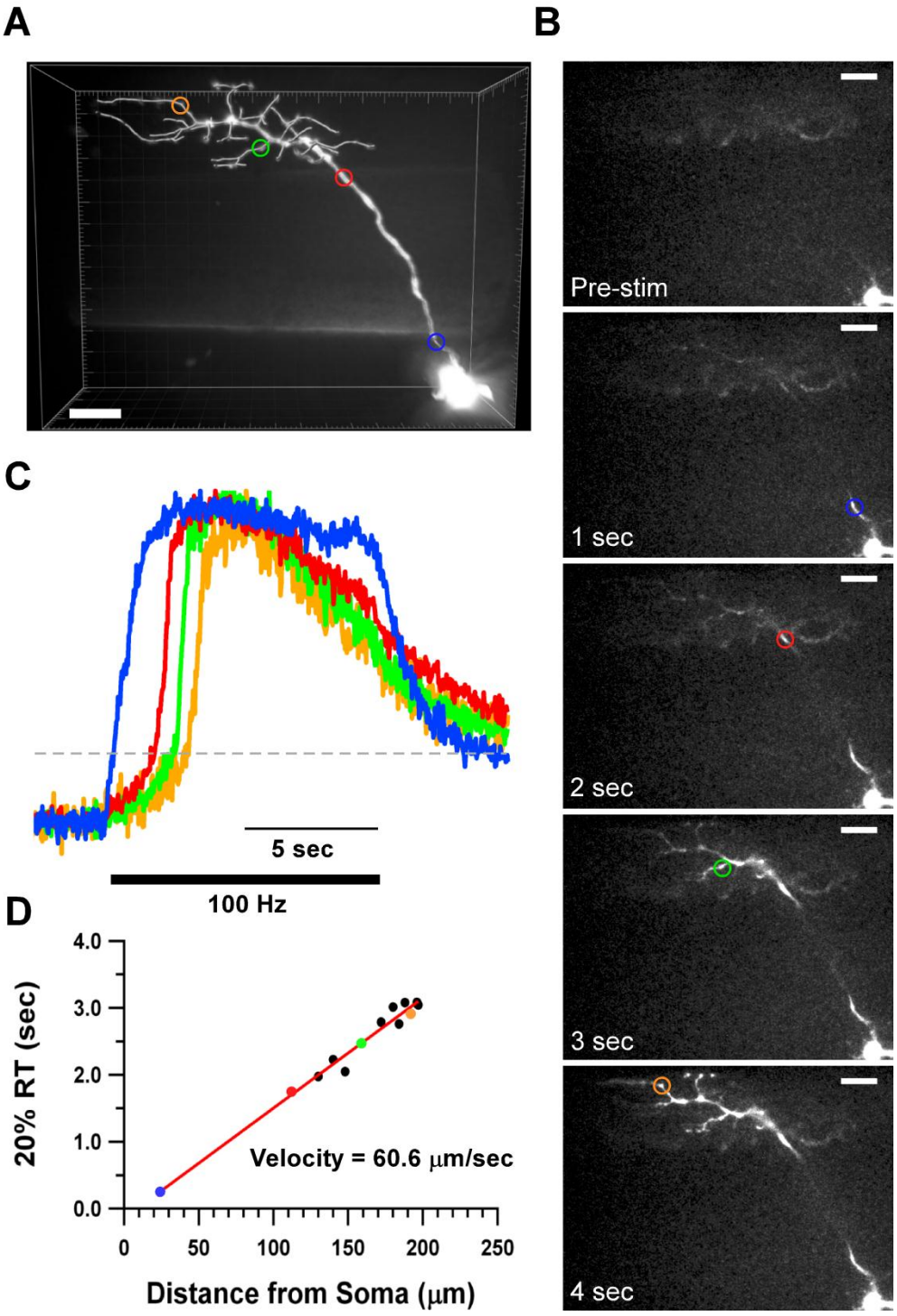
A
B
Pre-stim
1 sec
2 sec
3 sec
4 sec
C
5 sec
100 Hz
D
20% RT (sec)
4.0
3.0
2.0
1.0
0.0
0
50
100
150
200
250
Velocity = 60.6 μm/sec
Distance from Soma (μm)

Figure 5.8 – Cumulative Data Confirms the Distance Dependent Delay of Calcium in the Presence of ω-conotoxin GVIA

A distance vs. delay plot of individual ROIs binned according to distance from the soma (25 μm bins) both in the presence of ω-conotoxin GVIA (open circles, N = 85 boutons from 7 fish) and the control condition (closed circles, N = 91 boutons from 6 fish).

Fig. 5.8

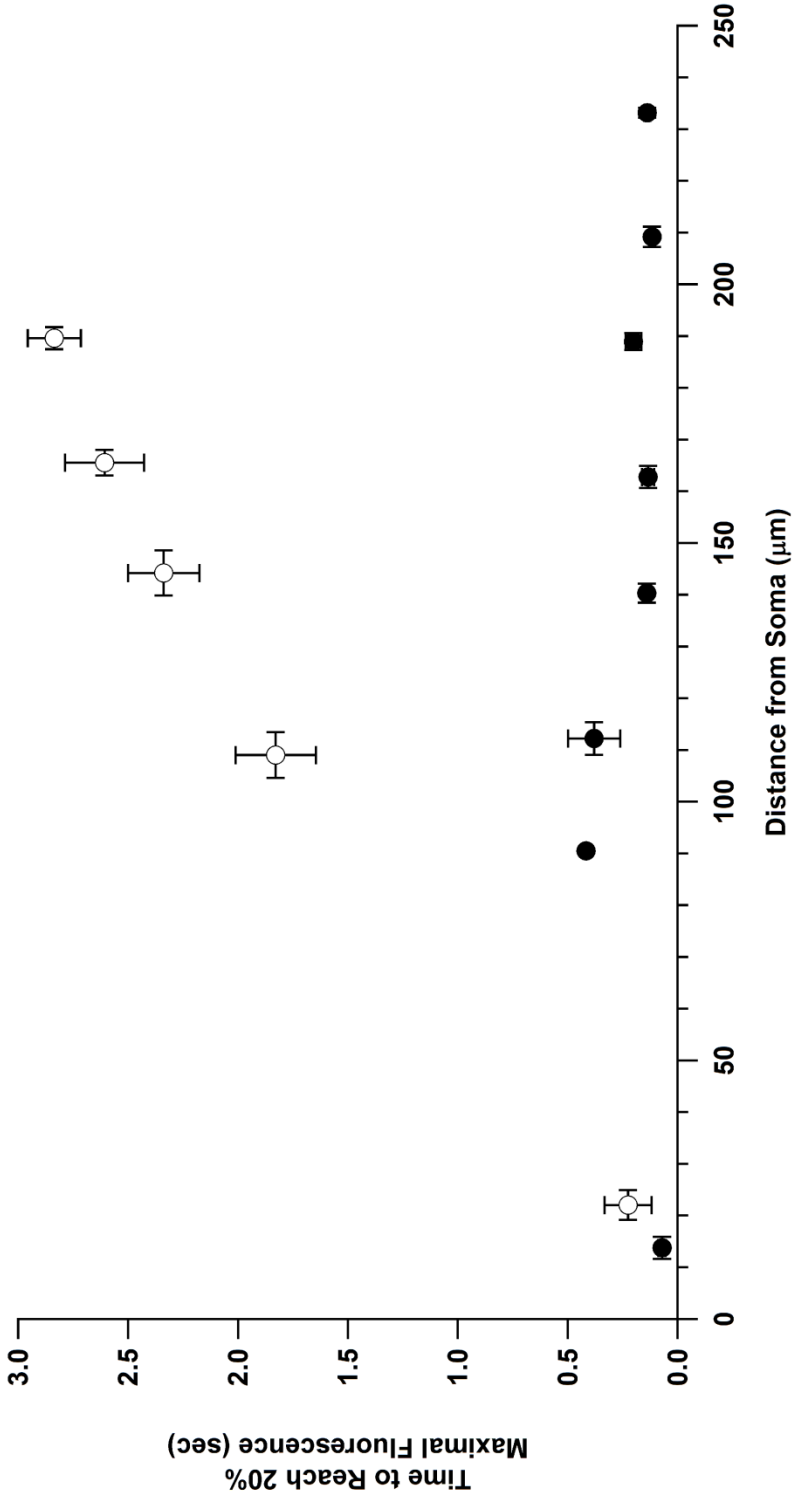
Time to Reach 20%
Maximal Fluorescence (sec)
3.0
2.5
2.0
1.5
1.0
0.5
0.0
0
50
100
150
200
250
Distance from Soma (μm)

Figure 5.9 – Distance dependent delayed Ca^{2+} rise in a CaP motor neuron

The imaging was performed at higher magnification (at 63x compared to 40x in Fig. 5.7) in order to focus on the area of innervation, where the axon branches extensively. (A) A series of timepoints of Fluo-5F Ca^{2+} imaging of a CaP motor neuron that was stimulated at 100 Hz for 10 seconds in the presence of ω-conotoxin GVIA. Five sample regions of interest are shown in the final panel (at the 4 second timepoint, scale bar = 10 μm for A and B). (B) The Imaris FilamentTracer reconstruction of the cell in A created from a 50 μm stack of images taken of the Alexafluor-647 dye fill (not shown), with the colored regions from A shown. (C) Fluo-5F fluorescence traces from a WT fish (cell not shown, black bar indicates the 100 Hz train). (D) Fluo-5F fluorescence traces from a ω-conotoxin GVIA treated WT fish (same cell as A and B, black bar indicates the 100 Hz train). The colored regions in A and B correspond to the colored traces in D. (E) Distance vs. delay plot of the control cell in C (black circles) and the ω-conotoxin GVIA treated neuron (open diamonds). The colored markers for both control and ω-conotoxin GVIA treated correspond to the colored traces in C and D.

Fig. 5.9

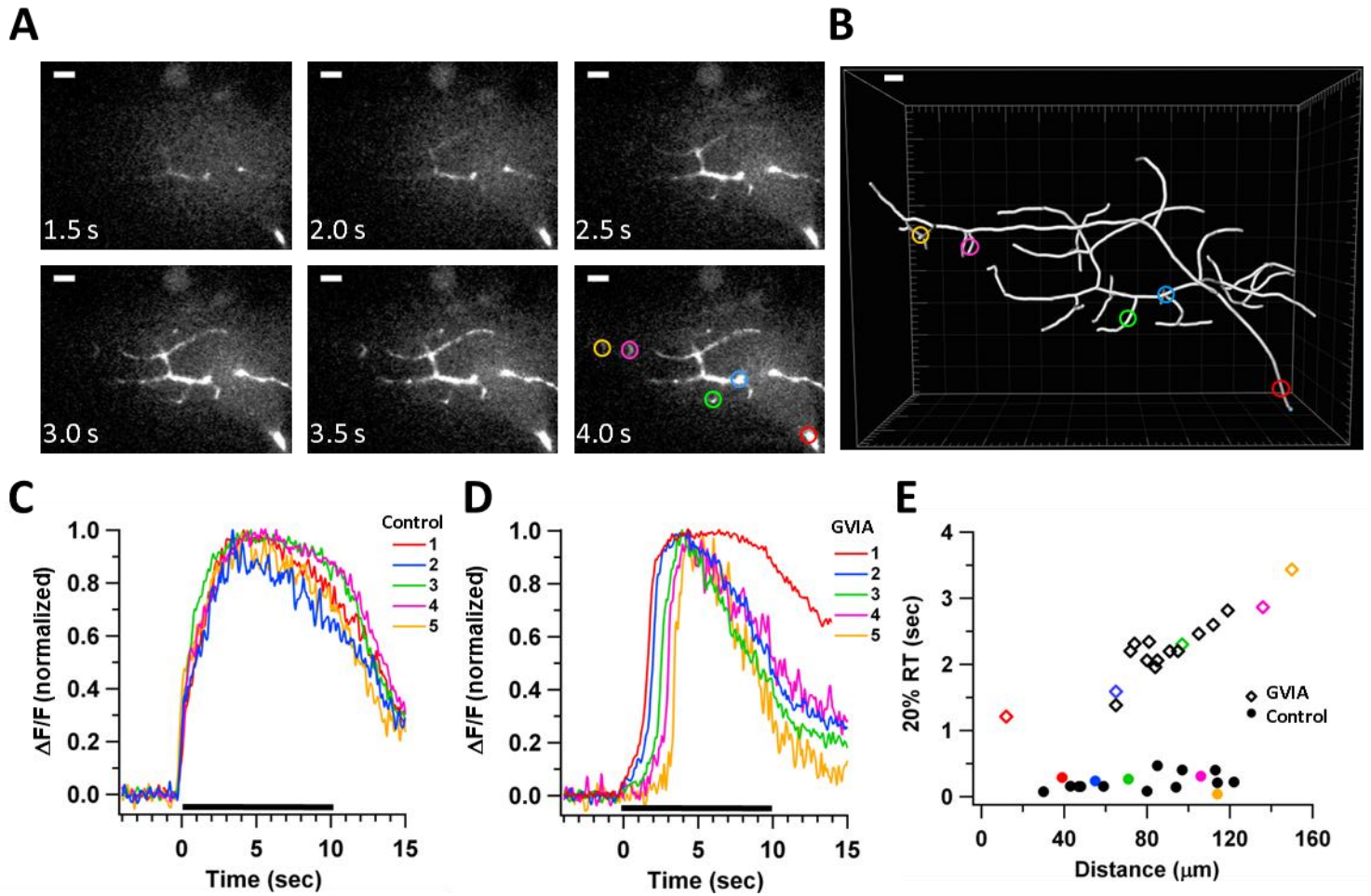
A
B
1.5 s
2.0 s
2.5 s
3.0 s
3.5 s
4.0 s
C
D
E
Control
GVIA
1
2
3
4
5
ΔF/F (normalized)
Time (sec)
20% RT (sec)
Distance (μm)

Figure 5.10 – Delayed Calcium Rise is Independent of Calcium Indicator Affinity and Mobility

(A) Comparison of the timing of bouton Ca^{2+} responses during 100 Hz stimulation in control and ω-conotoxin GVIA conditions for two Ca^{2+} indicators (Fluo-4 and Fluo-5F) which differ in their affinity for Ca^{2+} by approximately 10 fold. In control, Fluo-4 delay was 0.18 ± 0.02 seconds (N = 64 boutons from 4 fish), and Fluo-5F delay was 0.26 ± 0.02 seconds (N = 91 boutons from 6 fish). For ω-conotoxin GVIA treated motor neurons, the Fluo-4 bouton delay was 1.98 ± 0.1 seconds (N = 69 boutons from 6 fish), and Fluo-5F delay was 2.13 ± 0.07 seconds (N = 85 boutons from 7 fish). Data are presented as the mean ± S.E.M. For *** $P < 0.001$. N.S. denotes no significance. (B) The low mobility Ca^{2+} indicator, Oregon Green BAPTA-1 dextran, was tested in a single experiment. The CaP motor neuron was stimulated at 100 Hz for 10 seconds after allowing the dye to dialyze the neuron for 30 minutes. Distances and Ca^{2+} delay were determined in a similar manner as in Fig. 5.7 and 5.9 and were plotted with the cumulative data from Fig. 5.8 for comparison (green circles are Oregon Green BAPTA-1 dextran).

Fig. 5.10

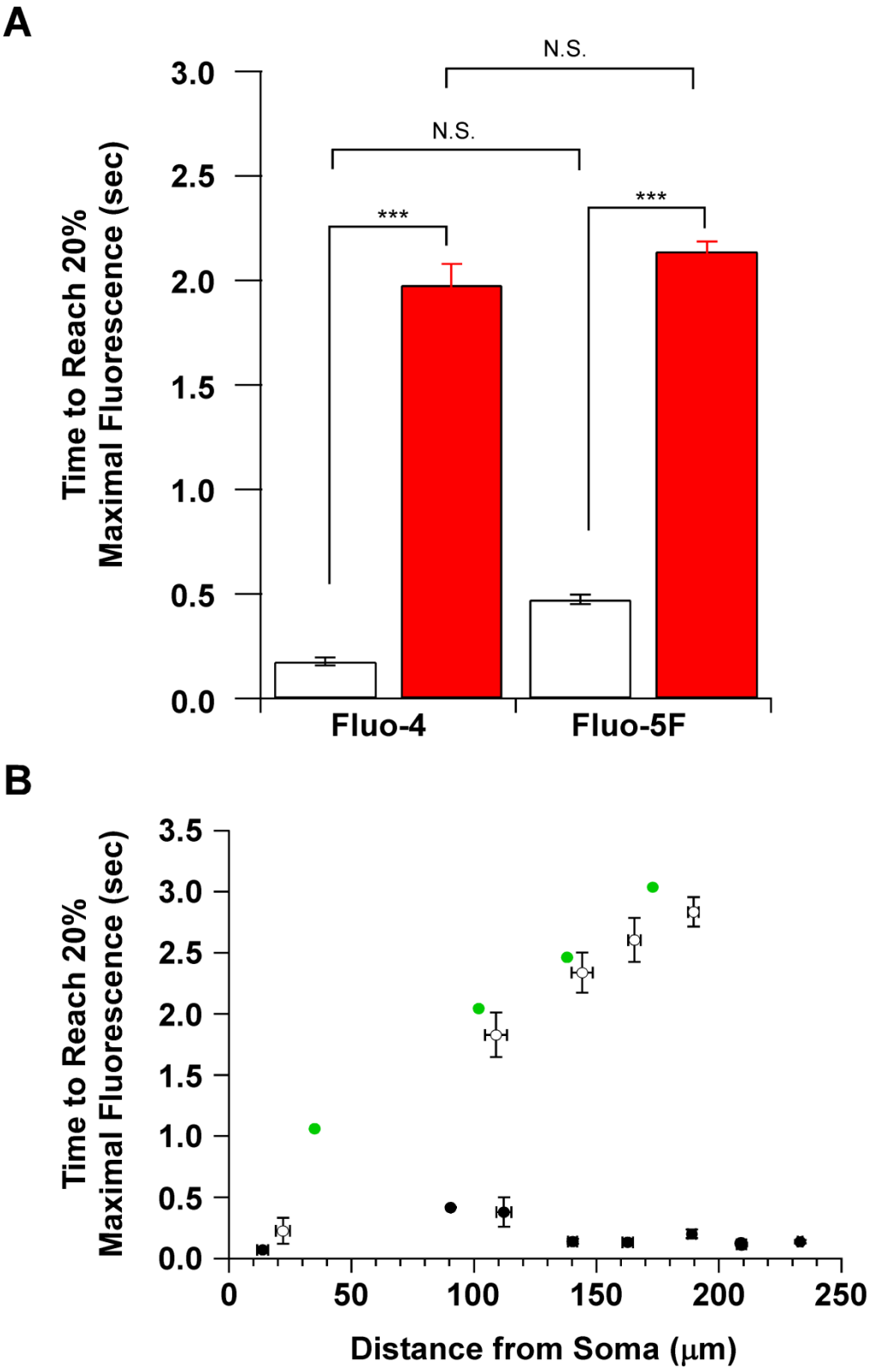
A
N.S.
N.S.
***
***
Time to Reach 20% Maximal Fluorescence (sec)
3.0
2.5
2.0
1.5
1.0
0.5
0.0
Fluo-4
Fluo-5F
B
Time to Reach 20% Maximal Fluorescence (sec)
3.5
3.0
2.5
2.0
1.5
1.0
0.5
0.0
0
50
100
150
200
250
Distance from Soma (μm)

Figure 5.11 – The Calcium Wave Can Propagate in the Absence of Sustained APs

(A) Paired recording from a CaP motor neuron stimulated at 100 Hz. The post-synaptic EPCs were monitored (red traces, below) and the AP train (black traces) was halted prior to the onset of the delayed asynchronous release. (B) Ca^{2+} imaging with Fluo-4 indicator in an untreated WT CaP motor neuron for comparison with C. The neuron was stimulated at 100 Hz for 10 seconds and the Ca^{2+} signal from a proximal (black trace) and a distal bouton (red trace) are shown to respond simultaneously. (C) Ca^{2+} imaging with Fluo-4 in a ω-conotoxin GVIA treated WT CaP motor neuron. This neuron was stimulated for 4 seconds at 100 Hz and the Ca^{2+} signal from a proximal (black trace) and a distal bouton (red trace). Note the delayed inflection in the distal bouton Ca^{2+} signal which occurs nearly 2 seconds after the APs have been halted.

Fig. 5.11

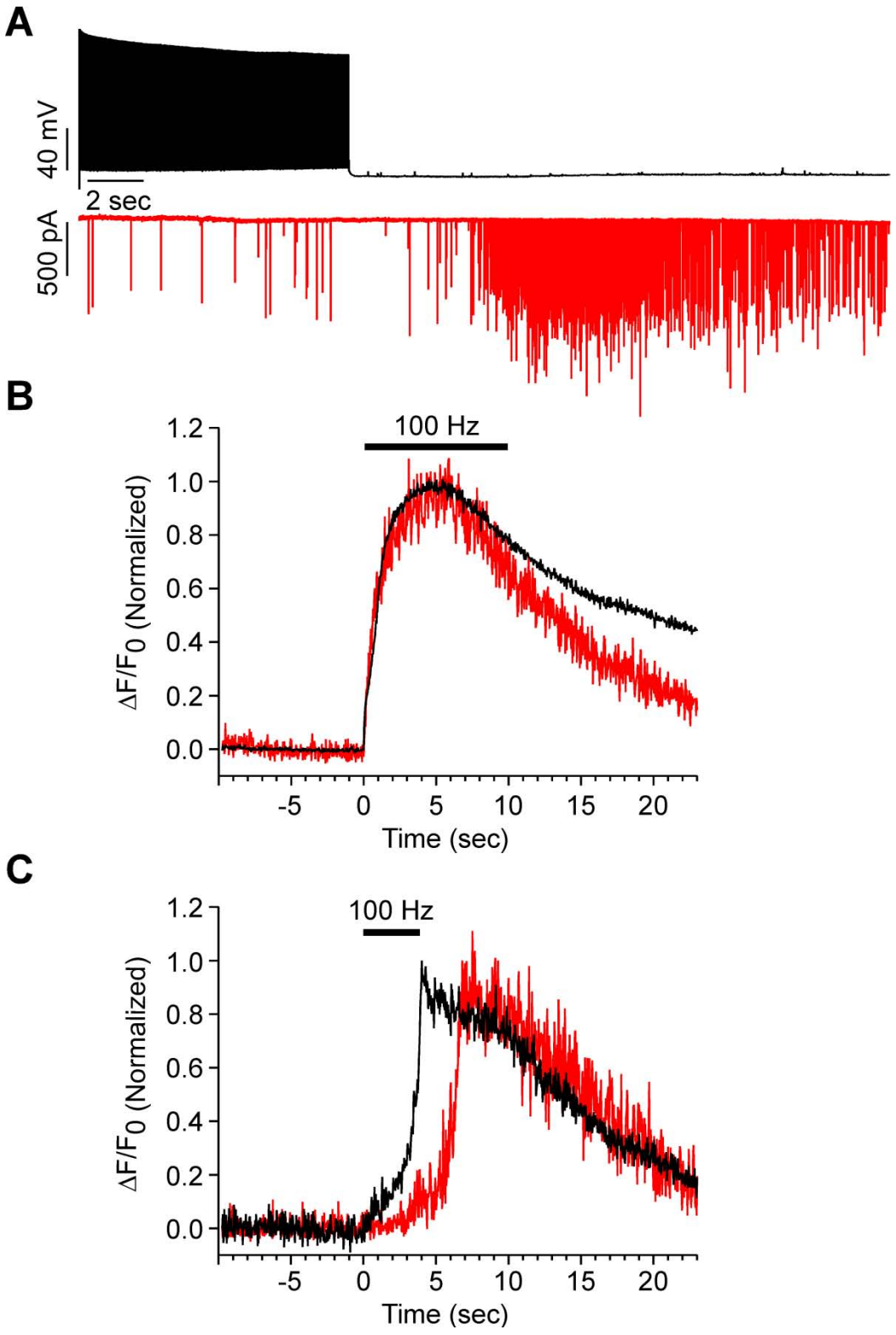
A
40 mV
2 sec
500 pA
B
100 Hz
ΔF/F0 (Normalized)
Time (sec)
C
100 Hz
ΔF/F0 (Normalized)
Time (sec)

Figure 5.12 – A Calcium Wave Can be Generated in the Absence of APs

The CaP motor neuron was bathed in 1 μM TTX and voltage clamped at -80 mV and subsequently depolarized to +50 mV. The Ca^{2+} signal from Oregon Green BAPTA-1 was monitored. (A) An image of the Ca^{2+} response showing ROIs which were measured and plotted in B. The colors of the regions correspond to the colored traces in B (scale bar = 20 μm). (B) Ca^{2+} responses from proximal and distal ROIs from A. The axon initial segment responds almost immediately to the voltage step (black trace) while other regions respond subsequently according to their relative distance from the soma, with proximal regions responding prior to distal regions.

Fig. 5.12

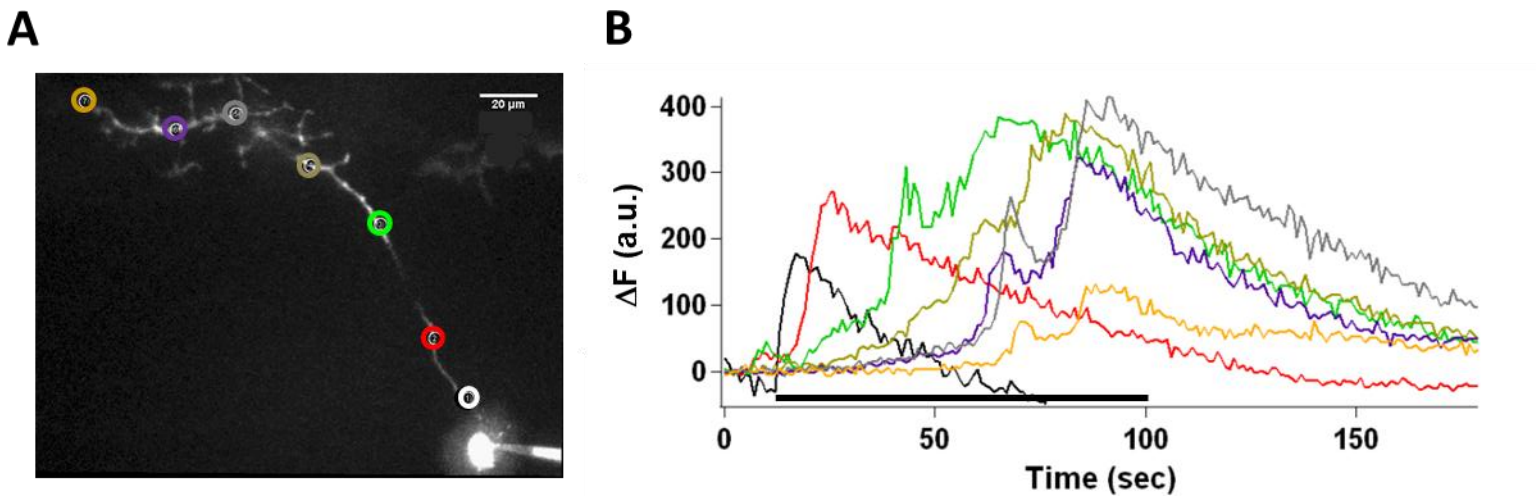

Figure 5.13 – Delayed Calcium Rise and Release are Sensitive to a Combination of Ni^{2+} and Mibefradil

(A) Paired recordings of wild type CaP motor neurons and target muscle showing the cumulative charge (binned in 1 second intervals) during a 20 second 100 Hz stimulation with 1 μM ω-conotoxin GVIA, 5 μM mibefradil and 100 μM Ni^{2+} (red traces, N = 4) and ω-conotoxin GVIA alone (black traces, N = 5, courtesy of Hua Wen). (B) Fluo-4 Ca^{2+} imaging of the axon of a CaP motor neuron stimulated at 100 Hz for 2 seconds (black bar) before (black trace) and after (red trace) application of ω-conotoxin GVIA, mibefradil and Ni^{2+}. (C) Ca^{2+} imaging of a bouton from a CaP motor neuron stimulated at 100 Hz for 2 seconds (black bar) before (black trace) and after (red trace) application of ω-conotoxin GVIA, mibefradil and Ni^{2+}.

Fig. 5.13

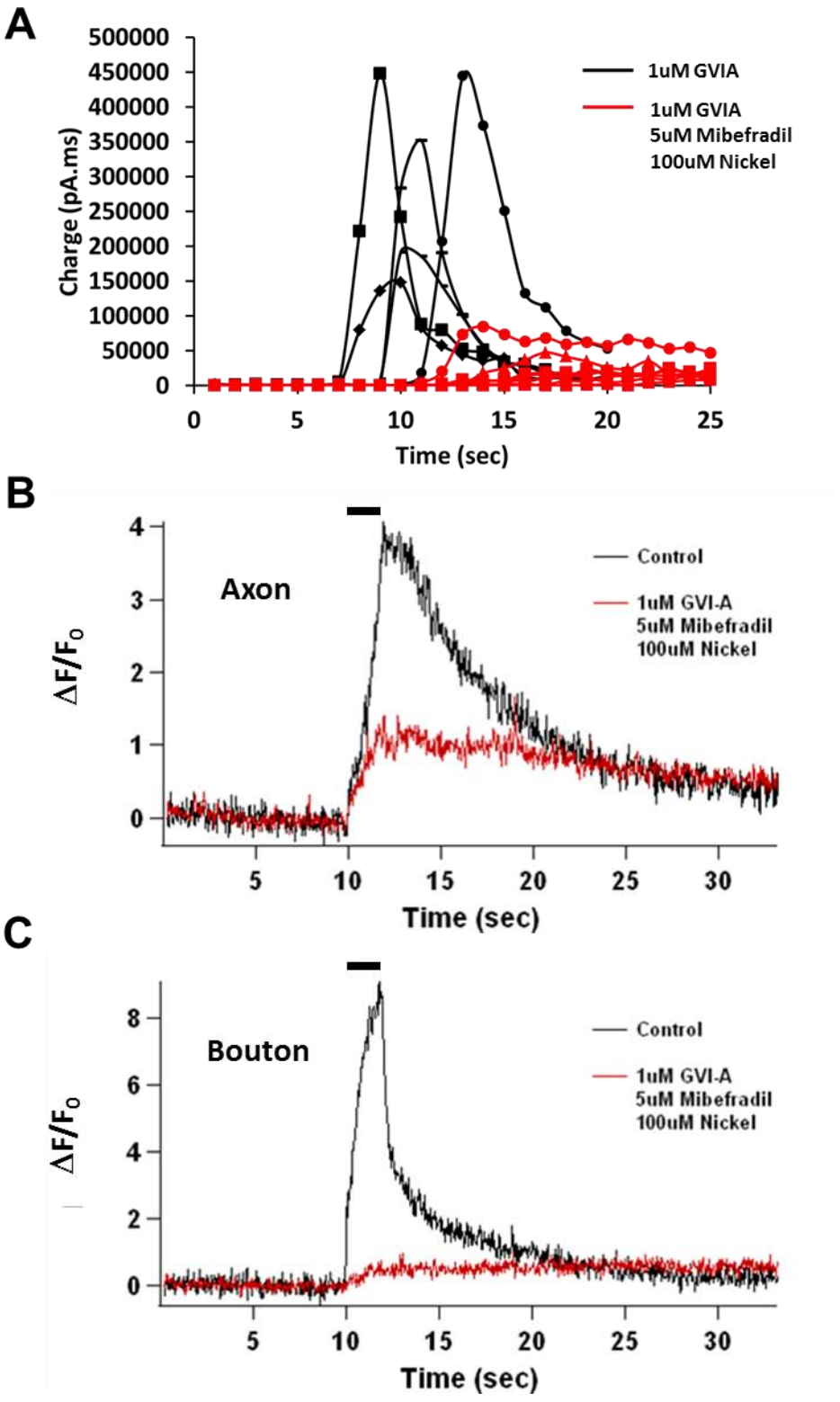
A
500000
450000
400000
350000
300000
250000
200000
150000
100000
50000
0
Charge (pA.ms)
0
5
10
15
20
25
Time (sec)
1uM GVIA
1uM GVIA
5uM Mibefradil
100uM Nickel
B
Axon
ΔF/F0
4
3
2
1
0
5
10
15
20
25
30
Time (sec)
Control
1uM GVI-A
5uM Mibefradil
100uM Nickel
C
Bouton
ΔF/F0
8
6
4
2
0
5
10
15
20
25
30
Time (sec)
Control
1uM GVI-A
5uM Mibefradil
100uM Nickel

Figure 5.14 – A T-type Calcium Channel Antagonist is Ineffective at Blocking the Calcium Wave

Fluo-5F calcium imaging of a CaP motor neuron stimulated at 100 Hz for 10 seconds (black bar) after the application of 1 μM ω-conotoxin GVIA and 5 μM TTA-P2. The red trace is the fluorescence response from the AIS. The small amplitude traces (dark purple and grey) are delayed responses from distal boutons.

Fig. 5.14

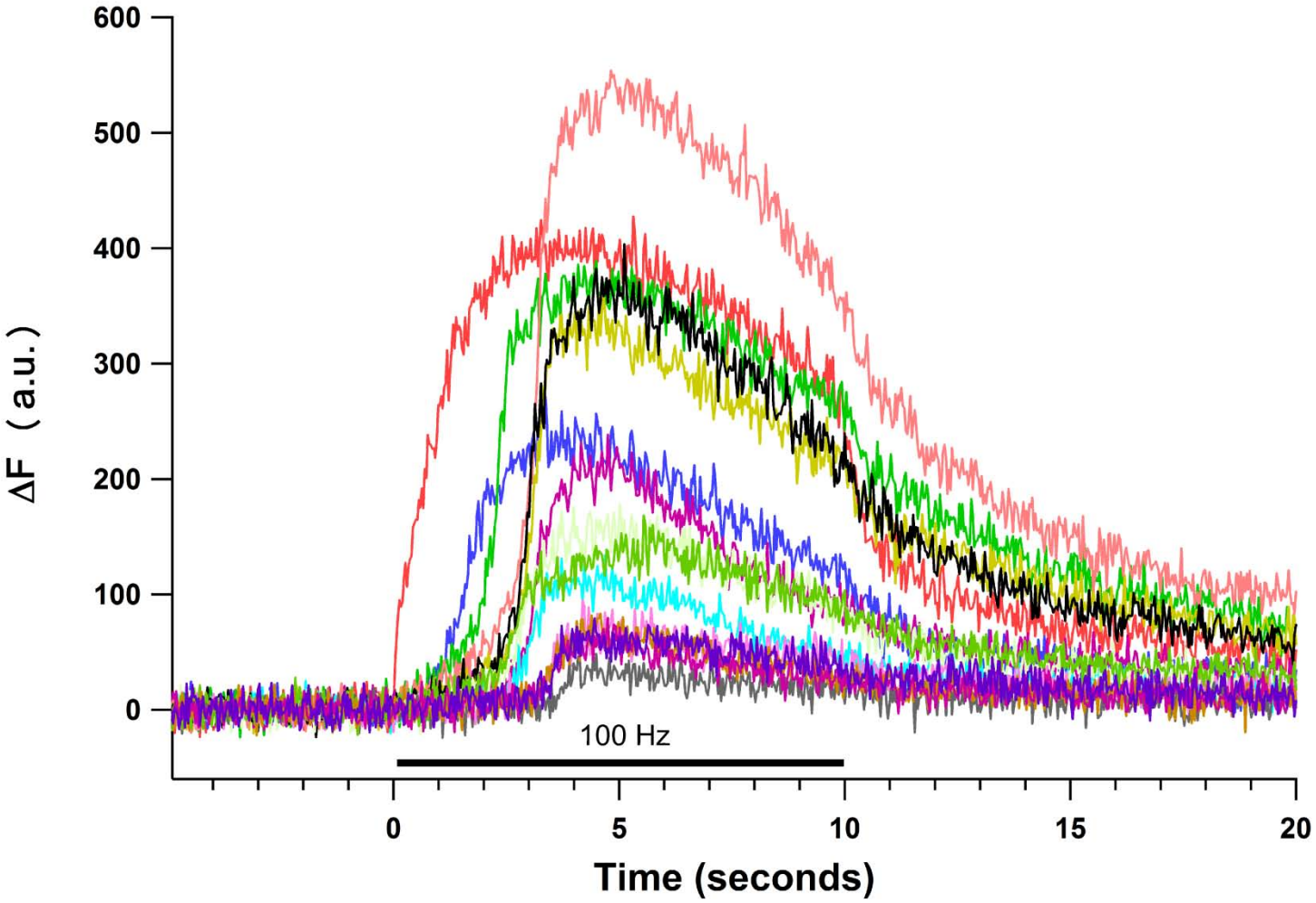

Figure 5.15 – Calcium Imaging In Low External Calcium Conditions the Wave is Nimodipine Sensitive

(A) Fluo-5F calcium imaging of the CaP motor neuron AIS in 200 μM Ca^{2+} external solution treated with ω-conotoxin GVIA (black circles, N = 5) or ω-conotoxin GVIA and 50 μM nimodipine (red squares, N = 5) and stimulated at 100 Hz for 20 seconds (black bar). (B) Calcium imaging of the axon (prior to branching) from the same cells as in A. Data are the mean ± S.E.M. (C) Integral of Ca^{2+} signals from the AIS (panel A) and axon (panel B) in the absence (black bars, N = 5) and presence of nimodipine (red bars, N = 5).

Fig. 5.15

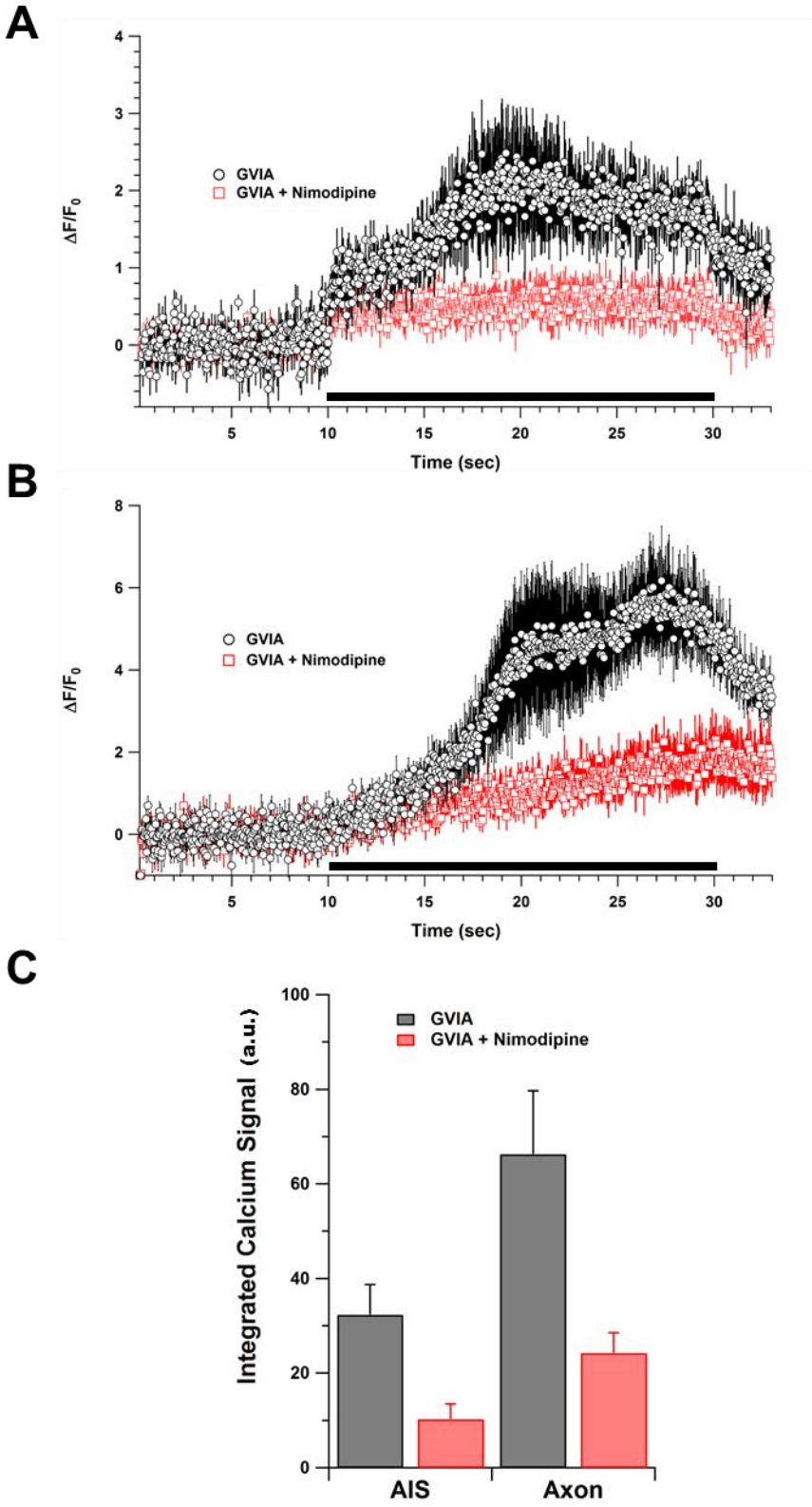
A
GVIA
GVIA + Nimodipine
ΔF/F0
Time (sec)
B
GVIA
GVIA + Nimodipine
ΔF/F0
Time (sec)
C
GVIA
GVIA + Nimodipine
Integrated Calcium Signal (a.u.)
AIS
Axon

Figure 5.16 – Nimodipine Consistently Eliminates the Wave Under Low Calcium Conditions

Individual cells from the experiment in Figure 5.15. (A) Ca^{2+} responses from the AIS of individual fish treated with ω-conotoxin GVIA alone show a slow increase in Ca^{2+} in 3 of 5 cells and an inflection with a rapid rise 2 of 5 cells. (B) When nimodipine and ω-conotoxin GVIA are applied together the AIS responses are small and flat with no rapid rise observed. (C) Ca^{2+} responses in the axon show a delayed increase in Ca^{2+} with variable amplitude and timing when ω-conotoxin GVIA alone is applied (same cells as A). (D) The axonal signal is nearly eliminated when CaP motor neurons are treated with both ω-conotoxin GVIA and nimodipine (same cells as B).

Fig. 5.16

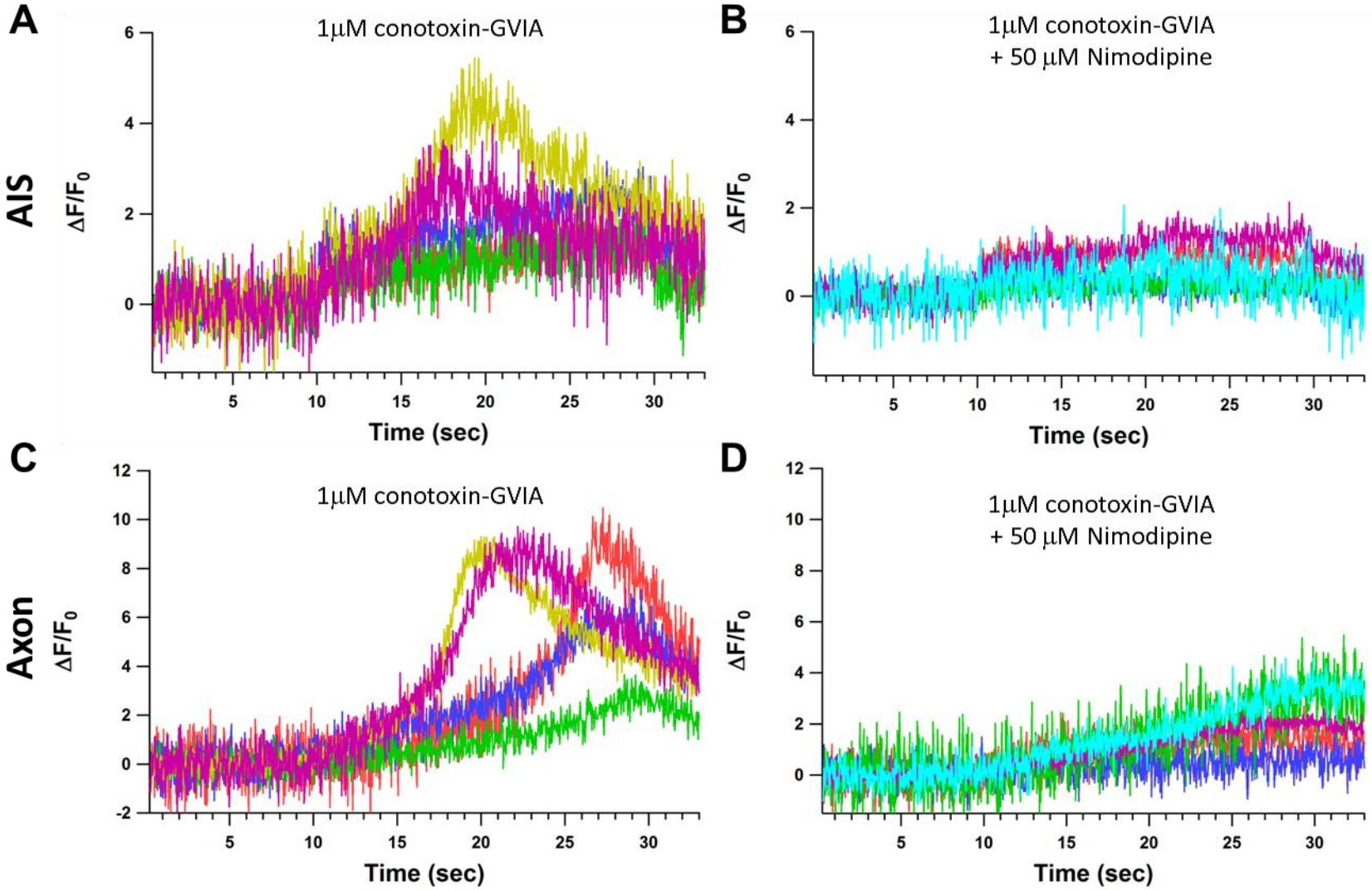
A
AIS
1μM conotoxin-GVIA
ΔF/F0
Time (sec)
B
1μM conotoxin-GVIA
+ 50 μM Nimodipine
ΔF/F0
Time (sec)
C
Axon
1μM conotoxin-GVIA
ΔF/F0
Time (sec)
D
1μM conotoxin-GVIA
+ 50 μM Nimodipine
ΔF/F0
Time (sec)

Chapter 6: General Discussion

My work in the Brehm lab has focused on synaptic transmission at the zebrafish neuromuscular junction, with a particular emphasis on presynaptic vesicle release. Close collaboration with Hua Wen, a postdoctoral fellow in lab, has been instrumental in furthering our understanding of the underlying mechanisms in play during evoked release. This collaboration has essentially evolved into a two pronged approach to attack questions which have arisen during my time in the lab. Using the power of the paired recording paradigm described in earlier chapters and imaging of both vesicle release and the Ca^{2+} dynamics responsible for transmission I believe that we have uncovered some previously unappreciated aspects of both synchronous and asynchronous transmitter release. Of course my hope is that these results may be borne out in other systems and stand the test of time at our synapse of choice as well.

Ca^{2+} channels and Synchronous Release

Voltage gated Ca^{2+} channels play a central role in neurotransmission at the neuromuscular junction as the gatekeepers of Ca^{2+} influx and thus the trigger for vesicle release. Therefore it has been of interest to learn the molecular identity of the Ca^{2+} channels involved. Curiously, some divergence has been reported between higher and lower vertebrates based on pharmacological studies. CaV2.2 channels (N-type) have been implicated at amphibian NMJ (Li et al., 2001; Sano et al., 1987; Thaler et al., 2001; Yazejian et al., 1997) while CaV2.1 channels (P/Q-type) are thought to be principally responsible for release at the mammalian NMJ (Bowersox et al., 1995; Katz et al., 1996; Protti and Uchitel, 1993; Uchitel et al., 1992). Experiments suggesting this difference were primarily based on pharmacology, using ω-

conotoxin GVIA purified from the venom of the sea snail, *Conus geographus*. The specificity of ω-conotoxin GVIA for N-type over P/Q-type channels had been established in mammalian preparations (Mintz et al., 1992a; Mintz et al., 1992b) and therefore presumed to extend to other vertebrates. The fact that ω-conotoxin GVIA application eliminates all synchronous release certainly supports the inclusion of zebrafish in the same group as other lower vertebrates such as frog. However, our experiments on the *tb204a* motility mutant line cause us to doubt the specificity of ω-conotoxin GVIA for N-type channels in these species. Synchronous release is compromised in *tb204a* fish (Fig. 4.1 and 4.2), and Ca^{2+} imaging indicates a lack of normal Ca^{2+} influx during stimulation (Fig. 4.3). These results suggested that the mutation in *tb204a* imparted a defect in the Ca^{2+} channel responsible for synchronous release, as opposed to a fault in another piece of fusion machinery. Given the steep Ca^{2+} dependence of vesicle release (Dodge and Rahamimoff, 1967), such a defect could have severely deleterious effects on neuromuscular transmission.

Subsequent mapping of the mutation to a region near S6 of Domain IV of CaV2.1 confirmed the molecular identity of this channel as a P/Q-type Ca^{2+} channel, much to our surprise. This revelation spurned additional experiments which were not discussed in chapter 4. Namely, the full length clones of both the Y1662N *tb204a* mutant and a corrected version of the CaV2.1 channel were expressed in HEK cells for pharmacological profiling, confirming the ω-conotoxin GVIA sensitivity of the zebrafish P/Q-type channel (Wen et al. submitted). Whether or not amphibian NMJ actually uses P/Q-type Ca^{2+} channels for vesicle release awaits molecular, rather than pharmacological, identification. Thus, it is possible that all vertebrates in fact use P/Q-type channels for fast synchronous release and that previous studies may have relied too heavily on the presumed specificity of a particular toxin, ω-conotoxin GVIA. But only additional experimentation will answer those riddles.

During low frequency stimulation (i.e. 0.2 or 1 Hz) of CaP motor neurons, transmitter release is invariably synchronous. This is also true of short bursts of high frequency stimulation (100 Hz) as long as the duration is limited to approximately 1 second or less (Fig. 4.1 and 4.6). From the work presented here we know that the Ca^{2+} responsible for this type of release emanates from a ω-conotoxin GVIA sensitive channel which corresponds to a P/Q-type. While calcium's role in transmitter release has long been appreciated, the significance of its spatial and temporal profile upon entry into nerve terminals has been a major focal point of research more recently. Experiments injecting the Ca^{2+} chelators, BAPTA and EGTA, into the squid giant synapse highlighted the importance of close proximity between vesicles and Ca^{2+} channels. Because BAPTA binds Ca^{2+} more quickly than EGTA, the effect was that transmitter release was abolished in BAPTA injected, but not EGTA injected preparations (Adler et al., 1991). It is widely accepted that when an action potential invades the presynaptic terminal, the subsequent opening of VGCCs causes a brief but large rise in the local Ca^{2+} concentration surrounding the channel. The limited region of high Ca^{2+} concentration as well as a low affinity trigger for exocytosis are thought to be key features of synchronous release (Neher and Sakaba, 2008; Sudhof, 2004).

Mechanisms of Asynchronous Release

At most synapses, synchronous release predominates, particularly during low frequency stimulation (Atluri and Regehr, 1998; Barrett and Stevens, 1972; Goda and Stevens, 1994). Although, in one peculiar instance, there is a report of an inhibitory synapse which releases transmitter almost exclusively asynchronously, even at low firing rates (Best and Regehr, 2009). Typically, asynchronous release becomes prominent at higher firing frequencies (Hefft and Jonas, 2005; Lu and Trussell, 2000). This is also true of the zebrafish NMJ. In the absence of any

inhibitor, asynchronous release always follows a period of phasic release if the motor neuron is stimulated at a high enough frequency (≥ 10 Hz, Hua Wen, personal communication). As the frequency increases, the time to onset of asynchronous release decreases. Two causes for asynchronous release are thought to be, 1) the accumulation of residual Ca^{2+} from prior stimuli (Zucker and Regehr, 2002), and 2) a Ca^{2+} sensor (possibly a synaptotagmin) for exocytosis different than that of synchronous release (Sun et al., 2007). First I will address the work that has been done recently on the Ca^{2+} sensors for different modes of release, as there is a recent report from our lab that speaks to this point. Then I will discuss how my data presented here relates to the notion of an expanding Ca^{2+} domain as causal to asynchronous release.

Clearly the triggering molecule plays an important role, and some studies posit that it is the Ca^{2+} sensor itself that is in fact the determining factor for synchronous vs. asynchronous release (Fernandez-Chacon et al., 2001; Maximov and Sudhof, 2005; Sun et al., 2007; Tang et al., 2006; Wen et al., 2010; Yao et al., 2011). Syt1 and Syt2 are two closely related Ca^{2+} sensors that appear to function similarly in regulating synchronous release. For example, at the calyx of Held synapse in mice, Syt2 knockdown blocks the majority of synchronous release, as assessed by paired recordings. However, at these synapses, asynchronous release remained intact. (Sun et al., 2007). While the asynchronous sensor was not explicitly identified, the authors proposed a model where dual Ca^{2+} sensors compete for and operate on the same vesicle pool. Their dual sensor model also predicts that while the Ca^{2+} affinity of each sensor is roughly the same (~ 40 μM), the on-rate for Ca^{2+} is much slower and the degree Ca^{2+} cooperativity is lower for the asynchronous sensor (Sun et al., 2007).

Results published from our lab show that synchronous release at the NMJ is mediated by Syt2 as well (Wen et al., 2010). This work implicated a second synaptotagmin, Syt7, as the

sensor for asynchronous release. Each mode of release could be isolated on the basis of knockdown of either Syt2 or Syt7 using morpholinos. The total release elicited by a 10 second 100 Hz stimulus train of the CaP motor neuron was similar in wild type, Syt2 morpholino, and Syt7 morpholino fish, arguing that each mode of release is drawing from a common pool of vesicles (Wen et al., 2010). In the presence of ω-conotoxin GVIA, I have shown that release is exclusively asynchronous in response to the 100 Hz train of APs (Fig. 5.1). This begs the question as to whether or not Syt7 is acting as the Ca^{2+} sensor when ω-conotoxin GVIA sensitive Ca^{2+} currents are blocked. To address this question, Syt7 expression was selectively knocked down using a morpholino. High frequency stimulation of the CaP motor neuron in ω-conotoxin GVIA treated Syt7 morpholino fish showed that asynchronous release was not abolished using paired recordings, suggesting that other Ca^{2+} sensors can mediate delayed release when Syt7 is eliminated (Hua Wen, personal communication). More recently, two other molecules have been identified which are also thought to selectively maintain asynchronous release, Doc2 (Yao et al., 2011) and VAMP4 (Raingo et al., 2012). The ability of these newly identified sensors to support asynchronous release at the zebrafish NMJ should be tested in the same manner as Syt7 (Wen et al., 2010).

Another important component of vesicle release is how closely coupled these sensors for neurotransmission are to the source of Ca^{2+}. As described previously, the distance between the Ca^{2+} source and the vesicles can be probed by loading exogenous Ca^{2+} chelators into the presynaptic terminal (Adler et al., 1991). BAPTA and EGTA are molecules which bind Ca^{2+} with similar affinities but the on-rate for BAPTA is larger than that of EGTA, which makes these buffers good tools to investigate the distance between the Ca^{2+} channels and the sensors. If BAPTA is required to disrupt release then the distance between vesicle and channel is thought to be small (< 100 nm), and thus considered a nanodomain. Whereas if release is disrupted by

EGTA the distance is generally thought to be greater. This weaker coupling is often referred to as a microdomain (Eggermann et al., 2012). A number of studies also show that delayed release tends to be particularly sensitive to EGTA (Atluri and Regehr, 1998; Hefft and Jonas, 2005; Lu and Trussell, 2000; Stevens and Wesseling, 1998). If delayed release is therefore more sensitive to EGTA than phasic release, then it stands to reason that the coupling is looser for delayed release than synchronous release. In one instance, the Ca^{2+} sensor, Syt2 may play an additional role of localizing the vesicle to the release site and stabilizing the coupling between Ca^{2+} influx and release (Young and Neher, 2009). The authors found that specific mutations in Syt2 could enhance the synaptic delay at the calyx of Held. Another active zone protein, RIM, has recently been shown to link the fusion apparatus to Ca^{2+} channels (specifically P/Q and N-type). When RIM1 and RIM2 are knocked out in cultured hippocampal neurons, release is desynchronized and EGTA-AM treatment blocks release more effectively (Han et al., 2011). Therefore, the synchronicity of release appears to be controlled by the extent to which Ca^{2+} can diffuse following the brief openings of VGCCs which occur during an AP and subsequently interact with the Ca^{2+} sensors that mediate fusion (Neher and Sakaba, 2008). In addition, the degree of coupling is not necessarily static, as developmental changes have been observed, again at the calyx of Held. This study demonstrated that EGTA was less effective at inhibiting release as the mice aged (Fedchyshyn and Wang, 2005).

A Propagating Ca^{2+} Wave Causal to Asynchronous Release

Asynchronous release is loosely defined as synaptic transmission that occurs in a delayed manner with respect to the action potential. Evidence of this delay comes in different forms experimentally and the amount of time that must pass between the AP and the post-synaptic response varies. There are several factors that are generally considered hallmarks of

asynchronous release: 1) it is delayed with respect to the stimulus, 2) it occurs in response to a global rise in Ca^{2+}, 3) it is persistent and, 4) sensitive to EGTA. I believe that my data presented in the previous chapters shows that a new model where a secondary source of Ca^{2+} ignites a propagating Ca^{2+} wave and induces delayed transmitter release can account for all of the above features of asynchronous release.

The global increase in presynaptic Ca^{2+} that is normally associated with slow or asynchronous release is typically thought to emanate from the same Ca^{2+} channels that evoke the fast synchronous release (Neher and Sakaba, 2008; Wadel et al., 2007). Perhaps because Ca^{2+} diffusion is generally thought to be extremely limited and tightly regulated (discussed below), the idea that a distal Ca^{2+} source could affect transmitter release has not been widely considered. The work presented here argues that a separate Ca^{2+} source, which is distal to the channels present at release sites, may initiate asynchronous transmitter release. In this scenario, the delayed onset of asynchronous release would be due to the convergence of two Ca^{2+} sources upon the vesicle population. The primary source is comprised of the active zone Ca^{2+} channels (P/Q-type) while the secondary source is distal to the release sites. The delay, I believe, is determined by the time it takes for the distal Ca^{2+} to arrive at the synaptic terminal. Several pieces of evidence which were determined by virtue of the fact that synchronous release could be entirely eliminated through the use of ω-conotoxin GVIA (Fig. 4.1B and 5.1B), support this line of reasoning. First, when isolated with ω-conotoxin GVIA, the asynchronous release could be further delayed by increasing the concentration of the exogenous buffer, EGTA (Fig. 5.3 and 5.4). The paired motor neuron target muscle recordings with simultaneous Ca^{2+} imaging indicate that the delayed Ca^{2+} increase is coincident with the delayed release (Fig. 5.5). Moreover, Ca^{2+} imaging performed on CaP motor neurons indicates that the distal Ca^{2+} travels to

release sites as a propagating Ca^{2+} wave. Evidence points to the propagation time for the wave as causal to the delayed Ca^{2+} rise in synaptic terminals (Fig. 5.6-5.9).

Morphological analysis was a key component in establishing the distance dependence of the Ca^{2+} delay. By filling the motor neuron with Alexafluor-647, in addition to a Ca^{2+} indicator, it was possible to create precise reconstructions of entire cells (Fig. 2.1 and 3.1). This was an important step because in order to maximize temporal resolution I was limited to acquiring images in a single focal plane for Ca^{2+} imaging. By matching the regions of interest from Ca^{2+} imaging to the morphological reconstruction produced offline in the Imaris FilamentTracer software, I could assign accurate distances from the soma for example to the ROIs chosen from the Ca^{2+} imaging movies (Fig. 2.2). In many ways the layout of the CaP motor neuron provided an ideal situation for these studies. At the appropriate magnification, it was possible to capture images of the soma, AIS, portions of axon and numerous synaptic boutons within a single focal plane which allowed me to sample relevant portions of the neuron simultaneously with good temporal resolution (30 FPS). While the Ca^{2+} imaging movies gave the impression of a Ca^{2+} wave, it was through the combination of the morphological measurements with the Ca^{2+} imaging data that I could actually quantitate the distance dependence of the observed delay (Fig. 5.7, 5.8 and 5.9).

Ca^{2+} Waves

Calcium waves have been widely reported in the literature and come in various forms, both intracellular and intercellular. Early examples of this include an intracellular Ca^{2+} wave in madeka (*Orysias latipes*) eggs induced upon fertilization (Gilkey et al., 1978). The hydrozoan coelenterate, *Obelia geniculata*, has specialized bioluminescent photocytes which are activated by an intercellular Ca^{2+} wave that propagates through gap junctions between endodermal cells

and the coupled photocytes (Brehm et al., 1989; Dunlap et al., 1987). Two types of Ca^{2+} wave have been described which both require the efflux of Ca^{2+} from the endoplasmic reticulum. Calcium induced Ca^{2+} release (CICR) from internal stores can be mediated by activation of ryanodine receptors (RyRs) or through IP_3 receptors to evoke regenerative waves (Berridge et al., 2000). IP_3R mediated waves were initially described in *Xenopus laevis* oocytes (Lechleiter et al., 1991; Lechleiter and Clapham, 1992). In neurons, Ca^{2+} waves can direct growth cone migration (Guan et al., 2007; Lautermilch and Spitzer, 2000), and have been measured in apical dendrites of CA1 pyramidal neurons (Nakamura et al., 1999; Nakamura et al., 2002). To my knowledge there are no reports of Ca^{2+} waves initiating neurotransmitter release, however a number of studies have proposed a roll for intracellular stores in exocytosis (Fitzjohn and Collingridge, 2002). Many of these reports involve CICR at synapses of CNS neurons (Bardo et al., 2006; Emptage et al., 2001; Isokawa and Alger, 2006; Sharma and Vijayaraghavan, 2003; Tang et al., 2011; Unni et al., 2004). But of particular interest with respect to my work are several studies which claim that CICR from RyRs is directly involved in asynchronous release at the frog NMJ (Kubota et al., 2005; Narita et al., 2000; Narita et al., 1998; Soga-Sakakibara et al., 2010). Blocking Ca^{2+} uptake into the ER as well as the inhibition of RyRs with ryanodine reduced the level of asynchronous release generated during tetanic stimulation (Soga-Sakakibara et al., 2010).

Properties of the Primary Motor Neuron Ca^{2+} Wave

Due to the fact that the NMJ has been studied so extensively, I was surprised that reports of axonal Ca^{2+} waves have not been published. However, the conditions necessary to generate the wave in the CaP motor neuron were unusual, and as described earlier the motor neuron orientation is ideal for imaging multiple cellular compartments simultaneously. To

visualize a wave, ω-conotoxin GVIA was applied to the preparation, and the motor neuron APs were fired at high frequency for 10 seconds or longer depending on the concentration of EGTA in the patch pipette (Fig. 5.7 and 5.9). In the paired recordings, no EPCs initially resulted from the high frequency stimulation, but fortunately the 10-20 second 100 Hz protocol had been commonly utilized previously and therefore was also used in the presence of ω-conotoxin GVIA. To our surprise the delayed asynchronous release manifested during the prolonged stimulation (Fig. 5.1B). Calcium imaging of the wave gives the impression that the signal begins at the AIS (Fig. 5.7). It is directional and almost always proceeds away from the soma toward the synaptic boutons. The only exception to this observation was an experiment using TTX and somatic depolarization in voltage clamp mode, where the wave initially moved from the soma toward the boutons and subsequently reflected back and traveled the length of the neuron arriving once again at the soma (not shown). The Ca^{2+} signal in the AIS is never delayed with respect to the onset of stimulation, whereas areas along the axon typically show a shallow rise in Ca^{2+} until they reach a point of inflection at which time the Ca^{2+} rise increases rapidly (Fig. 5.7). This indicates the presence of a VGCC which is not sensitive to ω-conotoxin GVIA at the AIS. The most distal synaptic boutons show no appreciable rise in Ca^{2+} signal prior to the arrival of the wavefront, but a sharp rise occurs upon its arrival (Fig. 5.9 and 5.14).

I was concerned that the apparent Ca^{2+} wave could be an artifact of the Ca^{2+} indicator itself. Initial experiments were performed using Oregon Green BAPTA-1 which has a relatively high affinity for Ca^{2+} as compared to other indicators (K_d = 170 nM). My worry was whether or not I was observing an intrinsic response from motor neurons or if the indicator was binding to Ca^{2+} and then diffusing, giving the impression of a wave-like process. I tested lower affinity indicators such as Fluo-4 (K_d = 345 nM) and Fluo-5F (K_d = 2.3 μM) but found that the Ca^{2+} wave persisted and the delay was similar (Fig. 5.10A). The low affinity Ca^{2+} indicators are well suited

for observing fast Ca^{2+} dynamics in small compartments of cells (Svoboda and Mainen, 1999). All of these indicators however are small molecules capable of diffusing readily, which like endogenous mobile buffers can extend the effective diffusion of Ca^{2+} (John et al., 2001). Therefore, I thought that perhaps any mobile indicator could produce a potential artifact. To address this concern I tested a version of Oregon Green BAPTA-1 which is conjugated to dextran, making it much more immobile as compared to the other Ca^{2+} indicators used. The result was the same, the Ca^{2+} wave remained intact and the wave velocity was consistent with that of the mobile indicators (Fig. 5.10B). According to Gabso et al., the use of less mobile indicators should be the least invasive method of measuring intracellular Ca^{2+} (Gabso et al., 1997). The result did not come as a complete surprise given that we were confident that delayed release existed in the paired recordings, experiments which did not include any fluorescent Ca^{2+} indicators.

Once I was convinced that a bona fide Ca^{2+} wave was present I wanted to know if it was regenerative. To test this possibility, paired recordings were made in the presence of ω-conotoxin GVIA, and the motor neuron was stimulated at high frequency while the appearance of muscle EPCs was monitored. Then, several seconds before the onset of the delayed asynchronous release the stimulation was shut down. It was remarkable to see post-synaptic currents manifest in the absence of motor neuron action potentials, and it lent support to the idea that the propagating wave was regenerative (Fig. 5.11). Furthermore, in the Ca^{2+} imaging experiment which included TTX, it was possible to generate a Ca^{2+} wave in the complete absence of APs (Fig. 5.12). Presumably the opening of Ca^{2+} permeable channels located on or near the soma during the depolarization is sufficient to initiate the Ca^{2+} wave.

Triggering the Ca^{2+} Wave – A Secondary VGCC?

Cadmium is known to block VGCCs (Catterall, 2000). Application of cadmium completely eliminates release during high frequency stimulation (Hua Wen, personal communication) leading me to believe that the Ca^{2+} influx which supports both synchronous and asynchronous release is mediated by VGCCs. Using ω-conotoxin GVIA to isolate the delayed asynchronous release, I began to test antagonists of other VGCCs, based on the hypothesis that a secondary Ca^{2+} channel, distal to the release sites, was triggering the Ca^{2+} wave and hence the delayed asynchronous release. The simultaneous paired recording and Ca^{2+} imaging experiment provided good evidence that the delayed Ca^{2+} and delayed release were coincident, and I reasoned that if I could eliminate the Ca^{2+} wave we would also abolish the delayed release. While the pharmacological approach yielded some interesting leads, as I showed in chapter 4, even the agents that are considered highly specific (i.e. ω-conotoxin GVIA) can affect other channels. Additionally, the specificity of most drugs is typically determined for mammalian channels and therefore their ability to block the same channels in fish could differ. Despite this potential pitfall, I decided that a drug screening approach stood a reasonable chance to successfully identify the secondary channel.

Of course there exists a great number of channels that are permeable to Ca^{2+}, so I hoped a bit of luck might be on my side. Initially, the pharmacology was tested using normal bath recording solution (2.1 mM Ca^{2+}). Focus was placed on the R-type, T-type, and L-type channels. The combination of Ni^{2+} and mibefradil, applied at concentrations thought to favor the block of T-type channels (Furukawa et al., 2005; Lee et al., 1999; Martin et al., 2000; Randall and Tsien, 1997), showed promise. Paired recordings indicate that this combination both delayed and reduced the total release. The idea of a T-type channel as the trigger for the Ca^{2+} wave was

appealing due to recent evidence that these channels can localize to the AIS (Bender and Trussell, 2012; Grubb and Burrone, 2010), which is a region where the Ca^{2+} response is always immediate in the CaP motor neurons, regardless of the inhibitors present. In addition, the kinetics of T-type channels differ from the high voltage activated Ca^{2+} channels, and are thought to play a role during bursts of APs and long periods of activity due to the fact that the recovery from inactivation for these channels is fast, as compared to their HVA cousins (Perez-Reyes, 2003). But when a newly developed T-type antagonist, TTA-P2 (Dreyfus et al., 2010) was tested, there was no apparent effect on release nor the Ca^{2+} wave (data not shown and Fig. 5.14). Perhaps this is a situation where the pharmacology differs in the zebrafish. Nickel and mibefradil are known to block other Ca^{2+} channel subtypes, including L-type channels, albeit at higher concentrations (Bezprozvanny and Tsien, 1995; Mehrke et al., 1994; Mishra and Hermsmeyer, 1994; Viana et al., 1997; Zamponi et al., 1996). Results from both paired recordings and Ca^{2+} imaging for L-type channel antagonists were inconsistent. Of the L-type blockers tested, nifedipine and nimodipine showed some promise, while others such as verapamil and amlodipine caused AP failures during the high frequency train, and as such the block of Ca^{2+} influx could not be attributed to a specific block of a VGCC. It is also important to note that the dihydropyridines have been shown to antagonize T-type currents in heterologously expressed in oocytes (Furukawa et al., 2005; Furukawa et al., 2009), leaving open the possibility of T-type involvement in wave initiation.

Due to the robust nature of the Ca^{2+} wave, I decided to lower the external Ca^{2+} concentration. The goal was to uncouple whatever was triggering the wave from the wave itself. For instance, using 200 μM external Ca^{2+} without antagonist present, it was possible to trigger an immediate but gradual rise of Ca^{2+}. In this condition, the inflection point in the Ca^{2+} response normally associated with the onset of the wavefront was more delayed than usual

(data not shown). The addition of ω-conotoxin GVIA reduced the overall Ca^{2+} signal in the neuron, particularly in the boutons, however a weak Ca^{2+} wave in the axon persisted (Fig. 5.15 and 5.16). Under these conditions, I again tested the L-type antagonists. Nimodipine was consistently able to abolish the weak Ca^{2+} wave, suggesting that perhaps an L-type Ca^{2+} channel acts as the triggering mechanism (Fig. 5.15 and 5.16). The L-type Ca^{2+} channels have long been known to be involved in excitation-contraction coupling in skeletal muscle (Franzini-Armstrong and Protasi, 1997; Franzini-Armstrong et al., 2005). Specifically, CaV1.1 channel activation in skeletal muscle triggers the Ca^{2+} release necessary for muscle contraction though a physical interaction with the ryanodine receptor (RyR) located on the sarcoplasmic reticulum (Tanabe et al., 1990). In this way, the depolarization caused by the activation of AChRs following transmitter binding at the NMJ, is ultimately transduced to cause contraction, with CaV1.1 acting as a critical link. In cardiac myocytes, the coupling between CaV1.2 channels and RyRs appears less direct but critical for function nonetheless. In this example, calmodulin may act as the mediator between CaV1.2 Ca^{2+} channels and release of internal Ca^{2+} stores via RyRs (Woo et al., 2003). These studies demonstrate that close coupling (and in the case of muscle, a physical link) of L-type channels and RyRs does exist in some cells. Perhaps in the motor neuron L-type Ca^{2+} channels are coupled (although not physically) to the intracellular Ca^{2+} release mechanism. However, I have no direct evidence for this type of coupling, and I have tested three different lines of zebrafish L-type Ca^{2+} channels mutants, *relaxed* (CaV1.1), *island beat* (CaV1.2), and *gemini* (CaV1.3) in conjunction with ω-conotoxin GVIA and the Ca^{2+} wave persists.

While the VGCCs are a principal mechanism for selective Ca^{2+} entry into cells, they are by no means the only Ca^{2+} permeable channels. Many non-selective cation channels are also permeable to Ca^{2+}, including TRP channels, CRAC channels, NMDA receptors, and AChRs (Clapham et al., 2001; Decker and Dani, 1990; Katz and Miledi, 1969; MacDermott et al., 1986;

Mulle et al., 1992; Parekh and Putney, 2005; Prakriya et al., 2006; Seguela et al., 1993). We do not know the extent to which other Ca^{2+} permeable channels are involved in the phenomena that are the subject of this work, but we continue to test the potential involvement of these channels pharmacologically. In the end, approaches other than pharmacology might ultimately be necessary to press forward. For instance, morpholinos have been a useful tool to selectively knock down expression of particular proteins in zebrafish. Protein expression, however, is not permanently suppressed using this approach and the effects typically only last several days into development. In addition, morpholinos can cause serious defects which may not be related to the protein of interest itself. New techniques, such as the use of TALENs, offer the possibility to specifically and permanently eliminate or alter particular genes and could be a powerful means by which the roles of various VGCCs could be investigated (Bedell et al., 2012; Huang et al., 2011).

Future Directions and Remaining Questions

A major unanswered question that this work leaves is what are the fundamental mechanisms involved in the Ca^{2+} wave propagation? Can passive diffusion of Ca^{2+} explain the observed phenomenon, or does the Ca^{2+} wave require an active process to maintain wave propagation? An early study measured the rate of Ca^{2+} diffusion by injecting radiolabeled calcium ($^{45}Ca^{2+}$) into squid giant axon, and found that the rate was incredibly slow. An upper estimate of 0.1 μm/second was determined (Hodgkin and Keynes, 1957). Given how tightly cells tend to regulate free Ca^{2+} within the cytosol any sort of diffusional model would likely require the saturation of these Ca^{2+} buffers. Even if the endogenous buffers were saturated, one would expect the rate of Ca^{2+} diffusion to decrease over time. Instead, the speed of the Ca^{2+} wave determined experimentally is constant (Fig. 5.8), which suggests an active process is involved in

order to propagate the wave (Wang and Thompson, 1995). In addition, the "killswitch" experiment where the AP train is turned off prior to the onset of EPCs and the TTX Ca^{2+} experiment both support the theory that the underlying mechanism is an active, regenerative process rather than passive diffusion (Fig. 5.11 and 5.12).

The highly linear distance dependence of the delayed rise in Ca^{2+} might reflect a propagating Ca^{2+} wave that is caused by an active process, such as CICR. Some studies suggest that the ER membrane is a continuous structure that can extend throughout processes such as axons and dendrites (Choi et al., 2006; Lindsey and Ellisman, 1985; Petersen et al., 2001; Petersen and Verkhratsky, 2007; Verkhratsky and Petersen, 2002). For the Ca^{2+} wave to travel hundreds of microns, a so-called reaction-diffusion mechanism might be necessary. For example, with RyR mediated CICR, a localized high concentration of Ca^{2+} is sufficient to cause Ca^{2+} release from the ER through a cluster of RyR receptors. The Ca^{2+} efflux from these Ca^{2+} "sparks" diffuses a short distance (~ 2-6 μm) and subsequently activates neighboring receptors on the ER (Berridge et al., 2003). The sequential opening and efflux of Ca^{2+} through RyRs therefore generates the wavefront (Berridge et al., 2000; Ross, 2012). In addition, the propagation of the wavefront can be directional because of the biphasic effect of Ca^{2+} on the RyRs themselves. While Ca^{2+} can open RyRs, further increasing the local Ca^{2+} concentration favors their closure (Bouchard et al., 2003; Capes et al., 2011). In this way, these receptors actually limit their own activity. Therefore, if the trigger for the wave were indeed located near the soma, and this type of reaction-diffusion mechanism were involved, then we might expect the observed linearity of the distance vs. delay as well as the directionality of the wave. An additional clue found in the Ca^{2+} imaging of CaP motor neurons which were treated with ω-conotoxin GVIA, is that the peak Ca^{2+} response normally occurs prior to the end of the AP train (Fig. 5.7 and 5.9). While not definitive evidence, the fact that the Ca^{2+} signal declines while the

stimulus is ongoing indicates that the source of Ca^{2+} is in some way shut down or inactivated. Perhaps this is the signature of the biphasic effect of Ca^{2+} on internal store release channels like RyRs. Ca^{2+} influx could also induce Ca^{2+} entry through Ca^{2+} permeable channels on the plasma membrane. This sort of mechanism has been proposed for some types of fast (~ 100 μM/sec) Ca^{2+} waves (Jaffe, 2007) and has garnered interest as a means by which intracellular stores can be refilled once emptied (so-called store operated Ca^{2+} entry or capacitive Ca^{2+} entry). Unfortunately, I have done little to directly address the underlying mechanism by which Ca^{2+} travels to ultimately affect transmitter release.

Rigorous experiments investigating the types of Ca^{2+} buffers present in zebrafish motor neurons and how they affect both synchronous and asynchronous transmitter release have not yet been performed. Endogenous Ca^{2+} buffers can have a range of affinities for Ca^{2+} (uM - mM) and are thought to be present in quantities of 100-300 uM (Allbritton et al., 1992). Mobile buffers such as parvalbumin and calbindin-D_{28k} effectively increase the range of diffusion of Ca^{2+} within the cell due to their small size and solubility. Whereas fixed endogenous buffers act to slow the diffusion of Ca^{2+}. Determining which buffers are present in the CaP motor neuron could be an important step toward gaining a better understanding of the Ca^{2+} wave. The buffer capacities of various cell types as well as the relative amount of mobile vs. immobile buffer can differ substantially. For example, rat motor neurons and adrenal chromaffin cells have low buffering capacities (Neher and Augustine, 1992; Palecek et al., 1999) while Purkinje cells and frog saccular hair cells have very high buffering capacities (Fierro and Llano, 1996; Roberts, 1994). Furthermore, individual compartments of cells can have different buffering capacities, so techniques have been developed to investigate small compartments such as dendritic spines and presynaptic terminals (Yasuda et al., 2004). The endogenous Ca^{2+} buffers present will determine the extent and delay with which Ca^{2+} can and will diffuse based on their intrinsic on

and off rates as well as their mobility in the cytoplasm or surface of a membrane, which in turn can ultimately influence synaptic transmission. In zebrafish CaP motor neurons, I have some limited evidence that Ca^{2+} buffering differs in the axon vs. the synaptic boutons. It appears as though Ca^{2+} buffering is higher in the synaptic terminals, as evidenced be the rapid rate of decay of the Ca^{2+} signal following short bursts of action potentials. For example, Ca^{2+} imaging of untreated wild type boutons following a train of 10 APs (Fig. 4.3) or 200 APs (Fig. 5.13) shows a rapid decay of the Ca^{2+} signal. Whereas the decay observed in the axon is slower (Fig. 5.13), suggesting lower levels of Ca^{2+} buffering in the axon. If this observation is substantiated, it could give some additional insight as to how the Ca^{2+} wave is able to efficiently propagate down the axon.

The proposition that Ca^{2+} arriving from a distal source could account for delayed asynchronous release, and that the Ca^{2+} arrives via a propagating wave will certainly be heavily scrutinized. Therefore, it is important to consider the types of additional experiments that could bolster (or indeed disprove!) this hypothesis. Two areas where we have very limited evidence deserve significant attention. First, positive identification of the triggering mechanism will be of great interest. As discussed earlier, a significant amount of time has been spent trying to pharmacologically identify a second Ca^{2+} channel which might initiate the Ca^{2+} wave. My evidence for a nimodipine sensitive channel as causal to the Ca^{2+} wave is an encouraging advance, but has not been supported to date by experiments on L-type Ca^{2+} channel mutant lines. In this case, a more targeted molecular approach may be warranted, either by using morpholinos or the newly developed TALEN technology. This is by no means an easy task, as there are many potential target channels, but starting with VGCCs seems appropriate.

Additional experimentation will also be necessary to understand the nature of the Ca^{2+} wave itself. I attempted some Ca^{2+} uncaging, but these experiments were very preliminary as the microscope had never been setup for this type of procedure. Additional modifications will be necessary to proceed with uncaging experiments, but once functional, Ca^{2+} uncaging could be a very useful technique to examine the wave. Ideally, one could both image and uncage Ca^{2+} and simultaneously record EPCs in skeletal muscle. This type of experiment could indicate where Ca^{2+} levels need to increase in order to generate a wave and ultimately produce asynchronous release. One could also determine if external Ca^{2+} is necessary for generating the Ca^{2+} wave using this approach. It may also be interesting to use genetically encoded Ca^{2+} indicators (GECIs) to track the Ca^{2+} wave. The advantage would be that the GECI could be specifically targeted to either the ER or the plasma membrane, potentially providing a means to examine the subcellular origin of the propagating Ca^{2+} wave.

Summary of Findings

- Synchronous Release is mediated by a ω-conotoxin GVIA sensitive P/Q-type Ca^{2+} channel.
- Asynchronous Release can be isolated by application of ω-conotoxin GVIA in conjunction with prolonged (~ 10 second) high frequency stimulation.
- The asynchronous release is caused by a delayed rapid rise in global Ca^{2+}.
- The delay in asynchronous release can be accounted for by the delayed arrival of a propagating Ca^{2+} wave.
- Limited evidence suggests a role for L-Type channels in wave initiation.

Nearly all of the experiments I have performed in the Brehm Lab involve live cell imaging, and as such the data are sometimes difficult to appreciate on a sheet of paper. Because of this limitation, I have created a YouTube channel called "TheRealBrehmLab" where you can find movies of experiments performed for this dissertation. In it you will see examples of the calcium wave, control experiments, CaP motor neuron reconstructions, and generally the latest interesting results. I hope that Brehm lab members will continue to add their own data, after all science is meant to be seen and shared.

Bibliography

Adler, E.M., Augustine, G.J., Duffy, S.N., and Charlton, M.P. (1991). Alien intracellular calcium chelators attenuate neurotransmitter release at the squid giant synapse. The Journal of neuroscience : the official journal of the Society for Neuroscience *11*, 1496-1507.

Ahrens, M.B., Li, J.M., Orger, M.B., Robson, D.N., Schier, A.F., Engert, F., and Portugues, R. (2012). Brain-wide neuronal dynamics during motor adaptation in zebrafish. Nature *485*, 471-477.

Allbritton, N.L., Meyer, T., and Stryer, L. (1992). Range of messenger action of calcium ion and inositol 1,4,5-trisphosphate. Science *258*, 1812-1815.

Andreae, L.C., Fredj, N.B., and Burrone, J. (2012). Independent vesicle pools underlie different modes of release during neuronal development. The Journal of neuroscience : the official journal of the Society for Neuroscience *32*, 1867-1874.

Atluri, P.P., and Regehr, W.G. (1998). Delayed release of neurotransmitter from cerebellar granule cells. The Journal of neuroscience : the official journal of the Society for Neuroscience *18*, 8214-8227.

Bai, J., Tucker, W.C., and Chapman, E.R. (2004). PIP2 increases the speed of response of synaptotagmin and steers its membrane-penetration activity toward the plasma membrane. Nature structural & molecular biology *11*, 36-44.

Bardo, S., Cavazzini, M.G., and Emptage, N. (2006). The role of the endoplasmic reticulum Ca2+ store in the plasticity of central neurons. Trends in pharmacological sciences *27*, 78-84.

Barrett, E.F., and Stevens, C.F. (1972). The kinetics of transmitter release at the frog neuromuscular junction. The Journal of physiology *227*, 691-708.

Bean, B.P. (1985). Two kinds of calcium channels in canine atrial cells. Differences in kinetics, selectivity, and pharmacology. The Journal of general physiology *86*, 1-30.

Beattie, C.E. (2000). Control of motor axon guidance in the zebrafish embryo. Brain research bulletin *53*, 489-500.

Bedell, V.M., Wang, Y., Campbell, J.M., Poshusta, T.L., Starker, C.G., Krug, R.G., 2nd, Tan, W., Penheiter, S.G., Ma, A.C., Leung, A.Y.*, et al.* (2012). In vivo genome editing using a high-efficiency TALEN system. Nature *491*, 114-118.

Bender, K.J., and Trussell, L.O. (2009). Axon initial segment Ca2+ channels influence action potential generation and timing. Neuron *61*, 259-271.

Bender, K.J., and Trussell, L.O. (2012). The physiology of the axon initial segment. Annual review of neuroscience *35*, 249-265.

Bender, K.J., Uebele, V.N., Renger, J.J., and Trussell, L.O. (2012). Control of firing patterns through modulation of axon initial segment T-type calcium channels. The Journal of physiology *590*, 109-118.

Berridge, M.J. (1998). Neuronal calcium signaling. Neuron *21*, 13-26.

Berridge, M.J., Bootman, M.D., and Roderick, H.L. (2003). Calcium signalling: dynamics, homeostasis and remodelling. Nature reviews Molecular cell biology *4*, 517-529.

Berridge, M.J., Lipp, P., and Bootman, M.D. (2000). The versatility and universality of calcium signalling. Nature reviews Molecular cell biology *1*, 11-21.

Best, A.R., and Regehr, W.G. (2009). Inhibitory regulation of electrically coupled neurons in the inferior olive is mediated by asynchronous release of GABA. Neuron *62*, 555-565.

Bezprozvanny, I., and Tsien, R.W. (1995). Voltage-dependent blockade of diverse types of voltage-gated Ca2+ channels expressed in Xenopus oocytes by the Ca2+ channel antagonist mibefradil (Ro 40-5967). Molecular pharmacology *48*, 540-549.

Borst, J.G., and Sakmann, B. (1996). Calcium influx and transmitter release in a fast CNS synapse. Nature *383*, 431-434.

Bouchard, R., Pattarini, R., and Geiger, J.D. (2003). Presence and functional significance of presynaptic ryanodine receptors. Progress in neurobiology *69*, 391-418.

Bowersox, S.S., Miljanich, G.P., Sugiura, Y., Li, C., Nadasdi, L., Hoffman, B.B., Ramachandran, J., and Ko, C.P. (1995). Differential blockade of voltage-sensitive calcium channels at the mouse neuromuscular junction by novel omega-conopeptides and omega-agatoxin-IVA. The Journal of pharmacology and experimental therapeutics *273*, 248-256.

Brehm, P., Lechleiter, J., Smith, S., and Dunlap, K. (1989). Intercellular signaling as visualized by endogenous calcium-dependent bioluminescence. Neuron *3*, 191-198.

Brunger, A.T. (2005). Structure and function of SNARE and SNARE-interacting proteins. Quarterly reviews of biophysics *38*, 1-47.

Cain, S.M., and Snutch, T.P. (2010). Contributions of T-type calcium channel isoforms to neuronal firing. Channels *4*, 475-482.

Capes, E.M., Loaiza, R., and Valdivia, H.H. (2011). Ryanodine receptors. Skeletal muscle *1*, 18.

Carlin, K.P., Jones, K.E., Jiang, Z., Jordan, L.M., and Brownstone, R.M. (2000). Dendritic L-type calcium currents in mouse spinal motoneurons: implications for bistability. The European journal of neuroscience *12*, 1635-1646.

Carter, A.G., Vogt, K.E., Foster, K.A., and Regehr, W.G. (2002). Assessing the role of calcium-induced calcium release in short-term presynaptic plasticity at excitatory central synapses. The Journal of neuroscience : the official journal of the Society for Neuroscience *22*, 21-28.

Catterall, W.A. (2000). From ionic currents to molecular mechanisms: the structure and function of voltage-gated sodium channels. Neuron *26*, 13-25.

Catterall, W.A. (2010). Signaling complexes of voltage-gated sodium and calcium channels. Neuroscience letters *486*, 107-116.

Catterall, W.A., and Few, A.P. (2008). Calcium channel regulation and presynaptic plasticity. Neuron *59*, 882-901.

Chad, J.E., and Eckert, R. (1984). Calcium domains associated with individual channels can account for anomalous voltage relations of CA-dependent responses. Biophysical journal *45*, 993-999.

Choi, Y.M., Kim, S.H., Chung, S., Uhm, D.Y., and Park, M.K. (2006). Regional interaction of endoplasmic reticulum Ca2+ signals between soma and dendrites through rapid luminal Ca2+ diffusion. The Journal of neuroscience : the official journal of the Society for Neuroscience *26*, 12127-12136.

Clapham, D.E., Runnels, L.W., and Strubing, C. (2001). The TRP ion channel family. Nature reviews Neuroscience *2*, 387-396.

Cohen, M.W., Jones, O.T., and Angelides, K.J. (1991). Distribution of Ca2+ channels on frog motor nerve terminals revealed by fluorescent omega-conotoxin. The Journal of neuroscience : the official journal of the Society for Neuroscience *11*, 1032-1039.

Decker, E.R., and Dani, J.A. (1990). Calcium permeability of the nicotinic acetylcholine receptor: the single-channel calcium influx is significant. The Journal of neuroscience : the official journal of the Society for Neuroscience *10*, 3413-3420.

Dodge, F.A., Jr., and Rahamimoff, R. (1967). Co-operative action a calcium ions in transmitter release at the neuromuscular junction. The Journal of physiology *193*, 419-432.

Dolmetsch, R.E., Pajvani, U., Fife, K., Spotts, J.M., and Greenberg, M.E. (2001). Signaling to the nucleus by an L-type calcium channel-calmodulin complex through the MAP kinase pathway. Science *294*, 333-339.

Dreyfus, F.M., Tscherter, A., Errington, A.C., Renger, J.J., Shin, H.S., Uebele, V.N., Crunelli, V., Lambert, R.C., and Leresche, N. (2010). Selective T-type calcium channel block in thalamic neurons reveals channel redundancy and physiological impact of I(T)window. The Journal of neuroscience : the official journal of the Society for Neuroscience *30*, 99-109.

Dunlap, K., Takeda, K., and Brehm, P. (1987). Activation of a calcium-dependent photoprotein by chemical signalling through gap junctions. Nature *325*, 60-62.

Eggermann, E., Bucurenciu, I., Goswami, S.P., and Jonas, P. (2012). Nanodomain coupling between Ca(2)(+) channels and sensors of exocytosis at fast mammalian synapses. Nature reviews Neuroscience *13*, 7-21.

Emptage, N.J., Reid, C.A., and Fine, A. (2001). Calcium stores in hippocampal synaptic boutons mediate short-term plasticity, store-operated Ca2+ entry, and spontaneous transmitter release. Neuron *29*, 197-208.

Evans, R.M., and Zamponi, G.W. (2006). Presynaptic Ca2+ channels--integration centers for neuronal signaling pathways. Trends in neurosciences *29*, 617-624.

Fatt, P., and Katz, B. (1952). Spontaneous subthreshold activity at motor nerve endings. The Journal of physiology *117*, 109-128.

Fedchyshyn, M.J., and Wang, L.Y. (2005). Developmental transformation of the release modality at the calyx of Held synapse. The Journal of neuroscience : the official journal of the Society for Neuroscience *25*, 4131-4140.

Fernandez-Chacon, R., Konigstorfer, A., Gerber, S.H., Garcia, J., Matos, M.F., Stevens, C.F., Brose, N., Rizo, J., Rosenmund, C., and Sudhof, T.C. (2001). Synaptotagmin I functions as a calcium regulator of release probability. Nature *410*, 41-49.

Fernandez, I., Arac, D., Ubach, J., Gerber, S.H., Shin, O., Gao, Y., Anderson, R.G., Sudhof, T.C., and Rizo, J. (2001). Three-dimensional structure of the synaptotagmin 1 C2B-domain: synaptotagmin 1 as a phospholipid binding machine. Neuron *32*, 1057-1069.

Few, A.P., Nanou, E., Watari, H., Sullivan, J.M., Scheuer, T., and Catterall, W.A. (2012). Asynchronous Ca2+ current conducted by voltage-gated Ca2+ (CaV)-2.1 and CaV2.2 channels and its implications for asynchronous neurotransmitter release. Proceedings of the National Academy of Sciences of the United States of America *109*, E452-460.

Fierro, L., and Llano, I. (1996). High endogenous calcium buffering in Purkinje cells from rat cerebellar slices. The Journal of physiology *496 (Pt 3)*, 617-625.

Fitzjohn, S.M., and Collingridge, G.L. (2002). Calcium stores and synaptic plasticity. Cell calcium *32*, 405-411.

Fox, A.P., Nowycky, M.C., and Tsien, R.W. (1987a). Kinetic and pharmacological properties distinguishing three types of calcium currents in chick sensory neurones. The Journal of physiology *394*, 149-172.

Fox, A.P., Nowycky, M.C., and Tsien, R.W. (1987b). Single-channel recordings of three types of calcium channels in chick sensory neurones. The Journal of physiology *394*, 173-200.

Franzini-Armstrong, C., and Protasi, F. (1997). Ryanodine receptors of striated muscles: a complex channel capable of multiple interactions. Physiological reviews *77*, 699-729.

Franzini-Armstrong, C., Protasi, F., and Tijskens, P. (2005). The assembly of calcium release units in cardiac muscle. Annals of the New York Academy of Sciences *1047*, 76-85.

Fredj, N.B., and Burrone, J. (2009). A resting pool of vesicles is responsible for spontaneous vesicle fusion at the synapse. Nature neuroscience *12*, 751-758.

Furukawa, T., Nukada, T., Miura, R., Ooga, K., Honda, M., Watanabe, S., Koganesawa, S., and Isshiki, T. (2005). Differential blocking action of dihydropyridine Ca2+ antagonists on a T-type Ca2+ channel (alpha1G) expressed in Xenopus oocytes. Journal of cardiovascular pharmacology *45*, 241-246.

Furukawa, T., Nukada, T., Namiki, Y., Miyashita, Y., Hatsuno, K., Ueno, Y., Yamakawa, T., and Isshiki, T. (2009). Five different profiles of dihydropyridines in blocking T-type Ca(2+) channel subtypes (Ca(v)3.1 (alpha(1G)), Ca(v)3.2 (alpha(1H)), and Ca(v)3.3 (alpha(1I))) expressed in Xenopus oocytes. European journal of pharmacology *613*, 100-107.

Gabso, M., Neher, E., and Spira, M.E. (1997). Low mobility of the Ca2+ buffers in axons of cultured Aplysia neurons. Neuron *18*, 473-481.

Galante, M., and Marty, A. (2003). Presynaptic ryanodine-sensitive calcium stores contribute to evoked neurotransmitter release at the basket cell-Purkinje cell synapse. The Journal of neuroscience : the official journal of the Society for Neuroscience *23*, 11229-11234.

Geppert, M., Goda, Y., Hammer, R.E., Li, C., Rosahl, T.W., Stevens, C.F., and Sudhof, T.C. (1994). Synaptotagmin I: a major Ca2+ sensor for transmitter release at a central synapse. Cell *79*, 717-727.

Gilkey, J.C., Jaffe, L.F., Ridgway, E.B., and Reynolds, G.T. (1978). A free calcium wave traverses the activating egg of the medaka, Oryzias latipes. The Journal of cell biology *76*, 448-466.

Goda, Y., and Stevens, C.F. (1994). Two components of transmitter release at a central synapse. Proceedings of the National Academy of Sciences of the United States of America *91*, 12942-12946.

Granato, M., van Eeden, F.J., Schach, U., Trowe, T., Brand, M., Furutani-Seiki, M., Haffter, P., Hammerschmidt, M., Heisenberg, C.P., Jiang, Y.J.*, et al.* (1996). Genes controlling and mediating locomotion behavior of the zebrafish embryo and larva. Development *123*, 399-413.

Groemer, T.W., and Klingauf, J. (2007). Synaptic vesicles recycling spontaneously and during activity belong to the same vesicle pool. Nature neuroscience *10*, 145-147.

Groffen, A.J., Martens, S., Diez Arazola, R., Cornelisse, L.N., Lozovaya, N., de Jong, A.P., Goriounova, N.A., Habets, R.L., Takai, Y., Borst, J.G.*, et al.* (2010). Doc2b is a high-affinity Ca2+ sensor for spontaneous neurotransmitter release. Science *327*, 1614-1618.

Grubb, M.S., and Burrone, J. (2010). Activity-dependent relocation of the axon initial segment fine-tunes neuronal excitability. Nature *465*, 1070-1074.

Guan, C.B., Xu, H.T., Jin, M., Yuan, X.B., and Poo, M.M. (2007). Long-range Ca2+ signaling from growth cone to soma mediates reversal of neuronal migration induced by slit-2. Cell *129*, 385-395.

Hagiwara, S., Ozawa, S., and Sand, O. (1975). Voltage clamp analysis of two inward current mechanisms in the egg cell membrane of a starfish. The Journal of general physiology *65*, 617-644.

Han, Y., Kaeser, P.S., Sudhof, T.C., and Schneggenburger, R. (2011). RIM determines Ca(2)+ channel density and vesicle docking at the presynaptic active zone. Neuron *69*, 304-316.

Hefft, S., and Jonas, P. (2005). Asynchronous GABA release generates long-lasting inhibition at a hippocampal interneuron-principal neuron synapse. Nature neuroscience *8*, 1319-1328.

Helton, T.D., Xu, W., and Lipscombe, D. (2005). Neuronal L-type calcium channels open quickly and are inhibited slowly. The Journal of neuroscience : the official journal of the Society for Neuroscience *25*, 10247-10251.

Hille, B. (2001). Ion channels of excitable membranes, 3rd edn (Sunderland, Mass.: Sinauer).

Hodgkin, A.L., and Keynes, R.D. (1957). Movements of labelled calcium in squid giant axons. The Journal of physiology *138*, 253-281.

Hua, Y., Sinha, R., Martineau, M., Kahms, M., and Klingauf, J. (2010). A common origin of synaptic vesicles undergoing evoked and spontaneous fusion. Nature neuroscience *13*, 1451-1453.

Huang, P., Xiao, A., Zhou, M., Zhu, Z., Lin, S., and Zhang, B. (2011). Heritable gene targeting in zebrafish using customized TALENs. Nature biotechnology *29*, 699-700.

Hutson, L.D., and Chien, C.B. (2002). Wiring the zebrafish: axon guidance and synaptogenesis. Current opinion in neurobiology *12*, 87-92.

Isokawa, M., and Alger, B.E. (2006). Ryanodine receptor regulates endogenous cannabinoid mobilization in the hippocampus. Journal of neurophysiology *95*, 3001-3011.

Jaffe, L.F. (2007). Stretch-activated calcium channels relay fast calcium waves propagated by calcium-induced calcium influx. Biology of the cell / under the auspices of the European Cell Biology Organization *99*, 175-184.

James, D.J., Kowalchyk, J., Daily, N., Petrie, M., and Martin, T.F. (2009). CAPS drives trans-SNARE complex formation and membrane fusion through syntaxin interactions. Proceedings of the National Academy of Sciences of the United States of America *106*, 17308-17313.

Jiang, Z., Rempel, J., Li, J., Sawchuk, M.A., Carlin, K.P., and Brownstone, R.M. (1999). Development of L-type calcium channels and a nifedipine-sensitive motor activity in the postnatal mouse spinal cord. The European journal of neuroscience *11*, 3481-3487.

Jockusch, W.J., Speidel, D., Sigler, A., Sorensen, J.B., Varoqueaux, F., Rhee, J.S., and Brose, N. (2007). CAPS-1 and CAPS-2 are essential synaptic vesicle priming proteins. Cell *131*, 796-808.

John, L.M., Mosquera-Caro, M., Camacho, P., and Lechleiter, J.D. (2001). Control of IP(3)-mediated Ca2+ puffs in Xenopus laevis oocytes by the Ca2+-binding protein parvalbumin. The Journal of physiology *535*, 3-16.

Katz, B., and Miledi, R. (1967). The timing of calcium action during neuromuscular transmission. The Journal of physiology *189*, 535-544.

Katz, B., and Miledi, R. (1969). Spontaneous and evoked activity of motor nerve endings in calcium Ringer. The Journal of physiology *203*, 689-706.

Katz, E., Ferro, P.A., Cherksey, B.D., Sugimori, M., Llinas, R., and Uchitel, O.D. (1995). Effects of Ca2+ channel blockers on transmitter release and presynaptic currents at the frog neuromuscular junction. The Journal of physiology *486 (Pt 3)*, 695-706.

Katz, E., Ferro, P.A., Weisz, G., and Uchitel, O.D. (1996). Calcium channels involved in synaptic transmission at the mature and regenerating mouse neuromuscular junction. The Journal of physiology *497 (Pt 3)*, 687-697.

Kerr, L.M., and Yoshikami, D. (1984). A venom peptide with a novel presynaptic blocking action. Nature *308*, 282-284.

Kochubey, O., and Schneggenburger, R. (2011). Synaptotagmin increases the dynamic range of synapses by driving Ca(2)+-evoked release and by clamping a near-linear remaining Ca(2)+ sensor. Neuron *69*, 736-748.

Koyano, K., Abe, T., Nishiuchi, Y., and Sakakibara, S. (1987). Effects of synthetic omega-conotoxin on synaptic transmission. European journal of pharmacology *135*, 337-343.

Kubota, M., Narita, K., Murayama, T., Suzuki, S., Soga, S., Usukura, J., Ogawa, Y., and Kuba, K. (2005). Type-3 ryanodine receptor involved in Ca2+-induced Ca2+ release and transmitter exocytosis at frog motor nerve terminals. Cell calcium *38*, 557-567.

Kucenas, S., Takada, N., Park, H.C., Woodruff, E., Broadie, K., and Appel, B. (2008). CNS-derived glia ensheath peripheral nerves and mediate motor root development. Nature neuroscience *11*, 143-151.

Lautermilch, N.J., and Spitzer, N.C. (2000). Regulation of calcineurin by growth cone calcium waves controls neurite extension. The Journal of neuroscience : the official journal of the Society for Neuroscience *20*, 315-325.

Leal, K., Mochida, S., Scheuer, T., and Catterall, W.A. (2012). Fine-tuning synaptic plasticity by modulation of CaV2.1 channels with Ca2+ sensor proteins. Proceedings of the National Academy of Sciences of the United States of America *109*, 17069-17074.

Lechleiter, J., Girard, S., Peralta, E., and Clapham, D. (1991). Spiral calcium wave propagation and annihilation in Xenopus laevis oocytes. Science *252*, 123-126.

Lechleiter, J.D., and Clapham, D.E. (1992). Molecular mechanisms of intracellular calcium excitability in X. laevis oocytes. Cell *69*, 283-294.

Lee, J.H., Gomora, J.C., Cribbs, L.L., and Perez-Reyes, E. (1999). Nickel block of three cloned T-type calcium channels: low concentrations selectively block alpha1H. Biophysical journal *77*, 3034-3042.

Li, W., Ono, F., and Brehm, P. (2003). Optical measurements of presynaptic release in mutant zebrafish lacking postsynaptic receptors. The Journal of neuroscience : the official journal of the Society for Neuroscience *23*, 10467-10474.

Li, W., Thaler, C., and Brehm, P. (2001). Calcium channels in Xenopus spinal neurons differ in somas and presynaptic terminals. Journal of neurophysiology *86*, 269-279.

Lindsey, J.D., and Ellisman, M.H. (1985). The neuronal endomembrane system. III. The origins of the axoplasmic reticulum and discrete axonal cisternae at the axon hillock. The Journal of neuroscience : the official journal of the Society for Neuroscience *5*, 3135-3144.

Lipscombe, D., Helton, T.D., and Xu, W. (2004). L-type calcium channels: the low down. Journal of neurophysiology *92*, 2633-2641.

Liu, H., Dean, C., Arthur, C.P., Dong, M., and Chapman, E.R. (2009). Autapses and networks of hippocampal neurons exhibit distinct synaptic transmission phenotypes in the absence of synaptotagmin I. The Journal of neuroscience : the official journal of the Society for Neuroscience *29*, 7395-7403.

Llano, I., Gonzalez, J., Caputo, C., Lai, F.A., Blayney, L.M., Tan, Y.P., and Marty, A. (2000). Presynaptic calcium stores underlie large-amplitude miniature IPSCs and spontaneous calcium transients. Nature neuroscience *3*, 1256-1265.

Llinas, R., Sugimori, M., Lin, J.W., and Cherksey, B. (1989). Blocking and isolation of a calcium channel from neurons in mammals and cephalopods utilizing a toxin fraction (FTX) from funnel-web spider poison. Proceedings of the National Academy of Sciences of the United States of America *86*, 1689-1693.

Lorenzon, N.M., and Beam, K.G. (2008). Disease causing mutations of calcium channels. Channels *2*, 163-179.

Lu, T., and Trussell, L.O. (2000). Inhibitory transmission mediated by asynchronous transmitter release. Neuron *26*, 683-694.

Luna, V.M., and Brehm, P. (2006). An electrically coupled network of skeletal muscle in zebrafish distributes synaptic current. The Journal of general physiology *128*, 89-102.

MacDermott, A.B., Mayer, M.L., Westbrook, G.L., Smith, S.J., and Barker, J.L. (1986). NMDA-receptor activation increases cytoplasmic calcium concentration in cultured spinal cord neurones. Nature *321*, 519-522.

Manseau, F., Marinelli, S., Mendez, P., Schwaller, B., Prince, D.A., Huguenard, J.R., and Bacci, A. (2010). Desynchronization of neocortical networks by asynchronous release of GABA at autaptic and synaptic contacts from fast-spiking interneurons. PLoS biology *8*.

Martin, R.L., Lee, J.H., Cribbs, L.L., Perez-Reyes, E., and Hanck, D.A. (2000). Mibefradil block of cloned T-type calcium channels. The Journal of pharmacology and experimental therapeutics *295*, 302-308.

Maximov, A., and Sudhof, T.C. (2005). Autonomous function of synaptotagmin 1 in triggering synchronous release independent of asynchronous release. Neuron *48*, 547-554.

Mehrke, G., Zong, X.G., Flockerzi, V., and Hofmann, F. (1994). The Ca(++)-channel blocker Ro 40-5967 blocks differently T-type and L-type Ca++ channels. The Journal of pharmacology and experimental therapeutics *271*, 1483-1488.

Miesenbock, G., De Angelis, D.A., and Rothman, J.E. (1998). Visualizing secretion and synaptic transmission with pH-sensitive green fluorescent proteins. Nature *394*, 192-195.

Mintz, I.M., Adams, M.E., and Bean, B.P. (1992a). P-type calcium channels in rat central and peripheral neurons. Neuron *9*, 85-95.

Mintz, I.M., Venema, V.J., Swiderek, K.M., Lee, T.D., Bean, B.P., and Adams, M.E. (1992b). P-type calcium channels blocked by the spider toxin omega-Aga-IVA. Nature *355*, 827-829.

Mishra, S.K., and Hermsmeyer, K. (1994). Selective inhibition of T-type Ca2+ channels by Ro 40-5967. Circulation research *75*, 144-148.

Mulle, C., Choquet, D., Korn, H., and Changeux, J.P. (1992). Calcium influx through nicotinic receptor in rat central neurons: its relevance to cellular regulation. Neuron *8*, 135-143.

Muto, A., Ohkura, M., Kotani, T., Higashijima, S., Nakai, J., and Kawakami, K. (2011). Genetic visualization with an improved GCaMP calcium indicator reveals spatiotemporal activation of the spinal motor neurons in zebrafish. Proceedings of the National Academy of Sciences of the United States of America *108*, 5425-5430.

Nakamura, T., Barbara, J.G., Nakamura, K., and Ross, W.N. (1999). Synergistic release of Ca2+ from IP3-sensitive stores evoked by synaptic activation of mGluRs paired with backpropagating action potentials. Neuron *24*, 727-737.

Nakamura, T., Lasser-Ross, N., Nakamura, K., and Ross, W.N. (2002). Spatial segregation and interaction of calcium signalling mechanisms in rat hippocampal CA1 pyramidal neurons. The Journal of physiology *543*, 465-480.

Narita, K., Akita, T., Hachisuka, J., Huang, S., Ochi, K., and Kuba, K. (2000). Functional coupling of Ca(2+) channels to ryanodine receptors at presynaptic terminals. Amplification of exocytosis and plasticity. The Journal of general physiology *115*, 519-532.

Narita, K., Akita, T., Osanai, M., Shirasaki, T., Kijima, H., and Kuba, K. (1998). A Ca2+-induced Ca2+ release mechanism involved in asynchronous exocytosis at frog motor nerve terminals. The Journal of general physiology *112*, 593-609.

Neher, E., and Augustine, G.J. (1992). Calcium gradients and buffers in bovine chromaffin cells. The Journal of physiology *450*, 273-301.

Neher, E., and Sakaba, T. (2001). Combining deconvolution and noise analysis for the estimation of transmitter release rates at the calyx of held. The Journal of neuroscience : the official journal of the Society for Neuroscience *21*, 444-461.

Neher, E., and Sakaba, T. (2003). Combining deconvolution and fluctuation analysis to determine quantal parameters and release rates. Journal of neuroscience methods *130*, 143-157.

Neher, E., and Sakaba, T. (2008). Multiple roles of calcium ions in the regulation of neurotransmitter release. Neuron *59*, 861-872.

Neher, E., and Zucker, R.S. (1993). Multiple calcium-dependent processes related to secretion in bovine chromaffin cells. Neuron *10*, 21-30.

Nowycky, M.C., Fox, A.P., and Tsien, R.W. (1985). Three types of neuronal calcium channel with different calcium agonist sensitivity. Nature *316*, 440-443.

Olivera, B.M., McIntosh, J.M., Cruz, L.J., Luque, F.A., and Gray, W.R. (1984). Purification and sequence of a presynaptic peptide toxin from Conus geographus venom. Biochemistry *23*, 5087-5090.

Otsu, Y., Shahrezaei, V., Li, B., Raymond, L.A., Delaney, K.R., and Murphy, T.H. (2004). Competition between phasic and asynchronous release for recovered synaptic vesicles at

developing hippocampal autaptic synapses. The Journal of neuroscience : the official journal of the Society for Neuroscience *24*, 420-433.

Palecek, J., Lips, M.B., and Keller, B.U. (1999). Calcium dynamics and buffering in motoneurones of the mouse spinal cord. The Journal of physiology *520 Pt 2*, 485-502.

Pang, Z.P., Bacaj, T., Yang, X., Zhou, P., Xu, W., and Sudhof, T.C. (2011). Doc2 supports spontaneous synaptic transmission by a Ca(2+)-independent mechanism. Neuron *70*, 244-251.

Panzer, J.A., Song, Y., and Balice-Gordon, R.J. (2006). In vivo imaging of preferential motor axon outgrowth to and synaptogenesis at prepatterned acetylcholine receptor clusters in embryonic zebrafish skeletal muscle. The Journal of neuroscience : the official journal of the Society for Neuroscience *26*, 934-947.

Parekh, A.B., and Putney, J.W., Jr. (2005). Store-operated calcium channels. Physiological reviews *85*, 757-810.

Perez-Reyes, E. (2003). Molecular physiology of low-voltage-activated t-type calcium channels. Physiological reviews *83*, 117-161.

Petersen, O.H., Tepikin, A., and Park, M.K. (2001). The endoplasmic reticulum: one continuous or several separate Ca(2+) stores? Trends in neurosciences *24*, 271-276.

Petersen, O.H., and Verkhratsky, A. (2007). Endoplasmic reticulum calcium tunnels integrate signalling in polarised cells. Cell calcium *42*, 373-378.

Prakriya, M., Feske, S., Gwack, Y., Srikanth, S., Rao, A., and Hogan, P.G. (2006). Orai1 is an essential pore subunit of the CRAC channel. Nature *443*, 230-233.

Protti, D.A., and Uchitel, O.D. (1993). Transmitter release and presynaptic Ca2+ currents blocked by the spider toxin omega-Aga-IVA. Neuroreport *5*, 333-336.

Pumplin, D.W., Reese, T.S., and Llinas, R. (1981). Are the presynaptic membrane particles the calcium channels? Proceedings of the National Academy of Sciences of the United States of America *78*, 7210-7213.

Radhakrishnan, A., Stein, A., Jahn, R., and Fasshauer, D. (2009). The Ca2+ affinity of synaptotagmin 1 is markedly increased by a specific interaction of its C2B domain with phosphatidylinositol 4,5-bisphosphate. The Journal of biological chemistry *284*, 25749-25760.

Raingo, J., Khvotchev, M., Liu, P., Darios, F., Li, Y.C., Ramirez, D.M., Adachi, M., Lemieux, P., Toth, K., Davletov, B.*, et al.* (2012). VAMP4 directs synaptic vesicles to a pool that selectively maintains asynchronous neurotransmission. Nature neuroscience *15*, 738-745.

Ramirez, D.M., Khvotchev, M., Trauterman, B., and Kavalali, E.T. (2012). Vti1a identifies a vesicle pool that preferentially recycles at rest and maintains spontaneous neurotransmission. Neuron *73*, 121-134.

Randall, A.D., and Tsien, R.W. (1997). Contrasting biophysical and pharmacological properties of T-type and R-type calcium channels. Neuropharmacology *36*, 879-893.

Richards, D.A., Guatimosim, C., Rizzoli, S.O., and Betz, W.J. (2003). Synaptic vesicle pools at the frog neuromuscular junction. Neuron *39*, 529-541.

Ritter, D.A., Bhatt, D.H., and Fetcho, J.R. (2001). In vivo imaging of zebrafish reveals differences in the spinal networks for escape and swimming movements. The Journal of neuroscience : the official journal of the Society for Neuroscience *21*, 8956-8965.

Rizzoli, S.O., and Betz, W.J. (2004). The structural organization of the readily releasable pool of synaptic vesicles. Science *303*, 2037-2039.

Rizzoli, S.O., and Betz, W.J. (2005). Synaptic vesicle pools. Nature reviews Neuroscience *6*, 57-69.

Roberts, W.M. (1994). Localization of calcium signals by a mobile calcium buffer in frog saccular hair cells. The Journal of neuroscience : the official journal of the Society for Neuroscience *14*, 3246-3262.

Robertson, J.D. (1956). The ultrastructure of a reptilian myoneural junction. The Journal of biophysical and biochemical cytology *2*, 381-394.

Robitaille, R., Adler, E.M., and Charlton, M.P. (1990). Strategic location of calcium channels at transmitter release sites of frog neuromuscular synapses. Neuron *5*, 773-779.

Ross, W.N. (2012). Understanding calcium waves and sparks in central neurons. Nature reviews Neuroscience *13*, 157-168.

Sand, O., Chen, B.M., and Grinnell, A.D. (2001). Contribution of L-type Ca(2+) channels to evoked transmitter release in cultured Xenopus nerve-muscle synapses. The Journal of physiology *536*, 21-33.

Sanes, J.R., and Lichtman, J.W. (2001). Induction, assembly, maturation and maintenance of a postsynaptic apparatus. Nature reviews Neuroscience *2*, 791-805.

Sano, K., Enomoto, K., and Maeno, T. (1987). Effects of synthetic omega-conotoxin, a new type Ca2+ antagonist, on frog and mouse neuromuscular transmission. European journal of pharmacology *141*, 235-241.

Sara, Y., Virmani, T., Deak, F., Liu, X., and Kavalali, E.T. (2005). An isolated pool of vesicles recycles at rest and drives spontaneous neurotransmission. Neuron *45*, 563-573.

Schiavo, G., Stenbeck, G., Rothman, J.E., and Sollner, T.H. (1997). Binding of the synaptic vesicle v-SNARE, synaptotagmin, to the plasma membrane t-SNARE, SNAP-25, can explain docked vesicles at neurotoxin-treated synapses. Proceedings of the National Academy of Sciences of the United States of America *94*, 997-1001.

Seguela, P., Wadiche, J., Dineley-Miller, K., Dani, J.A., and Patrick, J.W. (1993). Molecular cloning, functional properties, and distribution of rat brain alpha 7: a nicotinic cation channel highly permeable to calcium. The Journal of neuroscience : the official journal of the Society for Neuroscience *13*, 596-604.

Sharma, G., and Vijayaraghavan, S. (2003). Modulation of presynaptic store calcium induces release of glutamate and postsynaptic firing. Neuron *38*, 929-939.

Sheng, Z.H., Rettig, J., Cook, T., and Catterall, W.A. (1996). Calcium-dependent interaction of N-type calcium channels with the synaptic core complex. Nature *379*, 451-454.

Sheng, Z.H., Yokoyama, C.T., and Catterall, W.A. (1997). Interaction of the synprint site of N-type Ca2+ channels with the C2B domain of synaptotagmin I. Proceedings of the National Academy of Sciences of the United States of America *94*, 5405-5410.

Soga-Sakakibara, S., Kubota, M., Suzuki, S., Akita, T., Narita, K., and Kuba, K. (2010). Calcium dependence of the priming, activation and inactivation of ryanodine receptors in frog motor nerve terminals. The European journal of neuroscience *32*, 948-962.

Stevens, C.F., and Wesseling, J.F. (1998). Activity-dependent modulation of the rate at which synaptic vesicles become available to undergo exocytosis. Neuron *21*, 415-424.

Sudhof, T.C. (2004). The synaptic vesicle cycle. Annual review of neuroscience *27*, 509-547.

Sugita, S., Han, W., Butz, S., Liu, X., Fernandez-Chacon, R., Lao, Y., and Sudhof, T.C. (2001). Synaptotagmin VII as a plasma membrane Ca(2+) sensor in exocytosis. Neuron *30*, 459-473.

Sun, J., Pang, Z.P., Qin, D., Fahim, A.T., Adachi, R., and Sudhof, T.C. (2007). A dual-Ca2+-sensor model for neurotransmitter release in a central synapse. Nature *450*, 676-682.

Svoboda, K., and Mainen, Z.F. (1999). Synaptic [Ca2+]: intracellular stores spill their guts. Neuron *22*, 427-430.

Tanabe, T., Beam, K.G., Adams, B.A., Niidome, T., and Numa, S. (1990). Regions of the skeletal muscle dihydropyridine receptor critical for excitation-contraction coupling. Nature *346*, 567-569.

Tanabe, T., Takeshima, H., Mikami, A., Flockerzi, V., Takahashi, H., Kangawa, K., Kojima, M., Matsuo, H., Hirose, T., and Numa, S. (1987). Primary structure of the receptor for calcium channel blockers from skeletal muscle. Nature *328*, 313-318.

Tang, A.H., Karson, M.A., Nagode, D.A., McIntosh, J.M., Uebele, V.N., Renger, J.J., Klugmann, M., Milner, T.A., and Alger, B.E. (2011). Nerve terminal nicotinic acetylcholine receptors initiate quantal GABA release from perisomatic interneurons by activating axonal T-type (Cav3) Ca(2)(+) channels and Ca(2)(+) release from stores. The Journal of neuroscience : the official journal of the Society for Neuroscience *31*, 13546-13561.

Tang, J., Maximov, A., Shin, O.H., Dai, H., Rizo, J., and Sudhof, T.C. (2006). A complexin/synaptotagmin 1 switch controls fast synaptic vesicle exocytosis. Cell *126*, 1175-1187.

Taylor, C.W., and Prole, D.L. (2012). Ca(2+) Signalling by IP(3) Receptors. Sub-cellular biochemistry *59*, 1-34.

Thaler, C., Li, W., and Brehm, P. (2001). Calcium channel isoforms underlying synaptic transmission at embryonic Xenopus neuromuscular junctions. The Journal of neuroscience : the official journal of the Society for Neuroscience *21*, 412-422.

Torri Tarelli, F., Passafaro, M., Clementi, F., and Sher, E. (1991). Presynaptic localization of omega-conotoxin-sensitive calcium channels at the frog neuromuscular junction. Brain research *547*, 331-334.

Uchitel, O.D., Protti, D.A., Sanchez, V., Cherksey, B.D., Sugimori, M., and Llinas, R. (1992). P-type voltage-dependent calcium channel mediates presynaptic calcium influx and transmitter release in mammalian synapses. Proceedings of the National Academy of Sciences of the United States of America *89*, 3330-3333.

Unni, V.K., Zakharenko, S.S., Zablow, L., DeCostanzo, A.J., and Siegelbaum, S.A. (2004). Calcium release from presynaptic ryanodine-sensitive stores is required for long-term depression at hippocampal CA3-CA3 pyramidal neuron synapses. The Journal of neuroscience : the official journal of the Society for Neuroscience *24*, 9612-9622.

Urbano, F.J., Piedras-Renteria, E.S., Jun, K., Shin, H.S., Uchitel, O.D., and Tsien, R.W. (2003). Altered properties of quantal neurotransmitter release at endplates of mice lacking P/Q-type Ca2+ channels. Proceedings of the National Academy of Sciences of the United States of America *100*, 3491-3496.

Urbano, F.J., Rosato-Siri, M.D., and Uchitel, O.D. (2002). Calcium channels involved in neurotransmitter release at adult, neonatal and P/Q-type deficient neuromuscular junctions (Review). Molecular membrane biology *19*, 293-300.

Verkhratsky, A., and Petersen, O.H. (2002). The endoplasmic reticulum as an integrating signalling organelle: from neuronal signalling to neuronal death. European journal of pharmacology *447*, 141-154.

Verstreken, P., Ly, C.V., Venken, K.J., Koh, T.W., Zhou, Y., and Bellen, H.J. (2005). Synaptic mitochondria are critical for mobilization of reserve pool vesicles at Drosophila neuromuscular junctions. Neuron *47*, 365-378.

Viana, F., Van den Bosch, L., Missiaen, L., Vandenberghe, W., Droogmans, G., Nilius, B., and Robberecht, W. (1997). Mibefradil (Ro 40-5967) blocks multiple types of voltage-gated calcium channels in cultured rat spinal motoneurones. Cell calcium *22*, 299-311.

Wadel, K., Neher, E., and Sakaba, T. (2007). The coupling between synaptic vesicles and Ca2+ channels determines fast neurotransmitter release. Neuron *53*, 563-575.

Walter, A.M., Groffen, A.J., Sorensen, J.B., and Verhage, M. (2011). Multiple Ca2+ sensors in secretion: teammates, competitors or autocrats? Trends in neurosciences *34*, 487-497.

Wang, S.S., and Thompson, S.H. (1995). Local positive feedback by calcium in the propagation of intracellular calcium waves. Biophysical journal *69*, 1683-1697.

Weber, T., Zemelman, B.V., McNew, J.A., Westermann, B., Gmachl, M., Parlati, F., Sollner, T.H., and Rothman, J.E. (1998). SNAREpins: minimal machinery for membrane fusion. Cell *92*, 759-772.

Wen, H., and Brehm, P. (2005). Paired motor neuron-muscle recordings in zebrafish test the receptor blockade model for shaping synaptic current. The Journal of neuroscience : the official journal of the Society for Neuroscience *25*, 8104-8111.

Wen, H., and Brehm, P. (2010). Paired patch clamp recordings from motor-neuron and target skeletal muscle in zebrafish. Journal of visualized experiments : JoVE.

Wen, H., Linhoff, M.W., McGinley, M.J., Li, G.L., Corson, G.M., Mandel, G., and Brehm, P. (2010). Distinct roles for two synaptotagmin isoforms in synchronous and asynchronous transmitter release at zebrafish neuromuscular junction. Proceedings of the National Academy of Sciences of the United States of America *107*, 13906-13911.

Westenbroek, R.E., Hoskins, L., and Catterall, W.A. (1998). Localization of Ca2+ channel subtypes on rat spinal motor neurons, interneurons, and nerve terminals. The Journal of neuroscience : the official journal of the Society for Neuroscience *18*, 6319-6330.

Wilhelm, B.G., Groemer, T.W., and Rizzoli, S.O. (2010). The same synaptic vesicles drive active and spontaneous release. Nature neuroscience *13*, 1454-1456.

Woo, S.H., Soldatov, N.M., and Morad, M. (2003). Modulation of Ca2+ signalling in rat atrial myocytes: possible role of the alpha1C carboxyl terminal. The Journal of physiology *552*, 437-447.

Wyart, C., Del Bene, F., Warp, E., Scott, E.K., Trauner, D., Baier, H., and Isacoff, E.Y. (2009). Optogenetic dissection of a behavioural module in the vertebrate spinal cord. Nature *461*, 407-410.

Xu, J., Pang, Z.P., Shin, O.H., and Sudhof, T.C. (2009). Synaptotagmin-1 functions as a Ca2+ sensor for spontaneous release. Nature neuroscience *12*, 759-766.

Xu, W., and Lipscombe, D. (2001). Neuronal Ca(V)1.3alpha(1) L-type channels activate at relatively hyperpolarized membrane potentials and are incompletely inhibited by dihydropyridines. The Journal of neuroscience : the official journal of the Society for Neuroscience *21*, 5944-5951.

Yao, J., Gaffaney, J.D., Kwon, S.E., and Chapman, E.R. (2011). Doc2 is a Ca2+ sensor required for asynchronous neurotransmitter release. Cell *147*, 666-677.

Yasuda, R., Nimchinsky, E.A., Scheuss, V., Pologruto, T.A., Oertner, T.G., Sabatini, B.L., and Svoboda, K. (2004). Imaging calcium concentration dynamics in small neuronal compartments. Science's STKE : signal transduction knowledge environment *2004*, pl5.

Yazejian, B., DiGregorio, D.A., Vergara, J.L., Poage, R.E., Meriney, S.D., and Grinnell, A.D. (1997). Direct measurements of presynaptic calcium and calcium-activated potassium currents regulating neurotransmitter release at cultured Xenopus nerve-muscle synapses. The Journal of neuroscience : the official journal of the Society for Neuroscience *17*, 2990-3001.

Young, S.M., Jr., and Neher, E. (2009). Synaptotagmin has an essential function in synaptic vesicle positioning for synchronous release in addition to its role as a calcium sensor. Neuron *63*, 482-496.

Zamponi, G.W., Bourinet, E., and Snutch, T.P. (1996). Nickel block of a family of neuronal calcium channels: subtype- and subunit-dependent action at multiple sites. The Journal of membrane biology *151*, 77-90.

Zucker, R.S., and Regehr, W.G. (2002). Short-term synaptic plasticity. Annual review of physiology *64*, 355-405.